Automated Nozzle Design through Axis-Symmetric Method of Characteristics Coupled with Chemical Kinetics

by

Reid Britton Young

A thesis submitted to the Graduate Faculty of
Auburn University
in partial fulfillment of the
requirements for the Degree of
Master of Science

Auburn, Alabama
August 4, 2012

Keywords: rocket, propulsion, nozzle, design

Approved by

Roy J. Hartfield, Jr., Chair, Woltosz Professor of Aerospace Engineering
Andrew Shelton, Assistant Professor of Aerospace Engineering
Brian Thurow, Reed Associate Professor of Aerospace Engineering

Abstract

A method of designing axis-symmetric nozzles with included finite-rate chemical kinetics has been developed. The use of the axis-symmetric method of characteristics coupled with finite-rate chemistry allows for the design and performance prediction of nozzles for liquid rocket engines. The use of a particle swarm / pattern search optimizer enables viable pressure distributions to initiate the axis-symmetric method of characteristics. The method allows for the nozzle boundary to be formed through a full method of characteristics solution. The contour formed allows for a smooth throat, shock free nozzle.

This development allows the process for designing rocket nozzles to be automated, facilitating the design of axis-symmetric nozzles to meet a specific performance goal, while simplifying the effort of the designer. This thesis will describe the chemical kinetic coupled axis-symmetric method of characteristics, and the associated automated nozzle design methodology.

Acknowledgments

I would like to especially thank Dr. Roy Hartfield for his support and guidance throughout my graduate work at Auburn University.

I am also grateful for all of the support of my parents, they have been there through all of my endeavors.

I would like to dedicate this work to my grandfather, Donald R. Young. "Illigitimi Non Carborundum," these words will never let me down.

Table of Contents

List of Figures

List of Tables

Chapter 1

Introduction

The performance of a rocket engine is dependent upon the momentum imparted to the gaseous products of combustion by ejecting them through a nozzle. As these exhaust gases pass through the nozzle they are continually accelerated. The speed of the gases begins in the low subsonic range, in the head end of the thrust chamber, and increases to a highly supersonic flow. The thrust produced by a rocket engine accrues losses due to, among other things, flow divergence from the axial direction of the nozzle. Thus a nozzle that produces maximum thrust for a given exit condition is one with a uniform flow field across the exit that is directed axially. To achieve this maximum thrust condition, a nozzle contour must, also correctly expand the flow. However, contoured nozzles required to achieve such flows are generally extremely long, heavy, and undesirable for rocket nozzle applications.

The contour of a converging diverging nozzle is comprised of three sections: convergent section, throat section, and divergent section. Each section affects the flow differently and must be considered to produce the desired nozzle performance. Analysis of nozzle flows can be performed assuming that the exhaust gases expand adiabatically as an ideal gas with constant specific heat ratio. In addition, consideration of chemical reactions due to incomplete combustion, chemical properties in the exhaust gases, viscous boundary layer effects and radiative heat loss can be considered.

The design of a rocket engine nozzle can be developed using the method of characteristics. The method allows for physical boundaries to be found directly making the MOC an attractive design tool for finding the nozzle contours. The method can also be coupled with finite rate chemistry, allowing for the nozzle contour to be designed with chemical reactions

accounted for, including consideration of incomplete combustion, where the chemical properties of the exhaust gases are captured by analyzing the reactions and recombination of the combustion products.

The use of the axis-symmetric method of characteristics coupled with chemical kinetics of the combustion products has been developed by combining the method with the use of an optimization routine, which allows for an automated design approach to liquid rocket engines to meet desired performance goal.

1.1 A Brief History of Rockets

As early as 600 AD the Chinese had found that a mixture of charcoal, sulfur, and saltpeter could be used as a propellant allowing the creation of their rocket-propelled fire arrows[8]. These were the first true rockets. The use of such weapons slowly spread to western civilization. Despite the rockets early advent, technical understanding and development of the rocket did not begin until the end of the 19th century[9].

The Russian school teacher Konstantin Eduardovitch Tsiolkovsky is credited to be the first true rocket scientist[8]. As a student he was infatuated with space travel, he carried this with him into his career, and slowly worked on rocket theory without institutional support. His most known contribution is the Tsiolkovsky rocket equation.

$$\Delta v = I_{sp} g_o ln \frac{m_i}{m_t} \tag{1.1}$$

He also worked on a design for a liquid hydrogen, liquid oxygen rocket engine. He published his work on the design and the rocket equation in 1903, the same year as the first flight of a powered airplane[8]. However, due to his lack of funds he performed no practical experiments and generated no data on his design.

Convinced that rocketry was the key to space flight, Dr. Robert H. Goddard was the first to apply theory and develop practical working designs. As with Tsiolkovsky, Goddard

also determined that liquid hydrogen, liquid oxygen would be an efficient rocket propellant. In 1914, Goddard was granted patents on his designs for propellant feed systems, combustion chambers, nozzles, and multistage rockets. Obtaining a small grant from the Smithsonian Institution in 1917, he was able to secure his career in rocketry, allowing him to publish his work "Reaching Extreme Altitudes" in 1919[8]. Goddard went on to show how de Laval nozzles could be applied to the combustion exhaust gases to accelerate the flow. Most modern day rocket engines use some form of a Laval nozzle.

During the early 1920's, Goddard spent much of his time performing activities in his laboratory. This time was spent with testing and development of what would become the first liquid propellant rocket engine. Through these experiments, Goddard proved that a rocket can work in a vacuum, by showing that the rocket needs no air to push against[10]. On March 26, 1926 Goddard launched his 10ft long rocket that used a liquid oxygen and gasoline propellant. The rocket flew to an altitude of 184 ft and reached a maximum speed of 60 mph[8]. Seeming to be only a modest feat, this first flight is equivalent to that of the flight of the Wright brothers in importance to rocketry.

Larger and larger rockets were designed and tested during the 1930's, however the developments were slow and steady. The outbreak of World War II greatly accelerated the advancement of the rocket engine. This especially occurred in Germany with the development of the A-4 rocket, commonly known as the V-2 [11]. Much of this development was due to the work of Herman Oberth, who was considered the "founding father" of German rocketry. On October 3, 1942 the V-2 took its first flight, the significance of this flight was the demonstration that a rocket had the potential to obtain orbit[11].

Following World War II intense research lead to the evolution of liquid rocket propulsion from its rudimentary basis to a sophisticated science that has produced the engineering feats of modern day[12]. Arguably the most important development in liquid-propellant rocket engines came with the development of the Pratt and Whitney Aircraft RL10 powerplant. The RL10 was the first rocket engine to use liquid hydrogen as a fuel[13]. This technological

breakthrough ultimately allowed the first lunar landing and lead to the development of the Viking Spacecraft to Mars, and Voyager (to Jupiter and beyond[12]).

Today the state-of-the-art in high performance liquid-propellant rocket engines is represented by the Space Shuttle Main Engine. A single SSME delivers a vacuum thrust of 512,300 lb while the propulsion system weighs about 7775 lb [12, 14]. The SSME has a vacuum specific impulse of 452 seconds. This staged-combustion cycle engine is impressive machine from head to toe. The hydrogen fuel is fed using a 71,140 hp turbopump. The SSME has achieved a 100% flight success and demonstrated reliability of 0.9995[14]

1.2 The Liquid Rocket Engine

Liquid rocket engines are chemical rockets that use liquid propellants. A complete rocket engine is comprised of many highly integrated systems that allow for the operation and control of the engine. There are four major subsystems that a liquid-propellant rocket engine consists of:

- Thrust chamber
- Propellant feed system
- Propellant control system
- Thrust vector control system

The thrust chamber is used to convert stored chemical energy to directed kinetic energy through the combustion of propellants and the acceleration of the exhaust gases. The propellants are supplied to the thrust-chamber at the correct pressure by the propellant feed system.

The propellant feed system is comprised of storage tanks for the propellant, feed lines,and turbopumps or pressure regulators. There are two basic types of propellant feed systems,

direct pressurized gas fed and turbopump fed. Direct pressurized gas feed systems store propellants in pressurized tanks, limiting the chamber pressure to the design of the tank. High pressure tanks become heavy, due to tank thickness required to withstand such pressures[12].

Turbopump feeds use turbopump that are fed propellant at relatively low pressures. The pumps can raise the pressure of the propellant to high pressures. This allows for high pressures at much lower weight cost[12].

The turbine-drive system directs the appropriate gases through turbines in order to power the turbopumps used in the propellant feed system. The gases used to drive the turbans are directed from gas generators, preburners, heat exchangers, or tapped from the main combustion chamber.

The propellant control system provides regulation of the propellants in order to control the propellant mixture ratio and the total amount of propellant. This allows thrust control and proper operation. The propellant control system is typically a system of valves.

Other control systems allow for proper and desired operations of the rocket. The focus of the present development lies within the thrust chamber, which is be discussed in Sec 1.2.1

1.2.1 Thrust Chamber

The thrust chamber is the single most important system of a rocket engine as it is the system of the rocket designed for the generation of thrust. The thrust chamber for a liquid engine is comprised of three main sections: injector, combustion chamber, and supersonic nozzle. It is here that the liquid propellants are injected, atomized, vaporized, mixed, combusted, accelerated and ejected. Figure (1.1) displays the different zones of flow within a typical thrust chamber.

The injector injects both the fuel and oxidizer into the combustion chamber in such away that the liquids are separated into small droplets, this process is referred to atomization. The injectors are designed in such away that the injection streams of the fuel and oxidizer impinge on one another to form a well mixed solution in the correct mixture ratio for combustion.

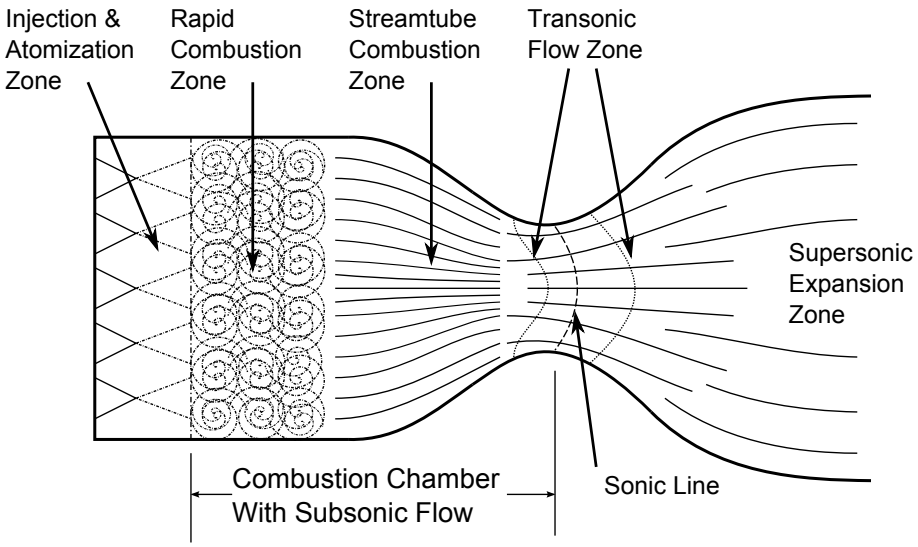

Figure 1.1: Flow Zones in a Typical Thrust Chamber[1]

This impingement in many cases aides to the atomization, through molecular interaction[1]. The design of these injectors is a complex subject beyond the scope of this investigation. It will be assumed henceforth that the injectors are designed in such away that proper mixing occurs at any specified mixture ratio.

The combustion chamber is the section of the thrust chamber where the burning of the propellants takes place. The combustion chamber is designed in such a way that it retains the mixture of propellants for enough time that it ensures complete mixing and combustion. The time that is required for this to happen is referred to as the combustion residence time and is effected by many parameters. Combustor geometry, injection condition, propellant combination are a few such parameters that must be considered in combustion chamber design[12]. Modern design of the combustion chamber typically calls for a cylindrical chamber. For this development, the combustion chamber will be assumed to be cylindrical and of the proper volume to ensure complete combustion to equilibrium conditions. Also, ignition processes are beyond the scope of this investigation therefore it will be assumed that the combustion process is taking place during operating conditions.

Following the combustion chamber is a converging diverging nozzle designed to produce supersonic exit conditions. This section of the thrust chamber is used to convert the chemical energy released in the combustion process to directed kinetic energy. This conversion of energy ultimately results in the production of thrust. De Laval, or converging diverging nozzles, are the focus of this investigation, and although other nozzle types exist they will not be discussed. A good discussion of annular nozzles can be found in Ref. [1],and Ref. [12]. The development of supersonic nozzle design will be discussed in great detail in Chapter 2.

1.2.2 Thrust Chamber Performance

The performance of a liquid propellant rocket engine is directly dependent on the combination of propellants used, the combustion efficiency of the propellants, and the expansion of the gases formed from the combustion process. For the most part the performance of a rocket engine can be expressed through the performance parameter called specific impulse, ISP. The specific impulse is defined as the thrust divided by the weight flow rate measured at sea level gravity[1]. This definition provides that the units of specific impulse are in time, typically in seconds.

$$I_{sp} = \frac{\int_0^t F dt}{go \int_0^t \dot{m} dt} \tag{1.2}$$

The thrust force generated by the rocket can be expressed as

$$F = \dot{m} u_e + A_e(p_e - p_a) \tag{1.3}$$

Where the exit velocity can be found through

$$u_e = \sqrt{\frac{2\gamma \frac{R_u}{MW} T_o}{\gamma - 1} \left[1 - \frac{p_e}{p_o}^{\frac{\gamma-1}{\gamma}}\right]} \tag{1.4}$$

From these relationships it is apparent that the specific impulse is dependent on the specific heat ratio, molecular weight and combustion temperature of the propellant. This can easily be shown by rewriting I_{sp} as

$$I_{sp} = \sqrt{\frac{2\gamma}{\gamma - 1}\frac{R_u T_o}{MW}\left[1 - \left(\frac{p}{p_o}\right)^{\frac{(\gamma-1)}{\gamma}}\right]} \tag{1.5}$$

Maximizing specific impulse has an important impact on the design of the total vehicle. From the definition of specific impulse above and the rocket equation, Eq. (1.1), the relationship between specific impulse and payload is apparent. Large values of Isp result in an increase in allowable payload. This is achieved by the minimization of the specific heat ratio and the molecular weight of the working fluid.

1.3 Liquid Propellants

As with all rockets, liquid propellant rocket engines are supplied internally with both the fuel and oxidizer. Unlike an air breathing propulsion device, which supplies the oxidizer in the form of air through some means of intake, rockets internal supply of both the fuel and oxidizer allows for the combustion of the propellant in a vacuum. Furthermore, the rocket is not limited by aerodynamics when supplying the oxidizer, allowing for a rocket to operate at very high speeds while in the atmosphere. There are three basic types of liquid rocket propellants: monopropellant, bipropellant, and tripropellant. The selection of the propellant is typically based on the application of the rocket. The main focus of this development is bipropellants, with liquid oxygen, LOX, as the oxidizer. However the development is designed so that other propellants can be used. A list of propellants that are readily available for analysis will be provided in a section 4.2 .

Clearly, from Eq 1.5, the performance of a rocket is dependent on the propellants used. The exit velocity, specific impulse, and thrust of a rocket are dependent on the specific heat ratio, molecular weight, and combustion temperature. This can easily be seen in Eqn. (1.2)

and Eqn. (1.4) and the thrust equation. From these relationships, it is clear that careful consideration of the chemical kinetics of the propellants will lead to a high fidelity solution to the design problem.

Selection of the propellants to be used is based on trade studies or optimization of mission design. This allows for the relationship between rocket performance, total weight of the vehicle, and other design considerations to be investigated. One characteristic of the propellant that lends to the selection is the density specific impulse. Defined as

$$I_d = I_{sp}\frac{\delta_o\delta_f(1+r)}{r\delta_f+\delta_o} \tag{1.6}$$

Where δ is the specific gravity of the propellant component, and r is the mixture ratio.

Fuel	Performance of LOX Oxidizer Propellants				
	Mixture Ratio	Bulk Density kg/m^3	Combustion Temp K	Vacuum I_{sp} sec	Density Specific Impulse $kg-s/L$
Hydrogen	6.0	358	3610	455.9	124
Methane	3.0	801	3589	368.3	235
Propane**	2.7	1014	3734	361.9	367.1
RP-1	2.5	1026	3803	354.6	294
*I_{sp} values based on 100:1 expansion into vacuum. Assumed chamber pressure 20 MPa. **Propane data based off of sub-cooled propane.					

Table 1.1: Performance factors of different hydrocarbon fuel compared to liquid hydrogen[6]

This characteristic of the propellant, can be useful in the overall design of a vehicle where any reduction in system mass can translate into an increase in payload mass for a given thrust capability. A comparison of a few hydrocarbon fuels and hydrogen is given in Table 1.1. It is clear hydrogen as a fuel yields the highest performance. However, the low density allows for the hydrocarbons to be a better choice for situations when mass savings outweighs overall performance. Ultimately the selection of the propellant is chosen as a vehicle design parameter and a rocket engine is designed for the specific propellant types[6].

1.4 Combustion of Liquid Propellants

For a chemical rocket, the working fluid of exhaust gases is produced by active combustion of propellant. Combustion allows the release of stored chemical energy in the propellant. This transfers the energy into the form of thermal, and random kinetic energy that can be directed by the use of a nozzle to impart momentum on the system for the generation of thrust[1]. The behavior of the combustion is dependent on the propellants being used. Investigation into the combustion process of the propellants results in more accurate predictions of the performance parameters of the rocket engine as well as the thrust produced[15, 1].

Typically, combustion of liquid propellants in thrust chambers is very efficient. Efficiencies in well-designed combustion chambers for liquid rocket engines can be found in the range of 95 to 99.5%[1]. The ability of the combustion chamber to provide thorough mixing through correct injection and atomization of the propellants along with the high reaction rates at the high chamber temperatures allow for such efficiencies. The nature of combustion provides that the exhaust gases are chemically active. The chemically active exhaust gases can be modeled by treating the gases as equilibrium, frozen, or non-equilibrium chemically reacting. Solutions to nozzle performance for equilibrium flow and frozen flow can readily be obtained using generalized one-dimensional flow analysis. However, these are the extreme cases. Equilibrium flow corresponds to the best case where the reaction rates of the flow are infinite. The lower limit corresponds to frozen flow where the reaction rates are zero. Both the equilibrium flow and frozen flow cases can be shown to be isentropic processes. For frozen flow the composition of the gas mixture has no change resulting in the entropy change in the system to be zero, while with equilibrium the sum of products of the chemical potential and changes in mass fraction of the reactants is equal to the sum of the changes in the products of the chemical potential and changes in mass fraction of the products resulting in no change in entropy in the system[4]. The two conditions can be shown through the effect of chemical reactions on the entropy of a mixture and is discussed in detail by Zucrow[4]

$$Tds = -\sum_{i}^{N} \mu_i dC_i \tag{1.7}$$

In reality, the chemically reacting flows have finite rates of reaction somewhere between these two limiting cases, and because the chemical reactions occur at a finite non-zero rate the entropy of the system will change.

The equilibrium composition and final equilibrium thermodynamic state can be found through the minimization of Gibbs free energy of the system, the minimization of Helmholtz free energy or the maximization of entropy of the system[16]. Characterizing the thermodynamic state by temperature and pressure lends itself to using the minimization of Gibbs free energy for equilibrium calculation due to temperature and pressure being natural variables of Gibbs free energy[16]. Gibbs free energy represents the amount of energy available to do work on an open system in which mass is exchanged within the surroundings. For a general reaction the Gibbs free energy change can be written as

$$\Delta G = \Delta H - T\Delta S \tag{1.8}$$

which can become

$$\Delta G = \sum \left[\nu_j (\Delta_f G^\circ)_j\right]_{products} - \sum \left[\nu_j (\Delta_f G^\circ)_j\right]_{reactants} \tag{1.9}$$

Gordon and McBride[16] used a Lagrangian multiplier technique for the minimization of Gibbs free energy to find the equilibrium composition of a reaction. Gordon and McBride's technique is used for the equilibrium calculation needed in this development. Their method and the program which they developed for a generic equilibrium composition calculation is discussed in Appendix B and a complete explanation of the their process can be found in [16][17].

When the exhaust gas velocities become primarily axial the gases are passing through the streamtube combustion zone. Although the gas composition is not truly uniform when

traversed radially across the combustion chamber, by time the exhaust gases become striated they have been well mixed and can be considered uniform composition for following the reactions through the subsonic portion of the nozzle. This allows to treat the problem as quasi-one-dimensional flow until the Mach number of the flow reaches just beyond unity, based on a prescribed pressure distribution through the combustion chamber, converging section and throat. As these streamlines of chemically reacting gases flow through the converging section of the nozzle they are accelerated more. Depending on the propellant this zone may become nearly chemically frozen if the axial velocity of the flow is at a rate that is faster than that at which the products can react.

Chapter 2

Review of Literature

2.1 Contoured Nozzle Design

It can easily be shown that in order to expand flow through a duct from subsonic flow to supersonic flow the area of the passage that the fluid is passing must first decrease in area and then increase in area. This area relationship is the basis in nozzle design given in Eq. (2.1). The relationship between local Mach number and the local area ratio was found through the study of quasi-one-dimensional flow. Although this relationship provides no information for the contour of such a duct[18] or the losses that are associated with a multidimensional flow field.

$$\frac{A}{A^*} = \frac{1}{M}\left[\frac{2}{\gamma+1}\left(1+\frac{\gamma-1}{2}M^2\right)\right]^{\frac{\gamma+1}{2(\gamma-1)}} \tag{2.1}$$

In early rocket engine designs, conical nozzles were used almost exclusively[12]. The geometry of a conical nozzle, depicted in Fig. 2.1, allows for ease of manufacturing. The simple design also allowed for any given expansion ratio to be created with simply extending the length of the nozzle.The flow in a conical nozzle is not turned to become axial and thus no strong shocks will form in the nozzled during operating conditions.

However, the conical nozzle has associated performance losses because the flow has a non-axial component[19]. In order to save weight on a potentially very long nozzle, large cone angles must to be used. As the cone angle is increased the loss of thrust,due to non-axial flow conditions at the exit, increases. The momentum losses are typically incorporated through the theoretical correction factor below[1]. This yields the percentage of the ideal

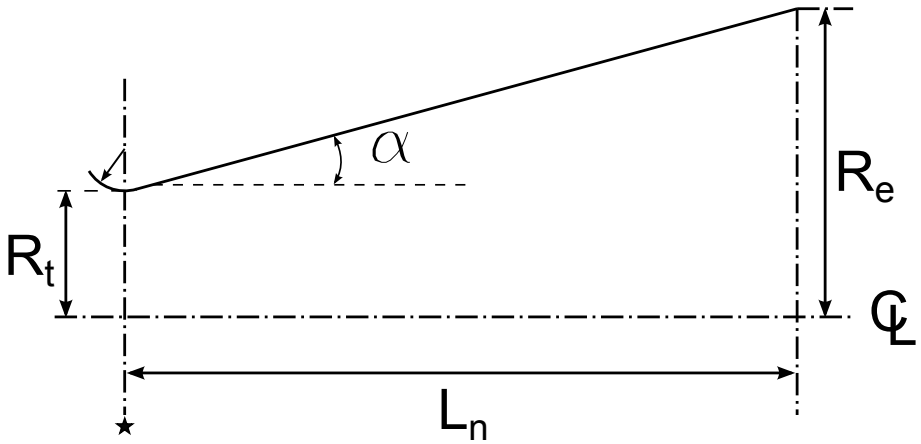

Figure 2.1: Typical Outer Mold Line of a Conical Nozzle

exhaust velocity that is axial. The influence as the cone half angle increases can be easily determined through [12, 1]

$$\lambda = \frac{1}{2}(1 + cos\alpha) \tag{2.2}$$

These losses and the extreme weights associated with small divergence angles make the conical nozzle a poor choice of geometry. In order to impart the momentum axially at the exit the contour nozzle or bell nozzle was developed, as depicted in Fig. 4.1[12]. The contoured nozzle increases performance the flow must be turned so that the exit flow of the nozzle is parallel to the centerline of the nozzle at the exit. This imparts all of the momentum axially. To develop this condition a contoured nozzle can be designed so that immediately behind the the throat the flow undergoes a pronounced expansion. As the flow continues throughout the nozzle the expansion continues to occur but the convex shape allows for the rate of expansion to diminish. Expansion waves in the fluid allow for the direction of the supersonic flow to change. As the gas flows through these expansion waves the fluid is allowed to change its direction and increase its velocity with little loss of energy, and a contour can be formed to follow these changes. The physicality of the flow lends itself to the method of characteristics for analysis, allowing the method to model these expansion

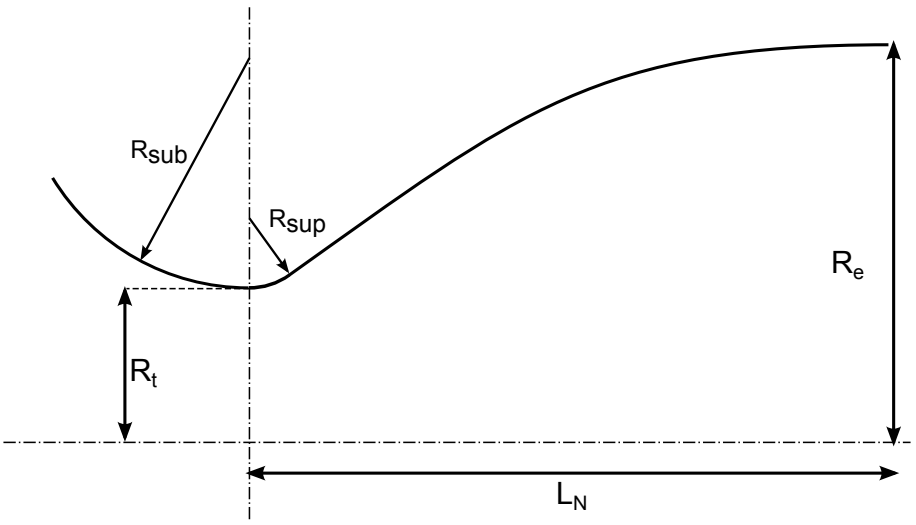

Figure 2.2: Typical Outer Mold Line of a Contoured Nozzle

waves as mathematical characteristics[1][20]. A detailed description of the method will be presented in a later section.

The first successful implementation method of characteristics for nozzle design was performed by Ludwig Prandtl and Adolf Busemann[18] in 1929. Since the implementation by Prandtl and Buseman, the method of characteristics has become a fundamental basis in nozzle design. This is because the method allows for physical boundaries to be located. Prandtl and Busemann implemented the method graphically to solve two-dimensional nozzle problems. A comprehensive presentation on both the graphical and the analytical approach to two-dimensional method of pharmacogenetics was completed by Shapiro and Edelman in 1947[21]. In 1949, Foelsch proposed a method for developing solutions to axis-symmetric supersonic streams using a method of characteristics approach[21]. Antonio Ferri extended the approach to axis-symmetric flows in 1954, through a theoretical adaptation to the mathematics[22, 21].

In 1959, Guerntert and Netmann implemented the analytical approach for the development of supersonic wind tunnels with desired mass flows[3, 21]. This implementation developed a solution based off of initial conditions along the nozzle centerline. The Guerntert

and Netmann consideration of the approach for wind tunnel design had no length requirement but required uniform exit flow. Their solution resulted in difficulties designing short length and large expansion ratio nozzles[3]. Their work also showed that truncation of nozzle lengths resulted in only a small reduction of vacuum specific impulse from the uniform flow case[3].

The work of G.V.R. Rao used the method of characteristics as part of his solution in developing contour nozzle designs. Rao developed a method of designing a contoured exhaust nozzle for optimum thrust of a fixed length nozzle. Rao's solution used a combination of Lagrangian multipliers and method of characteristics[19, 23].

Rao's solution used a control volume that does not span across the nozzle's exit. The prescribed control volume follows a characteristic. This creates a boundary on the control volume be at an oblique angle to the axis of the nozzle[19, 23], as illustrated in Fig (2.3). The control volume being set to an angle allowed Rao to integrate along a characteristic line to obtain mass flow rate and thrust.

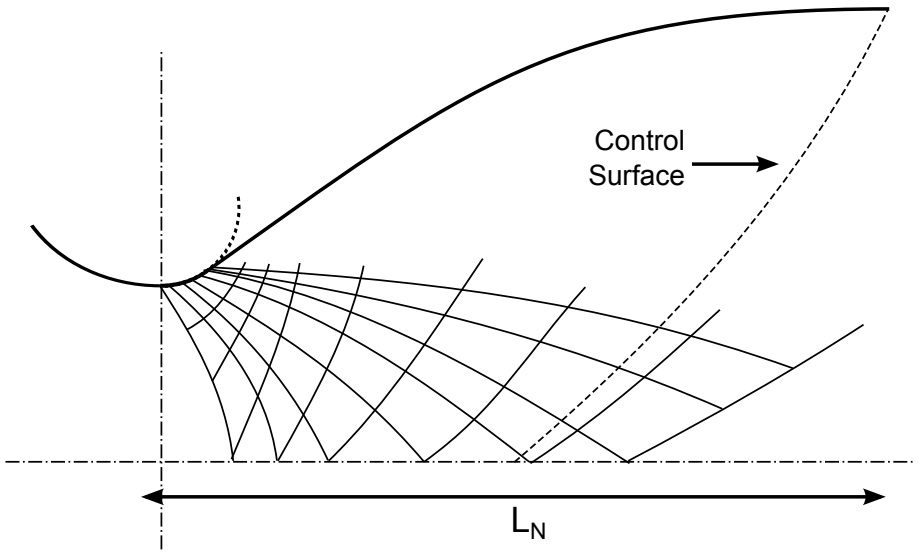

Figure 2.3: Typical characteristics net in a Rao nozzle with illustration of control surface

Rao's method for obtaining a nozzle contour, begins by prescribing the geometry of the throat. This sets the subsonic and supersonic radius as two unique values. The subsonic

radius of curvature is set to allow for substantially supersonic flow at the throat of the nozzle and was obtained on the basis of Sauer's solution[19], which will be explained in depth later. The supersonic radius of curvature is prescribed to a value that is large enough to ensure that flow separation at the throat is not a concern, yet kept short to allow for the minimization of total nozzle length[19, 23]. Rao's objective was to form nozzle contours that allowed for the maximization of thrust for a given nozzle length.

When examining a nozzle without uniform exit flow, following a line perpendicular to the centerline that intersects the nozzle exit, the Mach number will not be found to be constant. Starting at the exit, the Mach number along such a line will increase as the centerline is neared. With the exit Mach number selected, Rao finds the the wall slope at the exit under these flow conditions. From this point Rao's method constructs a characteristic net in the region between the exit, a calculated point on the control volume and the transition point on the nozzle wall where the contour will transform from convex to concave geometry with respect to the flow. The contour of the nozzle is then found following a stream line between the transition point and the exit point.

The method Rao presented in 1958 was the basis for the Rao parabolic approximation to bell nozzle contours. The parabolic nozzles are presented in detail in both Sutton[1] and Huzzel and Huang[12]. The Rao approximation method prescribes a set of parabolas that allow for a contour that is near the optimum thrust contours developed by his method. These nozzle contours are chosen by specifying the fractional nozzle length of a 15 degree half-angle conical nozzle, and the expansion area ratio. The appropriate parabola is chosen from these parameters. The parabola specifies the exit flow angle and the initial turning angle. The throat geometry is then found using a subsonic radius of curvature of $1.5r_t$ and a supersonic radius of curvature of $\approx 0.4r_t$[1, 12]. Neither Sutton or Huzel and Huang explain the selection of the supersonic radius of curvature. Sutton goes on to note that small changes in the supersonic radius have only small effect on the overall approximation. The method presented by Rao was widely used in the 1960's. However it has been found that

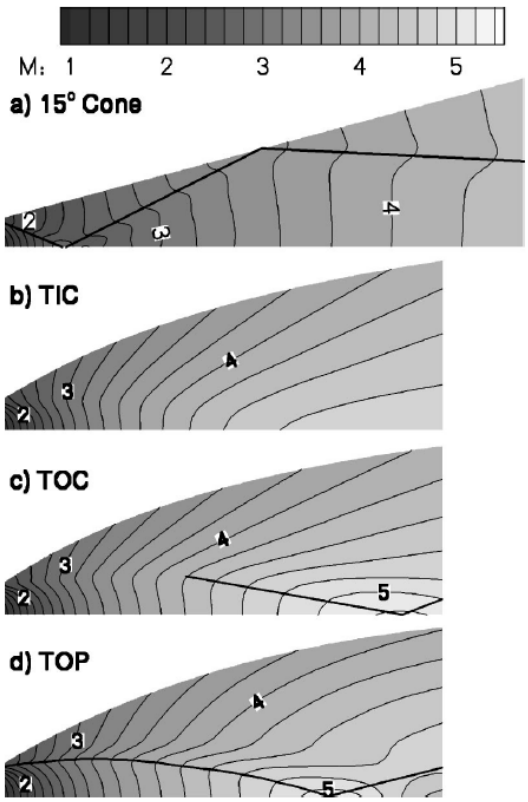

Figure 2.4: Formation of internal shocks in conical and contoured nozzles[2]

the contours formed by the Rao approach and the Rao parabolic approximation produce shocks. Shocks occur due to a pressure rise in the supersonic flow field. In nozzles, the formation of shocks can be caused by the presence of a downstream high pressure condition, as in ignition transients, or by the how the contour is constructed to control the expansion of the flow[2]. The formation of shocks due to the wall construction occurs as a result of turning the wall into the flow, allowing a compressive wave to form. Interaction between the compressive waves and expansion waves can cause a pressure rise. Figure (2.4) shows the formation of shocks in different contours[2]. The TIC nozzle is a truncated ideal contour, which is the focus of this thesis. TOC is a thrust optimized contour nozzle or Rao nozzle as described above. TOP is a parabolic bell nozzle contour. The nozzle wall can be formed such that a condition can be developed in which the compressive turn is exactly canceled

by an expansion wave. A viable solution can be obtained by specification of the centerline pressure distribution so that this condition for compressive cancelation occurs.

Obtaining viable axis-symmetric method of characteristics solutions can be a challenging exercise for large expansion ratio nozzles[21]. The solution is heavily dependent on a specified boundary condition along the nozzle centerline. This condition must be assumed prior to the implementation of the method of characteristics, as a result small deviations from viable conditions can cause characteristic lines in the solution to cross. Crossing of like characteristics may produce a solution however this solution cannot be considered valid, for a shock free contour.

In order to form a solution with axis-symmetric method of characteristics using the centerline as a boundary condition, a center line pressure distribution must be assumed. Three basic pressure distributions that have been used with success [21]. However, not every pressure distribution will yield a valid solution for any given nozzle. The pressure distribution must be fitted to the problem at hand. Three distributions that have previously been used with success are: [3]

$$\text{Cosine: } \ln p = \frac{1}{2}(\ln p_t - \ln p_e)cos\frac{\pi x}{l} + \frac{1}{2}(\ln p_t + \ln p_e) \tag{2.3}$$

$$\text{Parabolic: } \ln p = l^{-2}(x-l)^2(\ln p_t - \ln p_e) + \ln p_e \tag{2.4}$$

$$\text{Cubic: } \ln p = \left[\frac{ql + 2(\ln p_t - \ln p_e)}{l^3}\right]x^3 - \left[\frac{2ql + 3(\ln p_t - \ln p_e)}{l^2}\right]x^2 + qx + \ln p_t \tag{2.5}$$

The cubic pressure distribution has an additional factor that allows it to be manipulated. This can be used to create a valid pressure distribution. Examples of pressure distributions are illustrated in Figure (2.5) for a Mach 4 Nozzle with an expansion length that is $5.75r_t$. Chamber pressure is 4400 KPa and chamber temperature is 3000 K. As can be seen the cubic pressure distribution can be manipulated with the changes in q giving the cubic more flexibility

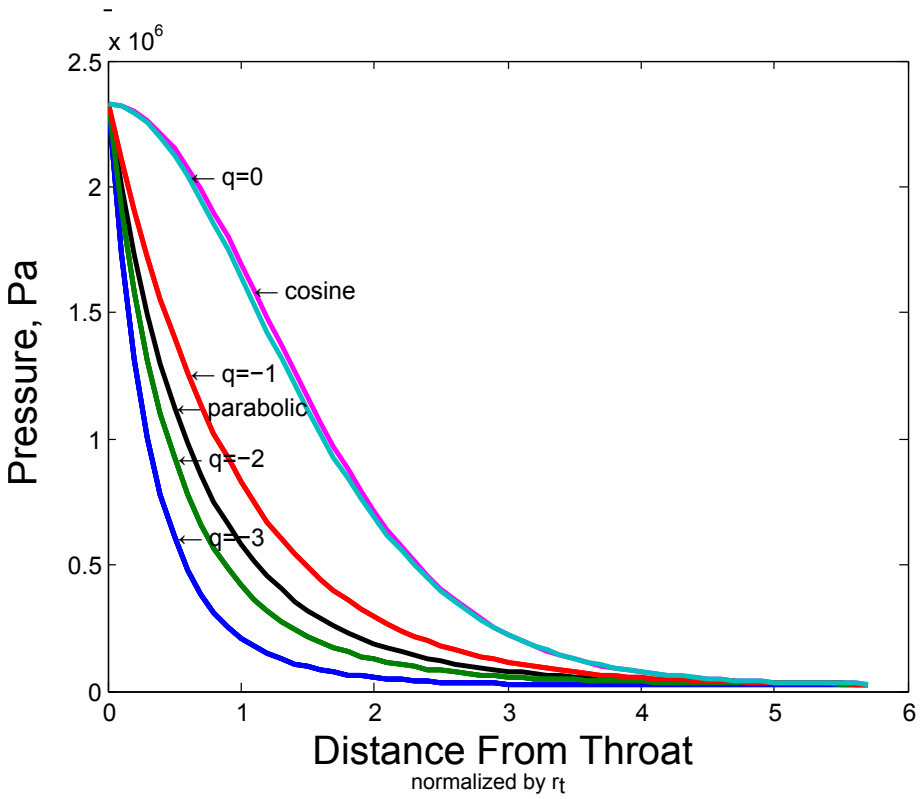

Figure 2.5: Pressure Distributions

Further examination into these pressure distribution shows that they are only valid for certain cases. The cosine pressure distribution is the least useful of all. For most expansion ratios the cosine distribution does not yield a realistic pressure distribution after the throat. The parabolic pressure distribution is valid for small expansion ratios. The cubic pressure distribution must be manipulated to the expansion ratios. For small expansion ratios the value of q must be close to zero to provide valid solutions. As the expansion ratio increases the value of q must decrease to provide valid pressure distributions. However as the expansion ratio increases further all of these distributions tend to form solutions with crossing characteristics. In order to produce a pressure distribution that allows for valid solutions through out a wide range of expansion ratios a different approach must be used to specify the centerline pressure distribution.

Haddad and Mosst[24] used a method of characteristics approach to axis-symmetric supersonic nozzle design, this was met with limited success when solving the pure axis-symmetric design requirements[21]. Wang and Hoffman[25] made use of the two-step predictor corrector algorithm on pre-specified flow field data. This has regularly been used since[21]. The work of Wayne and Mueller applied the rotational axis-symmetric method of characteristics employing a technique that allows the down stream characteristic point locations to be selected to fit the flow-field as it is developed. This technique was developed by Hartree. The technique is still subjected to the problem created by the centerline boundary condition. The problem can be overcome but the process to overcome the centerline boundary condition has become case dependent[21]. These methods result in heavy user interface and hit-and-trial solutions to find viable solutions to the case at hand[21].

In 1978 Allman and Hoffman presented a procedure for the design of a maximum thrust contours by a direct optimization method. The contour used was a second-degree polynomial fitted to a prescribed initial expansion contour. The contours produced were similar to that of a Rao nozzle. Allman and Hoffman showed that a polynomial could be used to develop the nozzle boundary with comparable results to a Rao nozzle, however the flow field was solved in much the same way, and the solution differed only slightly in the formation of the nozzle boundary. Essentially, their solution was a Rao nozzle with a polynomial fitted boundary instead of a boundary determined by the solution[26].

In 2011 Hartfield and Ahuja[21] put forth an effort to automatically determine a viable centerline pressure distribution when the centerline pressure distribution is chosen as the governing boundary condition. The technique used by Hartfield and Ahuja was to remove the ability of the characteristics to cross despite using a non-viable axial centerline pressure distribution. The method is a non-physical solution to the internal flow, however the resulting contour of the nozzle allowed for the appropriate expansion lending the contour to a physical solution.

2.2 Transonic Flow Zone

Transonic flow is the flow regime where the fluid transitions from subsonic to supersonic velocities[5]. The transonic flow regime has been intensely studied. The work of Sauer[5] detailed the complexities and the mathematical treatment of such flows, especially as applied to the passage of flow through Laval nozzles. The flow in the throat region of a converging-diverging nozzle under choked flow conditions is transonic[4].

The work of Sauer has been the primary basis for the treatment of the transonic flow zone in supersonic nozzle design, because Sauer's method is a closed form solution for the flow field in the nozzle throat[4], and it can produce excellent approximate solutions for nozzles with a large subsonic radius of curvature relative to the throat radius. In 1958, Rao[19] used Sauer's approach in his treament of transonic flow region. The work of Nickerson et al. [7] based their work in the transonic analysis off of Sauer, applying the analysis to zoned expansions. Nickerson et al. applied this transonic model to striated flow for flows with variable mixture ratios[7]. Because of the importance of Sauer's work on the treatment of the transonic flow zone his work is outlined and described in Appendix A.

The transonic solution is important to the method of characteristics solution. It allows for the determination of a subsonic radius of curvature that allows for substantially supersonic flow at the nozzle wall at the minimum area point and also locates the position where like flow is on the axis of symmetry. In determining this line of constant substantially supersonic Mach number, an initial value line can be formed so that the flow satisfies the wall boundary condition at the throat exactly. Hence, the flow at the wall boundary of the throat will have a radial component of velocity exactly equal to zero.

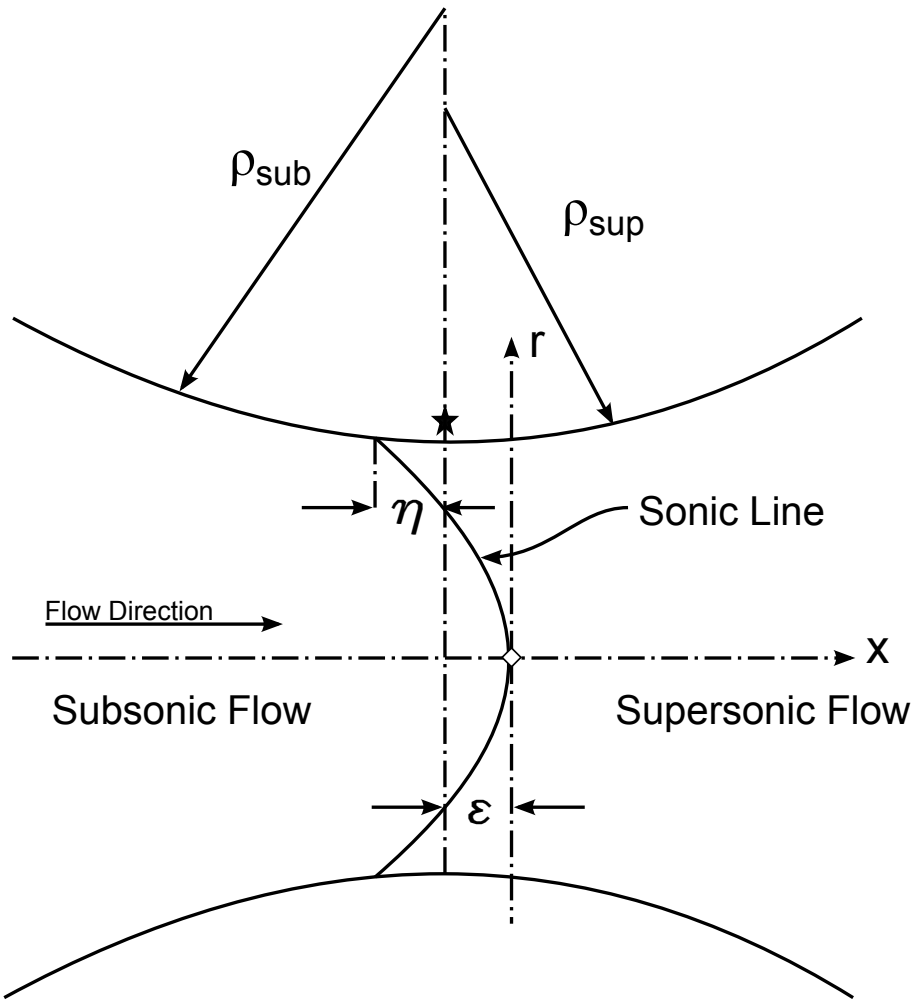

Figure 2.6: Flow in the throat region of the nozzle with Sauer's solution to the sonic line.

2.3 Method of Characteristics

The method of characteristics is a technique for solving partial differential equations based on absolute differential calculus. The method is a numerical approach, but the nature of the approach differs from finite differencing schemes in that the solution provides the information necessary for the location of a physical boundary in which produces shock free flow within the nozzle. The method was developed by the mathematicians Jaques Saloman Hadamard in 1903 and by Tullio Levi-Civita in 1932[21]. The method of characteristics uses a technique of following propagation paths in order to find a solution to partial differential equations. This is done through the reduction of the partial differential equation to ordinary

differential equations or algebraic expressions if appropriately restricted. These propagation paths are called the characteristics. These characteristics can represent such things as geometrical form, discontinuities, or physical disturbances[20]. For the case of irrotational supersonic flow the characteristics follow the propagation of Mach waves. Because the flow is supersonic and these Mach waves have no influence of the flow upstream of themselves and the method of characteristics may be used.

In 1949, it was proposed that an analytical solution to an all axial supersonic stream could be developed using the axis-symmetric method of characteristics[21]. Working at NASA Lewis, Guentert and Neumann implemented the analytical approach for designing axis-symmetric supersonic windtunnels[3]. The approached used may be extended to form the contour of a propulsive nozzle as well.

The applications of the method of characteristics for nozzle flows are not limited to the design of contours. The method may also be used to analyze the flow field inside a known contour as well[4]. The method is also not limited to the flow within the nozzle. The approach can be extended to analyze the exhaust plume for both underexpanded and overexpanded nozzle flow using the free pressure boundary of the exhaust plume.

2.3.1 Axis-symmetric Method of Characteristics

Assuming that the flow through the nozzle is comprised of an ideal gas that is both steady and maintains constant total enthalpy, the second law of thermodynamics, the continuity equation and the momentum equation can be used to model the flow. With the assumption that there are no shocks or viscous effects present in the flow the second law of thermodynamics can be reduced to the condition for irrotationality. Thus the governing equations are given as[21]:

$$\vec{\nabla} \times \vec{V} = 0 \tag{2.6}$$

$$\vec{\nabla} \cdot (\rho \vec{V}) = 0 \tag{2.7}$$

$$\rho \frac{D\vec{V}}{Dt} - \vec{\nabla} = 0 \tag{2.8}$$

It can be shown that combining these equations and solving using Cramer's rule for the indeterminate case yields the characteristic equations[21]. They can also be found using a linear algebra approach as shown by Ferri[22]. These equations are devided into two families, one that follows the left running characteristics and one that follows the right running characteristics. The characteristic equations are[3]:

$$\frac{dy}{dx} = \tan(\theta \mp \mu) \tag{2.9}$$

From the governing equations the compatability equations are also derived. These two equations are grouped into the two families. The compatability equations are:

$$\frac{dV}{V} \mp \tan\mu d\theta - \frac{\tan\mu \ \sin\mu \ \sin\theta}{\cos(\theta \pm \mu)} \frac{dx}{y} = 0 \tag{2.10}$$

A complete derivation of the characteristic and compatibility equations can be found in Ferri[22] and Zucrow[27, 4]. Both present a similar approach to the derivation.

The angle μ is the Mach angle. Because μ is dependent on the specific heat ratio, γ and Mach number, M, it is a variable at every point in the flow field. The characteristic points will be described by the Mach angle, the flow angle, and the velocity at each point in the characteristics web. Although the characteristics are actually curves, they can be represented as a line segment between characteristic points when distance between characteristic points is kept small[3]. Figure (2.7) shows how each characteristic point is described.

Practical implementation of the above equations requires that they be discretized. The differential equations are discretized by rewriting them into a finite-difference solution. This allows for point to point calculation of the flow properties throughout the given flow field. Figure (2.8), shows a typical characteristic mesh. In order to form the solution information must be known at points A and B in order for the information at point C to be found[3].

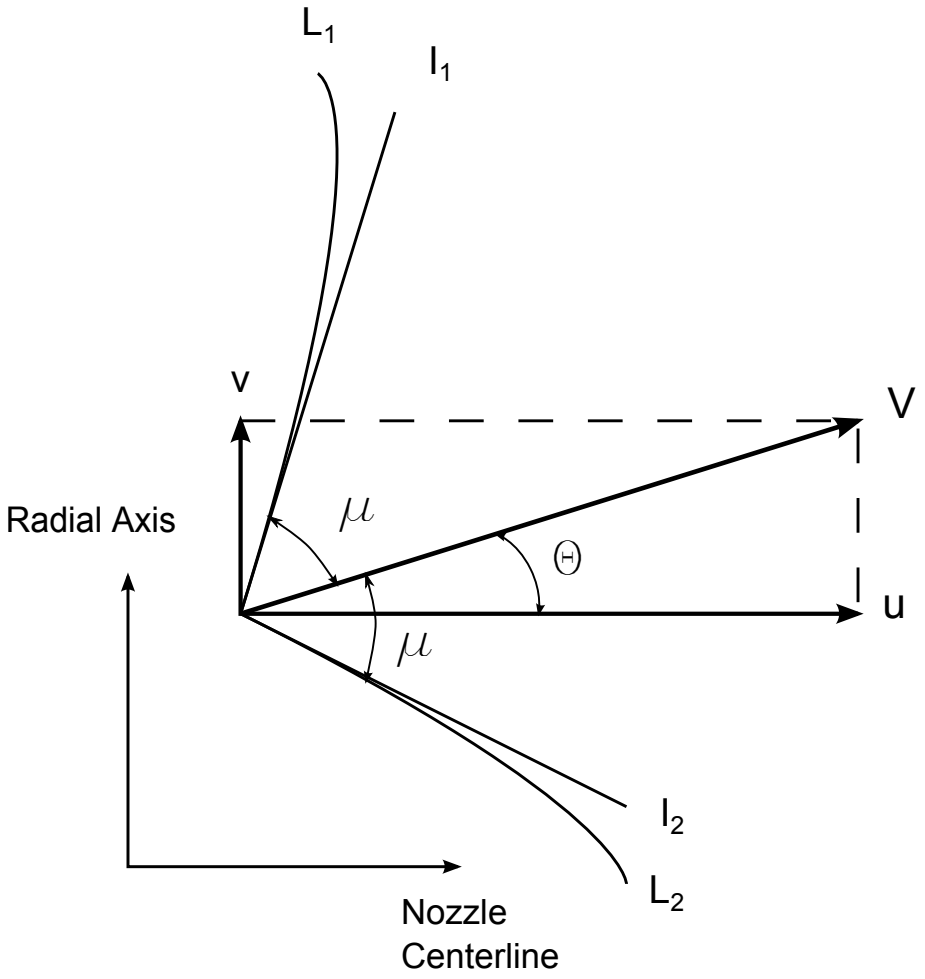

Figure 2.7: Characteristic Point and its Associated Angles[3]

For a first approximation it is common to treat the location of the characteristics as the characteristics themselves. That is the location of C may be calculated using the first order finite-difference form of the characteristic equations if the location of points A and B are known[3].

$$\frac{y_C - y_A}{x_C - x_A} = \tan(\theta_A + \mu_A) \tag{2.11}$$

$$\frac{y_C - y_B}{x_C - x_B} = \tan(\theta_B - \mu_B) \tag{2.12}$$

Solving these equations simultaneously results in the location of C. This essentially is using the slope of the left running characteristic from A and the slope of the right running

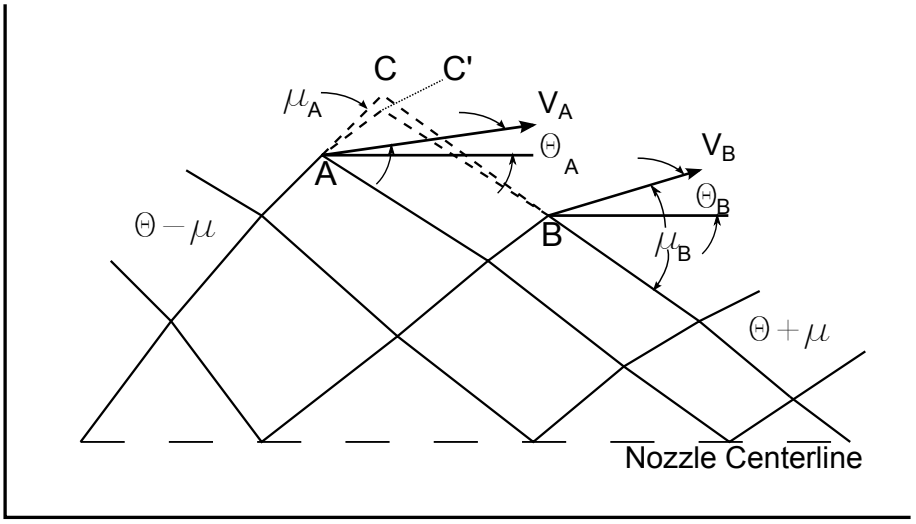

Figure 2.8: Characteristic Mesh

characteristic from B and their associated angles to find the intersection of the characteristics. It is most practical to solve for the x location of C and then the y location. This is simple algebra and results in the following[3]

$$x_C = \frac{y_A - y_B + x_B \tan(\theta_B - \mu_B) - x_A \tan(\theta_A + \mu_A)}{\tan(\theta_B - \mu_B) - \tan(\theta_A + \mu_A)} \tag{2.13}$$

$$y_C = y_A + (x_C - x_A) tan(\theta_A + \mu_A) \tag{2.14}$$

The compatibility equations may be discretized and combined to form a finite difference form of the differential equations. The result of the discretization is then solved for the velocity of the point C. Because the velocity at the point C is dependent on the flow angle at the point, velocity is determined through elimination of θ_c resulting in the following equations[3].

$$V_C = \frac{1}{\frac{\cot \mu_A}{V_A} + \frac{\cot \mu_B}{V_B}} \{\cot \mu_A (1 + \pounds (x_C - x_A)) + \cot \mu_B (1 + \mathfrak{M}(x_C - x_B)) + \theta_B - \theta_A\} \tag{2.15}$$

where

$$\pounds = \frac{\tan\mu_A \ \sin\mu_A \ \sin\theta_A}{y_A \cos(\theta_A + \mu_A)} \tag{2.16}$$

and

$$\mathfrak{M} = \frac{\tan\mu_B \ \sin\mu_B \ \sin\theta_B}{y_B \cos(\theta_B - \mu_B)} \tag{2.17}$$

In turn the flow angle of the characteristic may be obtained by solving the compatibility equations for θ_c yeilding:

$$\theta_C = \theta_A + \cot\mu_A \left(\frac{V_C - V_A}{V_A}\right) - \pounds(x_C - x_A)) \tag{2.18}$$

The solution at point C with the equations in presented thus far yields a first order solution. However, it may be necessary to use a second order approach to form a valid solution. The second order solution can be developed by solving Eqs 4.50, 4.53 for velocity and flow angle and then performing a second iteration upon the point C producing point C'.

In turn the flow velocity of the characteristic may be obtained by solving the compatibility equations for θ_c yeilding[3, 22]:

$$x_c' = \frac{y_A - y_B + \frac{1}{2}(\tan(\theta_B - \mu_B) + \tan(\theta_C - \mu_C))x_b - \frac{1}{2}(\tan(\theta_A + \mu_A) + \tan(\theta_C + \mu_C)x_A}{\frac{1}{2}(\tan(\theta_B - \mu_B) - tan(\theta_A + \mu_A) + tan(\theta_C - \mu_C) - tan(\theta_C + \mu_C)} \tag{2.19}$$

$$y_C' = y_A + (x_C - x_A)\frac{1}{2}(\tan(\theta_A + \mu_A) + \tan(\theta_C + \mu_C)) \tag{2.20}$$

$$V_C' = \frac{\mathfrak{F} + \mathfrak{G} + \theta_B - \theta_A}{4((V_A + V_C)^{-}1(tan\mu_A + \tan\mu_C)^{-}1 + (V_B + V_C)^{-}1(\tan\mu_B + \tan\mu_C)^{-}1)} \tag{2.21}$$

where

$$\mathfrak{F} = \frac{2}{\tan\mu_A + tan\mu_C}\left(\frac{2V_A}{V_A + V_C} + \frac{\pounds_A + \pounds_C}{2}(x_C - x_A)\right) \tag{2.22}$$

$$\mathfrak{G} = \frac{2}{\tan\mu_B + \tan\mu_c}\left(\frac{2V_B}{V_B + V_C} + \frac{\mathfrak{M}_B + \mathfrak{M}_C}{2}(x_C - x_B)\right) \tag{2.23}$$

and

$$\theta'_C = \theta_A + \frac{2}{\tan\mu_A + \tan\mu_C}\left(\frac{2(V'_C - V_A)}{V_C + V_A} - \frac{\pounds_A + \pounds_C}{2}(x_C - x_A)\right) \tag{2.24}$$

Using these equations the flow properties are determined at C', which becomes the location of the characteristic and the starting point for future calculations. Because the characteristic points are described by velocity and Mach angle the Mach angle and thermodynamic conditions are determined through the Mach number at this point. This can easily be calculated by using the definition of enthalpy

$$T_o = T + \frac{V^2}{2cp} \tag{2.25}$$

From Eq. (2.25) here the Mach number, pressure, and density of the flow may be found through the isentropic process and definition of Mach number.

2.3.2 Valid Pressure Distribution Selection

In order to produce a pressure distribution that allows for valid solutions throughout a wide range of expansion ratios a direct approach must be used to specify the centerline pressure distribution. The functions presented in section 2.1 are difficult to implement while obtaining solutions without crossing characteristics, and have the potential to produce non-physical pressure distribution. A direct selection method together with a simple particle swarm/pattern search optimizer[28] can produce valid pressure distributions for a much larger range of expansion ratios than with the three provided in section 2.1. Two direct methods are presented here.

Lagrange Polynomial Pressure Distribution

A method for developing pressure distributions is to form the pressure distribution with a Lagrange polynomial, through the direct selection of pressure points. The associated method for developing the pressure distribution is similar to that of polynomial interpolation. With

this method it is essential to use an optimization process so that the polynomial is generated to the case and known to be valid.

Much like polynomial interpolation, the process in developing a pressure distribution using Lagrange polynomials use points spread across an interval that describes the function fitting a curve that passes through each point[29]. Although the exact pressure distribution is not known, points along the interval are given a value that is assumed to be the known pressure at that point and the distribution is determined by the curve that best fits these points. The location of the points along the interval is held constant yet the amplitude of the points is allowed to change. Small changes are made until the pressure distribution allows for a viable solution.

To select a pressure distribution using a lagrange polynomial a design interval $[0, l]$ is used. Along this interval there are set $n + 1$ distinct nodes $x_0, ..., x_n$ and the corresponding values $y_0, ..., y_n$. It can be shown that with these distinct nodes and their corresponding values a unique polynomial exists which exactly intersects each node at its corresponding value[29]. This polynomial is expressed in the form

$$L(x) = \sum_{i=0}^{n} y_i l_i(x) \tag{2.26}$$

where

$$l_i(x) = \prod_{\substack{0 \le j \le k \\ j \ne i}}^{n} \frac{x - x_j}{x_i - x_j} \tag{2.27}$$

If the distinct nodes $x_0, ..., x_n$ are distributed uniformly across $[0, l]$ then for functions of the type needed to model a viable pressure distribution

$$\lim_{n \to \infty} |f(x) - Lf(x)| \neq 0 \tag{2.28}$$

This is the phenomenon that occurs in Runge's counterexample[29]. This phenomenon occurs due to the equally spaced nodes. In order for the interpolating polynomial to have uniform convergence an appropriate choice of the distribution of the nodes must be made.

Use of Gaussian quadratures considered with respect to the Chebyshev weight can produce a distribution of the nodes that will allow for uniform convergence. With this consideration the nodes on the interval $[-1, 1]$ are distributed by[29]

$$x_i = \cos \frac{(2i-1)\,\pi}{2 * n} \tag{2.29}$$

This distribution is not defined on the appropriate interval. The distribution of the nodes over the desired interval, $[0, l]$, can be found by an affine transformation. The result of the transformation gives for an arbitrary interval $[a, b]$

$$x_i = \frac{1}{2}\,(a+b) + \frac{1}{2}\,(b-a) \cos\left(\frac{(2i-1)\,\pi}{2n}\right) \tag{2.30}$$

With the distribution of the nodes selected. The corresponding values of the nodes are arbitrarily selected while following the scheme

$$y_0 > y_1 > y_2 > ... > y_n \tag{2.31}$$

while

$$y_0 = 1\, and\, y_n = 0 \tag{2.32}$$

Once a set of values is selected the corresponding pressures are set when both the exit pressure and the initial method of characteristics pressure is known. Piecewise multiplication and scaling as follows will provide the correct pressure values for the polynomial produced above

$$p = (p_t - p_e)\,[y] + pe \tag{2.33}$$

Direct Selection Method

A very simple approach that can easily be implemented for solutions using a moderate number of characteristics is direct selection of the pressures at each point. In order to produce a valid pressure distribution a optimizer should be used.

Choosing the expansion length and the number of characteristics, the center line points are distributed evenly across the expansion length. For each of these points a unique pressure distribution is chosen, and the method of characteristics mesh can be generated and checked for viability

This is a simple brute force approach that can be implemented quite successfully for moderate numbers of characteristics using an optimizer.

2.4 Chemical Kinetics with Finite Reaction Rates

When considering a chemically reacting gas mixture with finite reaction rates, a system of reactions that model the mixture must be developed. This system of elementary reactions is referred to as the reaction mechanism[4]. The reaction mechanism can be written as a system of arbitrary chemical reactions with Eq. (2.34), where ν and ν' are the stoichiometric coefficients, A is the molecular formula, i is the ith species of the mechanism and j is the jth reaction.

$$\sum_{i=1}^{N} \nu_{ij} A_i \Leftrightarrow \sum_{i=1}^{N} \nu_{ij}^{'} A_i \tag{2.34}$$

(note: ν and ν' are the stoichiometric coefficients of the reactants and products respectively)

For example a LOX Hydrogen system the reaction mechanism is described by the following reactions, where M denotes a third body [30]:

$$2H + M \rightleftharpoons H_2 + M \tag{2.35}$$

$$H + OH + M \rightleftharpoons H_2O + M \tag{2.36}$$

$$O + H + M \rightleftharpoons OH + M \tag{2.37}$$

$$2O + M \rightleftharpoons O_2 + M \tag{2.38}$$

$$O_2 + H \rightleftharpoons O + OH \tag{2.39}$$

$$H_2 + O \rightleftharpoons H + OH \tag{2.40}$$

$$H_2 + OH \rightleftharpoons H_2O + H \tag{2.41}$$

$$OH + OH \rightleftharpoons H_2O + O \tag{2.42}$$

It is clear that this reaction mechanism has a total of eight reactions and the total number of species for the mechanism is six. For a given reaction mechanism the production rate σ can be calculated for each species of the mechanism. The production rate of the species of a reaction rate is called the species source function and is a function of local thermodynamic properties as well as properties that are unique to the individual reaction, the equilibrium constant, and the reaction rate. From the Law of Mass Action it can be shown that the reaction rate is proportional to the collision rate between appropriate molecules and the collision rate is proportional to the product of concentrations, thus the source function is also proportional to product of concentrations of the species in the gas mixture[15].

$$\sigma_i = MW_i \sum_{j=1}^{k} \left(\nu'_{ij} - \nu_{ij}\right) \left[K_{fj} \prod_{i=1}^{N} \left(\frac{\rho c_i}{MW}\right)^{\nu_{ij}} - K_{bj} \prod_{i=1}^{N} \left(\frac{\rho c_i}{MW}\right)^{\nu'_{ij}} \right] M_j \tag{2.43}$$

Where K_f and K_b are the forward and reverse reactions rates respectively and M_j is the third body influence of the reaction. The rate constants are equated by the equilibrium constant which is the ratio of reverse to forward reaction rates

$$K_c = \frac{K_f}{K_b} \tag{2.44}$$

Typically either the forward or the backward rate for a given reaction is known, or available. From the relation above the unknown rate can be calculated once the equilibrium constant is calculated. There are many forms of the equilibrium constant and selection of the correct definition is essential to a correct solution. The form to be used to find the species production rate must be expressed in terms of concentration. Data available for reaction rates typically results in corresponding units of cm, mol, K, s for units. Thus the equilibrium constant must be found in the form

$$K_c = \frac{101.325}{R_u T}^{\Delta\nu} e^{\frac{\Delta S^\circ}{R_u}} e^{\frac{-\Delta H^\circ}{R_u T}} \tag{2.45}$$

where the universal gas constant $R_u = 8.31447 Jmol^-1K^-1$ the exponent $\Delta\nu$ is the change in total moles of the reaction[31]. For reaction in Eq.2.42 this value would be -1. The value 101.325 comes from the value of 1 standard atmosphere in units of N/cm^2 or kPa. The enthalpy and entropy exponentials are equivalent to

$$\Delta G_f^\circ = \sum_{i=1}^{NS} (\nu_i' - \nu_i) g_f^\circ \tag{2.46}$$

where ΔG_f° is the standard state change in Gibbs free energy for the reaction at temperature[32]. The gibbs free energy of formation for a individual species g_f° can be found simply through the enthalpy and entropy for the species at the specified temperature through

$$g_f^\circ = \Delta h_{f,298}^\circ + h_T - h_{298} - T s_T \tag{2.47}$$

The values above can be found in the JANAF database or through the CAP program[33]. See Appendix C.

The reaction rate can be expressed as a function of temperature, fit to the reaction data found through experiments. Data is usually provided as forward rates taking the same form as the equilibrium constant equation above. The rate equation is

$$K_j = a_j T^{-n_j} e^{(-b_j/R_u T)} \tag{2.48}$$

where a_j is the pre-exponential coefficient, n_j is the temperature dependence of the pre-exponential factor, and b_j is the activation energy, these coefficients are tabulated for each elementary reaction for many reaction mechanisms. They can readily be found in Kushida[30] and Nickerson[7] for many oxidizer/propellant combinations.

The third body influence of a reaction determines how the rates are changed with the interaction of a third body to the reaction. Nominally if a M is introduced in the reaction all other bodies besides the species of the reaction itself act as third bodies. However, some species have more of an effect on the reaction rates than others. The ratio that expresses this influence is given for each reaction that is influenced by a third body and the the influence is calculated through

$$M_j = \sum_{i=1}^{NS} m_{thr} \frac{\rho c_i}{MW_i} \tag{2.49}$$

2.4.1 One Dimensional Chemical Kinetics

The development of the one-dimensional governing equations for non-equilibrium chemically reacting gas is presented. Considering steady flow that progresses in only a single positively increasing direction the following equations are obtained.
Momentum:

$$\rho V \frac{dV}{dx} + \frac{dp}{dx} = 0 \tag{2.50}$$

Energy:

$$h + \frac{V^2}{2} = constant \tag{2.51}$$

In the above equation h is the total enthalpy which comprises of the sum of the sensible enthalpy plus the energy of formation. Eq (2.51) can be rewritten on a mass basis with the following equation.

$$h = \sum_{i=1}^{N} c_i h_i = \sum_{i=1}^{N} c_i \left[\int_{T_o}^{T} c_{pi} dT + h_i^o \right] \tag{2.52}$$

Continuity Equation:

Because of the chemical reactions the composition of the gas varies along the flow path. Thus conservation of mass must be applied to individual chemical species in the gas. Assuming no mass diffusion or thermal non-equilibrium occur the continuity equation becomes

$$d\dot{m} = d(\rho_i A V) = \sigma_i (A dx) \tag{2.53}$$

Where σ is the source function as shown in Eq (2.43).

Substituting $\rho_i = c_i \rho$ into Eq (2.53) yields

$$d(c_i \rho A V) = (\rho A V) dc_i + c_i d(\rho A V) = \sigma_i (A dx) \tag{2.54}$$

Combining Eq (2.54) with the global continuity equation $\dot{m} = \rho A V$ yeilds the differential equation

$$\frac{dc_i}{dx} = \frac{\sigma_i}{\rho A} \tag{2.55}$$

Equation of State:

The equation of state for a gaseous mixture is written as the sum of the product of the species massfraction and the species spific gas constant yeilding the equation:

$$p = \rho T \sum_{i=1}^{N} c_i R_i = \rho R T \tag{2.56}$$

The equations may be solved numerically for a non-equilibrium chemically reacting gas mixture. In order to avoid singularities near the sonic point it is recommended to use a specified pressure method to solve the system of equation simultaneously. This results in the following equations and requires a known pressure distribution to solve the system[4]

$$\frac{dV}{dx} = \frac{-1}{\rho V}\frac{dp}{dx} \tag{2.57}$$

$$\frac{d\rho}{dx} = \left[\frac{1}{\gamma p}\frac{dp}{dx} - \bar{A}\right]\rho \tag{2.58}$$

$$\frac{dT}{dx} = \left[\frac{\gamma - 1}{\gamma}\frac{1}{p}\frac{dp}{dx} - \bar{B}\right]T \tag{2.59}$$

$$\frac{dc_i}{dx} = \frac{\sigma_i}{\rho V} \tag{2.60}$$

$$Area = \frac{\dot{m}}{\rho V} \tag{2.61}$$

Where

$$\bar{A} = \frac{1}{PV}\left[\sum_{i=1}^{N} \sigma_i R_i T - \frac{\gamma - 1}{\gamma}\sum_{i=1}^{N} \sigma_i h_i\right] \tag{2.62}$$

and

$$\bar{B} = \frac{\gamma - 1}{\gamma}\frac{1}{pV}\sum_{i=1}^{N} \sigma_i h_i \tag{2.63}$$

It is worth noting that for non-equilibrium chemically reacting gases the constant pressure specific heat and hence the specific heat ratio of the gaseous mixture cannot be assumed constant[34]. To calculate the constant pressure specific heat the CAP program developed by Zehe, Gordon, and McBride[33] was found to be useful. This program allows for the calculation not only of constant pressure specific heat of numerous constituents but many other thermodynamic properties as well.

Chapter 3

Axis-Symmetric Method of Characteristics Nozzle Design

The general approach in the design of an axis-symmetric nozzle based on a prescribed centerline pressure distribution uses a three zone method of characteristics solution. This approach produces a "smooth throat" design, where the entire expansion contour is determined through the method of characteristics. This differs from Rao's approach and the approaches outlined by Zucrow, in that the initial expansion section of the nozzle was prescribed for these approaches. If this initial expansion section is not prescribed correctly, crossing of like characteristics, will occur. To avoid crossing characteristics with a prescribed initial turn, small radius turns near the throat are required. The coalescence of like characteristics represents the formation of an oblique shock wave. If the oblique shock waves are relatively weak they can be ignored without serious error in the solution[4]. However by using the method of characteristics solution that contains no crossing of like characteristics a shock free nozzle contour can be formed.

3.1 Nozzle Contour Design Process

The following describes the process for axis-symmetric method of characteristics nozzle design, assuming isentropic flow. Providing the chamber conditions and propellant properties, a contour will be formed to produce a nozzle of specified exit Mach number, with uniform axial exit flow.

1. Select Converging Section Geometry
2. Analysis of Transonic Region
3. Select Pressure Distribution

4. Select Number of Characteristic Points
5. Select Expansion Length
6. Determine Centerline Distribution
7. Perform Method of Characteristics
8. Check Solution for Viability
9. Perform Method of Characteristics Near the Throat
10. Form Nozzle Boundary

In order to design the smooth throat nozzle using the method of characteristics transonic flow at the throat must be analyzed. The smooth throat design takes inconsideration the geometry in the throat region bring importance into how the geometry effects the flow both in the subsonic region and the supersonic region of the nozzle. The sonic line cannot be assumed to be a vertical line spanning the throat. The geometry of the throat will be curved both in the subsonic and supersonic regions of the nozzle, thus the geometry effect on the transition from subsonic to supersonic flow must be considered.

This entails a three fold analysis of the method of characteristics. The first being the method of characteristics performed along the prescribed pressure distribution, called the "Kernel". The second method of characteristics analysis is performed between the line of substantial supersonic flow from the transonic solution and the first left running characteristic from the first analysis, this in the "Non-simple region". The third is the extension of the characteristic mesh in the rest of the flow field, called the "Boundary Region". These zones are depicted in Fig 3.1.

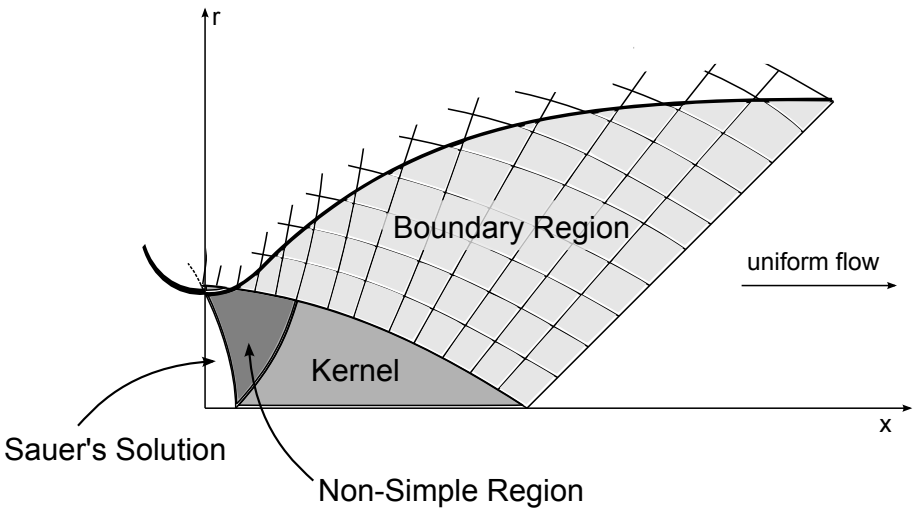

Figure 3.1: Method of characteristics solution zones

3.1.1 Comparison of Processes

The process described in Sec. 3.1 is not fundamentally different than the process used by Rao, Zucrow, and others [19][4][12][1]. However the approach to the solution has some key differences. A comparison to the method at hand and the method used by Rao to design nozzle contours shows the key differences between the two approaches.

Both approaches begin with the selection of the converging section geometry. With the geometry known, an analysis of the transonic region is performed to produce a set of initial conditions for the solution. Figure 3.2

The next step in the process is to set the initial conditions. In an approach such as Roa's approach, the geometry of the initial expansion region downstream of the throat is

(a) Rao Method (b) Proposed Method

Figure 3.2: Initial step for both nozzle design approaches

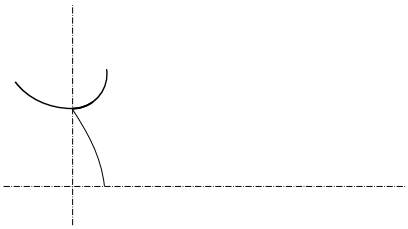

(a) Rao Method

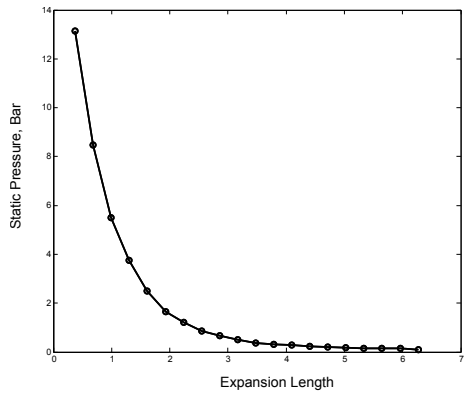

(b) Proposed Method

Figure 3.3: Establishing the boundary conditions for both approaches

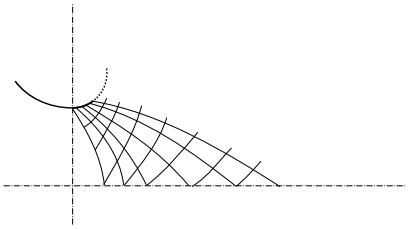

(a) Rao Method

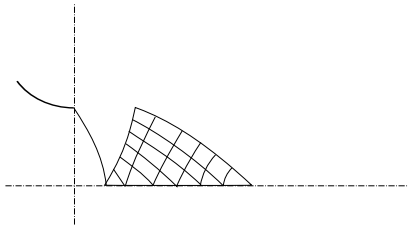

(b) Proposed Method

Figure 3.4: Kernel solution developed for both design approaches

prescribed. In the proposed method, the pressure distribution along the centerline of the nozzle is prescribed, as can be seen in Fig. 3.3

With the initial conditions and the boundary conditions for both approaches determined, the next step is to form and analyze the "kernel" solution through the method of characteristics. As shown in Fig. 3.4, an approach such as Rao's, the "kernel" will contain the solution from the transonic solution through the expansion length. For the proposed approach the "kernel" solution will contain only the solution produced along the expansion length.

For the proposed approach the method of characteristics is then used to form a solution to the non-simple region, as depicted in Fig. 3.5. The solution is allowed to extend beyond where the physical boundary will be, allowing for the physical geometry near the throat to be determined. This is a main difference in the result between the two approaches at hand.

(a) Rao Method (b) Proposed Method

Figure 3.5: Form method of characteristic solution to fill the non-simple region

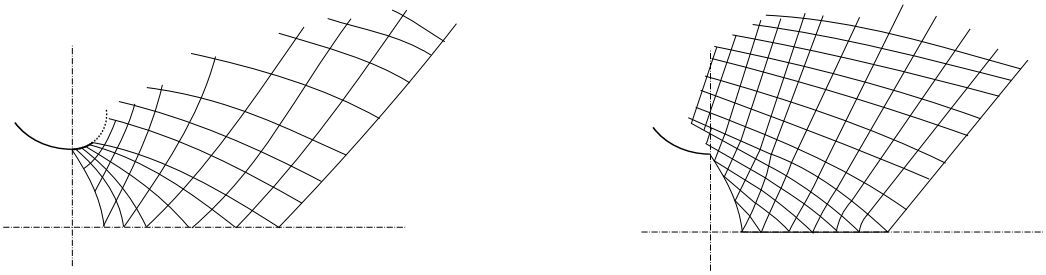

(a) Rao Method (b) Proposed Method

Figure 3.6: Form boundary region solution with the method of characteristics

An approach like Rao's, the geometry just down stream of the throat was prescribed. With the proposed approach and the extension of a method of characteristics solution near the geometric throat, the geometry near the throat can be found.

From here, the solutions to each approach are carried on in the same manor. The boundary region solution is formed using the method of characteristics, as shown in Fig. 3.6. This provides for a solution space that allows for the boundary to be located.

With the boundary region solution formed, the location of the physical boundary can be found, as depicted in Fig. 3.7. The location of the boundary allows for the contour of the nozzle to be described. Either flow tangency or characteristic continuity can be used to obtain the location of the boundary along the characteristic lines. The location of the physical boundary completes the solution to the nozzle design.

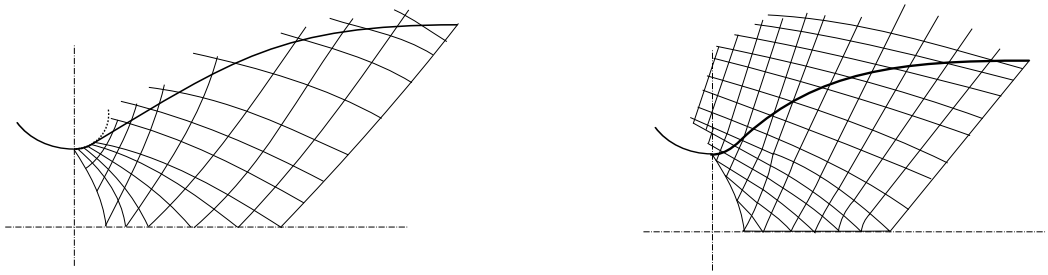

(a) Rao Method

(b) Proposed Method

Figure 3.7: Formation of nozzle contour for both approaches

3.1.2 Converging Section Geometry

In order to design the smooth throat nozzle using the method of characteristics the geometry throughout the throat region is considered. The subsonic geometry has a large role in the transonic region of the nozzle and must be selected so that the location of where the flow becomes substantially supersonic, where the flow downstream has does not affect the current position in the flow. If the flow is not substantially supersonic the method of characteristics solution can not produce a viable solution. A rule of thumb for the converging geometry that allows for substantially supersonic flow near the throat is a radius of curvature that is $2.0r_t$. This geometry allows for Sauer's solution to hold, and is very similar to that of the RL-10. This is not necessarily the optimal geometry for the subsonic region but clearly suits its purpose of generating substantially supersonic flow near the throat.

3.1.3 Analysis of Transonic Region

An analysis of the transonic region must be completed to provide a boundary condition that is is substantially supersonic near the throat and to provide an axial location to start the method of characteristics. For the transonic region analysis will be performed by using the technique presented by Sauer[5]. The assumption of the sonic line being a vertical line spanning the minimum area point is no longer considered. The sonic line will be a curve that starts at some point upstream of the throat, crosses through the minimum area point,

and lies up-stream of the throat at the centerline of the nozzle.

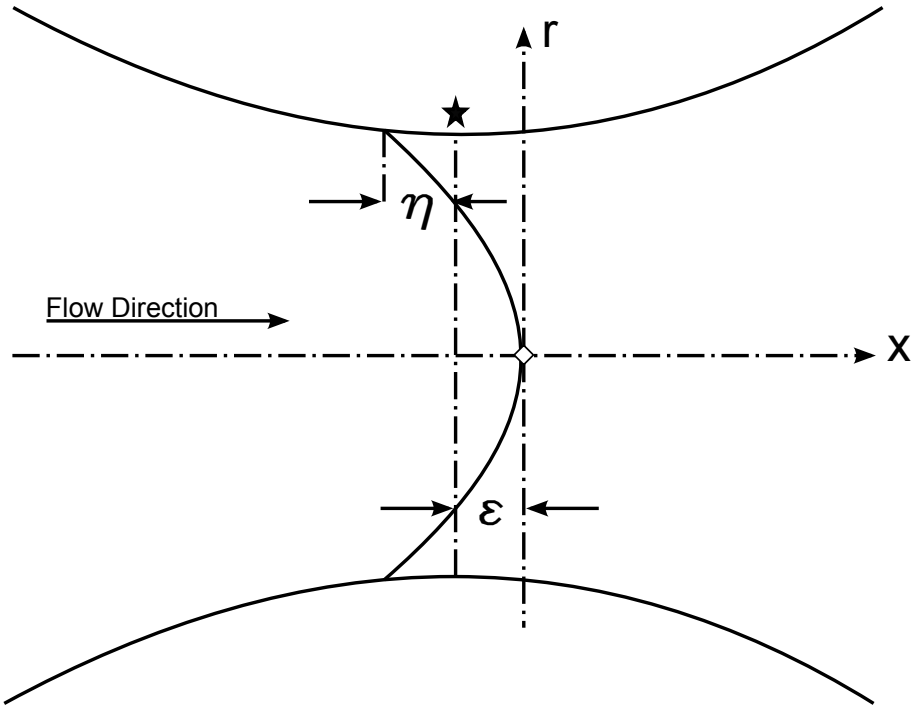

Figure 3.8: Transonic Region of Nozzle

Given a subsonic radius of curvature, the shape of the sonic line can be found. With this information The Mach number at the boundary of the throat will be calculated and determined if substantially supersonic. If so, the constant Mach number line will be developed and followed to the centerline. This will be the initial point for the method of characteristics solution as well as the starting point of the pressure distribution. Note that the coordinate system for Sauer's solution has an origin located where the sonic line intersects the nozzles axis of symmetry[5].

From Sauer[5] the following equations are needed

$$\eta = \frac{r^*}{8}\sqrt{\frac{2(\gamma+1)r^*}{\rho_{sub}}} \tag{3.1}$$

Equation [3.1] is the axial displacement from the throat in which the sonic line intersects the nozzle wall. For an axis-symmetric nozzle this distance is equal to that of the displacement of the sonic line upstream of the throat. Resulting in

$$\eta = \epsilon \tag{3.2}$$

The location of the throat is

$$x^* = -\eta = -\epsilon \tag{3.3}$$

The Mach number in the transonic region is then calculated by finding transonic components

$$u = \alpha x^* + \frac{\gamma + 1}{4}\alpha^2 r^{*2} \tag{3.4}$$

$$v = \frac{\gamma + 1}{2}\alpha^2 x^* r^* + \alpha^3 r^{*3}\frac{(\gamma + 1)^2}{16} \tag{3.5}$$

where

$$\alpha = \sqrt{\frac{2}{(\gamma + 1)\rho_{sub} r^*}} \tag{3.6}$$

The Mach number can now be found from

$$M = \sqrt{(1 + u)^2 + v^2} \tag{3.7}$$

Using the above equations the position where the same Mach number, as found above, is located on axis of symmetry can be found. Recall that the coordinate system for the transonic analysis is based off of the location that the sonic line crosses the axis of symmetry. Thus η must be added to the supersonic location found, representing this point in throat fixed coordinates.

Solving the above equations for the sonic condition yields the sonic line which can be projected as

$$x_K = -\frac{\gamma+1}{4}\alpha r_k^2 \tag{3.8}$$

At every point along this line the Mach number is unity. The solution method of characteristic solution cannot begin where the sonic line intersects the centerline at this point. The flow along this line is at Mach 1 which causes singularities in the Prandtl Myer Expansion equation as well as with the slope of the characteristic because the flow angle along the centerline is $\theta = 0$. When the solution is initiated at a point where the flow is substantially supersonic the right running characteristic quickly intersects the sonic line. Because the method of characteristics is only valid for supersonic flow, the solution does not encompass the entire supersonic portion of nozzle[3]. This zone has been referred to in literature as the undefined region or the non-simple region of the flow, as illustrated in Fig. 3.9.

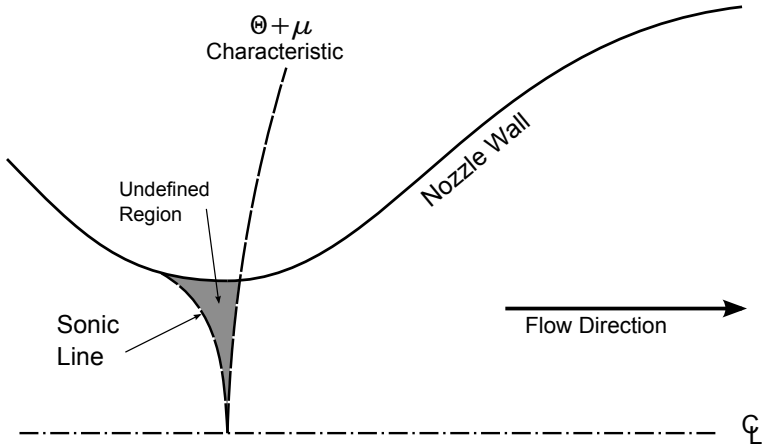

Figure 3.9: Undefined Region[3]

To determine the location of the substantially supersonic point on the centerline the Mach number is determined at the boundary of the geometric throat by Sauer's solution. The geometric throat lying upstream of the sonic line will have a flow that is substantially supersonic. Using Sauer's solution a line of constant Mach number eminating from the physical minimum area point along the wall. can be found and its intersection with the

centerline provides the location and Mach number of the initial centerline characteristic point.

3.1.4 Select Number of Charcteristic Points

The number of characteristic points is chosen arbitrarily. The use of a small number of allows for greater spacing in the characteristic mesh allowing for greater accumulation of error. However, when a large number of characteristics is used the computational time increases. When developing a method of characteristics code, the use of small numbers of characteristics can be helpful for debugging purposes but will not result in highly accurate solutions.

3.1.5 Select Pressure Distribution And Expansion Length

Through the isentropic process the pressure at the initial characteristic point can be found. The location of the initial point will be the location that the constant Mach number line emanated from Sauer's solution. Starting the pressure distribution at this known location avoids the singularities. The even distribution of expansion points can be

$$dx = \frac{l}{n_c} \tag{3.9}$$

Where n_c is the number of characteristics used in the solution and l is the expansion length.

The expansion length l is the distance along the centerline that it takes for the flow to expand from the Mach number of the initial expansion point to the desired exit Mach number along the centerline of the nozzle. It is important to understand that the expansion length is not the length of the physical nozzle. This is because the flow will expand to the desired Mach number at the centerline upstream of where it becomes fully expanded at the boundary. Thus, the most downstream point in the initial characteristic mesh is located at $l + 2\eta$ along the centerline and the pressure distribution chosen describes the

change of pressure between the constant Mach line and this point. At first this length can arbitrarily be selected, but for for a given exit condition, pressure distribution and number of characteristics there exists a unique expansion length that provides the correct expansion through the nozzle, while minimizing the nozzle length. This can be found using an iterative technique or an optimization process.

With the pressures selected by the chosen pressure distribution for each characteristic point along the centerline the problem has been initialized for the the method of characteristics

3.1.6 Perform Method of Characteristics

Following the scheme presented above the method of characteristics solution along the centerline can be determined. This first method of characteristics solution will be referred to as the "kernel".

3.1.7 Check Solution for Viability

The viability of the first method of characteristics solution is checked before additional analysis is to be performed. Checking kernel for viability allows for the solution to be discarded before trying to perform the second method of characteristics solution. Validity of the solution as a whole is only possible if both solutions are viable. When the solution is found to be nonviable the pressure distribution prescribed for the analysis is incorrect.

The contour being designed is to be a nozzle contour that produces shock free flow. Due to this goal a viable solution can only occur if none of the like characteristics intersect. The viability of the solution can be performed easily. The characteristic lines between the points of the characteristic mesh are treated as line segments. By calculating the location where corresponding lines with equivalent slopes intersects, it can be determined if the two characteristic segments cross. The segments cross if the location of the intersection is between the points in question.

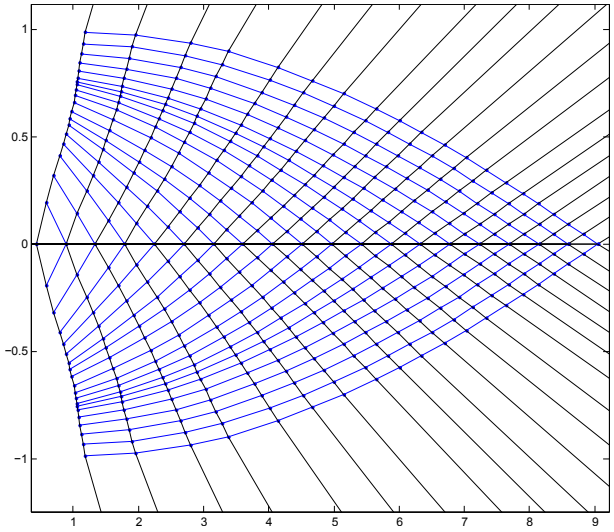

Figure 3.10: Viable Kernel solution, MOC mesh contains no crossing characteristics

As the solution unfolds, the characteristics may not initially cross but the grid points are aligned to result appropriate spacing of characteristic lines, resulting in coalescence. The result shown in Fig. 3.11 shows a MOC mesh with crossing characteristics. This mesh was created using the same pressure distribution as that in Fig. 3.10, but with a different exit Mach numbers.

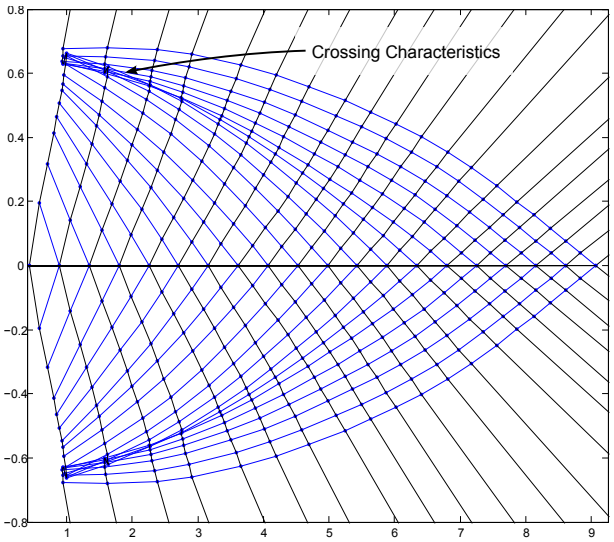

Figure 3.11: Non-viable method of characteristics solution, crossing like characteristics in MOC mesh

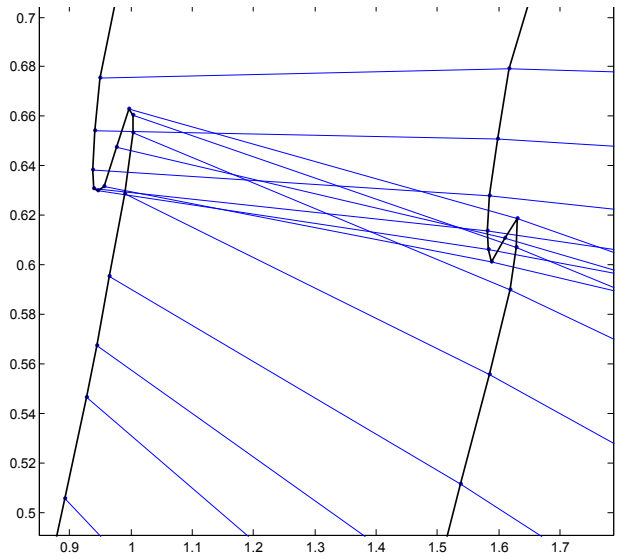

Figure 3.12: Close inspection of a non-viable method of characteristics solution, crossing like characteristics in MOC mesh

It is important to note that the viability of the entire solution is not solely dependent on the kernel The prescribed pressure distribution may produce a initial analysis that allows for none of the characteristics to coalesce. However, this pressure distribution may allow for the characteristics near the throat to cross. This requires a check on the viability of the solution after the non-simple region has been formed as well.

To count the number of characteristics that cross the following checks are made:

1. Let x and r be the positions of the characteristic points of the MOC solution. The x location of the intersection of the line segments conjoining between four characteristic points can be found by

$$x = \begin{vmatrix} \begin{vmatrix} x_{i,j} & r_{i,j} \\ x_{i,j+1} & r_{i,j+1} \end{vmatrix} & x_{i,j} - x_{i,j+1} \\ \begin{vmatrix} x_{i+1,j} & r_{i+1,j} \\ x_{i+1,j+1} & r_{i+1,j+1} \end{vmatrix} & x_{i+1,j} - x_{i+1,j+1} \end{vmatrix} \Bigg/ \begin{vmatrix} x_{i,j} - x_{i,j+1} & r_{i,j} - r_{i,j+1} \\ x_{i+1,j} - x_{i+1,j+1} & r_{i+1,j} - r_{i+1,j+1} \end{vmatrix} \tag{3.10}$$

The characteristic lines between these four points intersect in the solution if $x_{i+1,j} < x \leq x_{i+1,j+1}$

2. If $r_{i+1,j} < r_{i,j} \rightarrow n = n + 1$

3. If $r_{i+1,j} < r_{i,j}$ and $r_{i+1,j+1} < ri, j + 1 \rightarrow n = n + 1$

4. If $x_{i+1,j} < x_{i,j} \rightarrow n = n + 1$

3.1.8 Analysis Near Throat

With a viable method of characteristics solution carried out along the prescribed pressure distribution. The analysis of the flow between the kernel and the line of substantial supersonic flow can be analyzed.

Using Sauer's method a line of constant Mach number is formed, beginning at the wall of the geometric throat and extending to the centerline of the nozzle. This is the same line that provided for the location of the first characteristic point. The zone between this line and the first characteristic line running from the centerline is considered part of the non-simple region, see Fig. (3.9). The flow along the Sauer constant Mach number line is found to be substantially supersonic, allowing for the method of characteristics solution to be applied to the region. The line of constant Mach number can be produced using Sauer's solution to the transonic region. And can be well modeled by

$$x = \frac{-(\gamma + 1)}{4} \alpha r^2 + \eta \tag{3.11}$$

Through Sauer's solution the Mach number components U and V are known anywhere along this line. From these components the flow angle at any point along the line can be found. All of the other flow variables can be found through the isentropic relations from the Mach number. Although the flow is known at every location along this line, where characteristic lines can be launched so that the solution is influenced by the prescribed

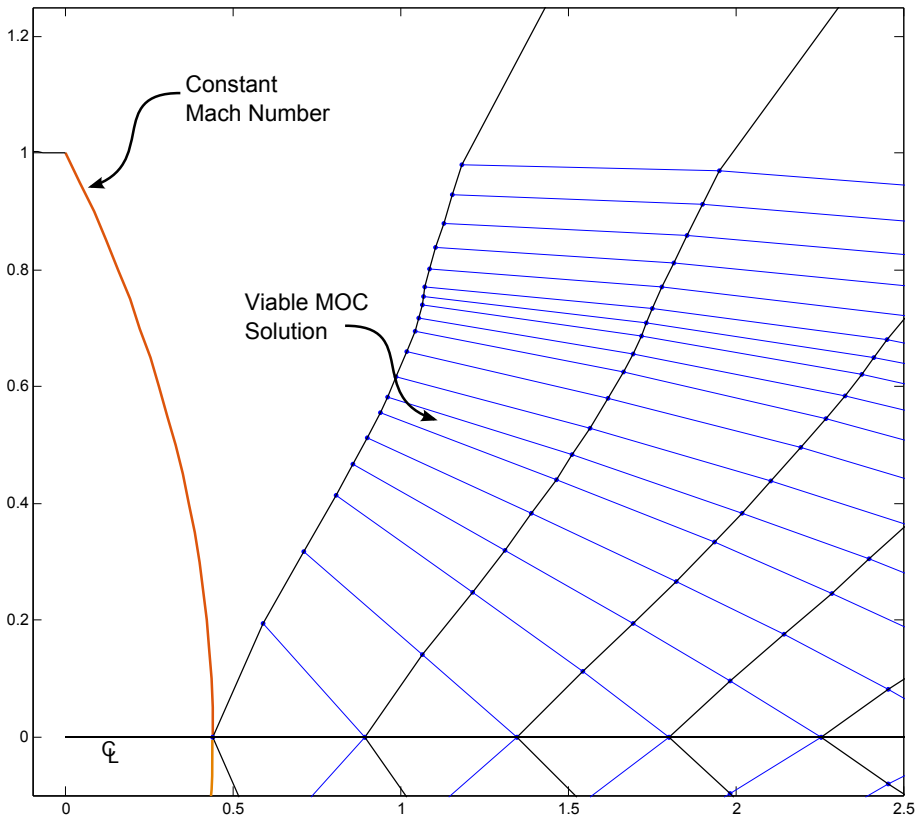

Figure 3.13: Specification of the undefined region

centerline pressure distribution has not been determined. Having the flow known along this line allows for a solution to be found for the non-simple region. Although the line of constant Mach number is not a characteristic line as has been previously defined, it will be treated as one for the solution of the undefined region. This can be done because the flow variables are known along the line. When finding the solution of the undefined zone, when a right running characteristic line intersects the constant Mach number the point of intersection becomes the characteristic point and a left running characteristic line is launched. The solution of the undefined region begins by using the first left running characteristic line of the viable MOC solution as the initial conditions. From the solution the slopes of the right running characteristics are known at each characteristic point along this line. This allows the points along this characteristic to be characteristic points in both the initial solution and the undefined solution.

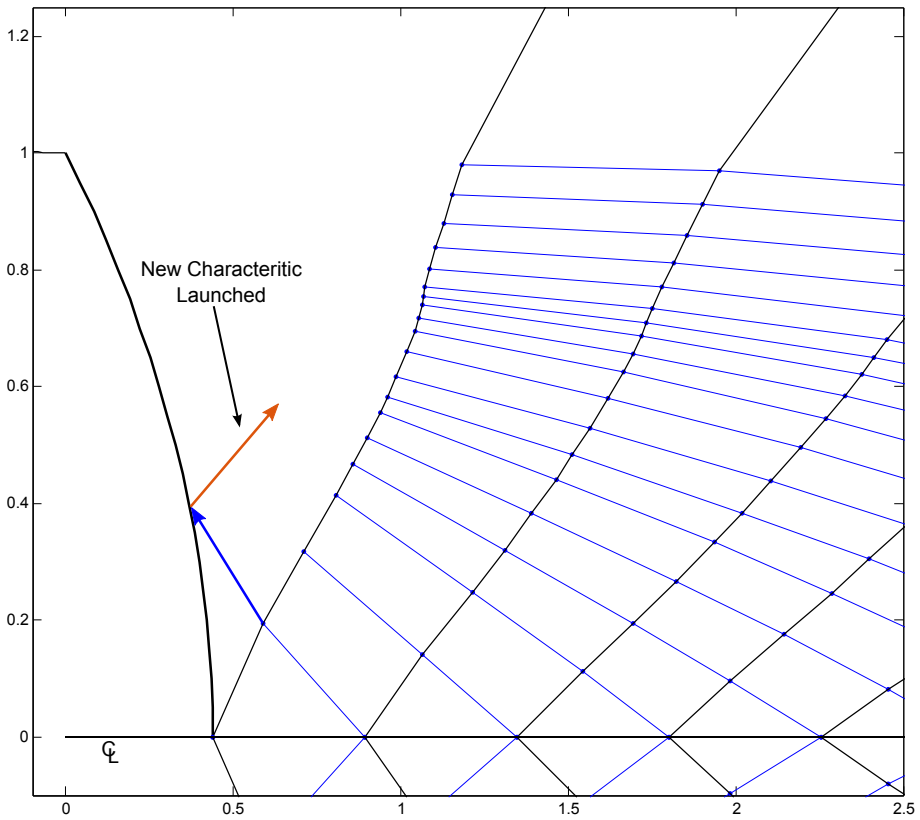

Figure 3.14: Launching characteristic off of the constant Mach number line

The process for the solution in the undefined region is the same as the method of characteristics solution presented with one distinct difference. When the solution nears the constant Mach line, a characteristic points must lie along this line. These points can be found through the intersection of the right running characteristics from the initial solution and the constant Mach line. They are found through

$$x = \frac{\left(\frac{(\gamma+1)}{2}\alpha\lambda\left(-\lambda x_A + r_A\right) + 1\right) \pm \sqrt{\left(\frac{-(\gamma+1)}{2}\alpha\lambda\left(\lambda x_A + r_A\right) - 1\right)^2 + ((\gamma+1)\alpha)^2\lambda^2(-\lambda x_A + r_A)^2}}{\frac{-(\gamma+1)}{2}\alpha\lambda^2} \tag{3.12}$$

where

$$\lambda = tan(\theta - \mu) \tag{3.13}$$

At this point the flow properties are known from the conditions of the constant Mach number line and a characteristic line can be launched back into the solution space, allowing the method of characteristics is to be carried out in the usual way.

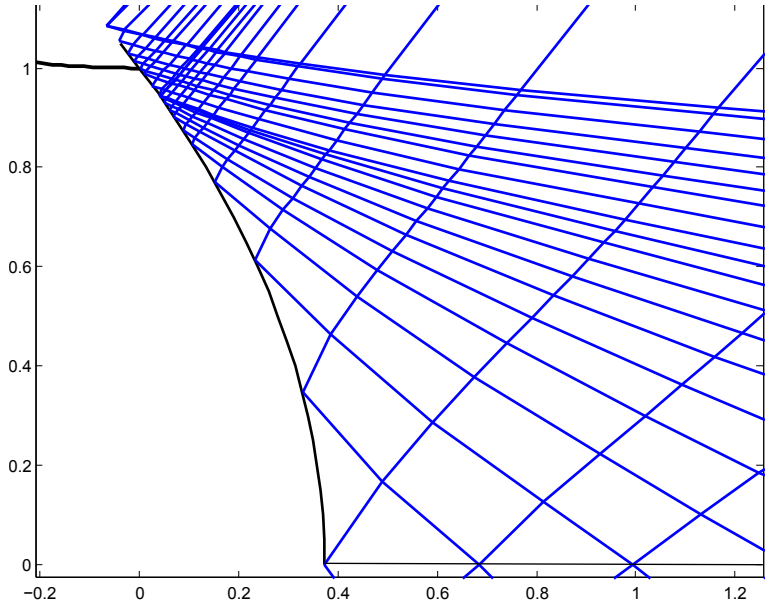

Figure 3.15: Solution to the non-simple region

3.1.9 Determining The Boundary

In the design of a two-dimensional planar nozzle the region between the kernel and where the boundary is treated as a simple wave region. The left running characteristics continue outward and a stream line that matches tangency at each of these characteristics can be treated as the boundary. This is not the case for axis-symmetric flow, and the axis-symmetric method of characteristics must be applied to this region. Once applied the boundary can then be determined by flow tangency through the solution or by applying continuity along left running characteristics as developed by Rao[19].

To form the extended characteristic mesh the initial conditions are based off of the last right and left running characteristics. Downstream of the last left running characteristic the flow is become uniform and axial. Along this characteristic the flow angle and the Mach

number are constant. To initiate the characteristic mesh a number of points are distributed along the characteristic line and form the initial value points. The other set of initial value points lies along the last right running characteristic and all needed information is known.

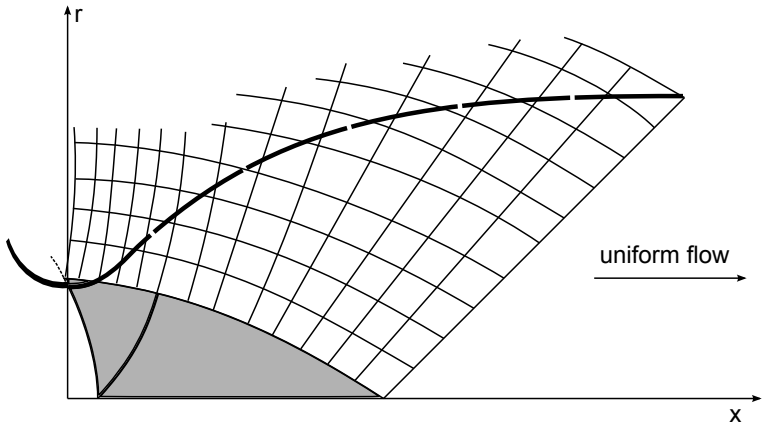

Figure 3.16: Illustration of boundary formation through extended characteristic mesh

Following the axis-symmetric method of characteristics, the left and right running characteristic lines are propagated from each initial value point. Forming a mesh similar to that in Fig. (3.17). The final initial point placed on the last left running characteristic should be set to achieve the correct area ratio for the chosen exit Mach number. This is found through

$$r = \sqrt{\frac{A}{A^*}} \tag{3.14}$$

$$x = \frac{\sqrt{\frac{A}{A^*}}}{tan(\theta + \mu)} + x_c \tag{3.15}$$

This point is also the point at which the contour will end. Insuring that the exit area is correct. As with the other portions of the solution the prescribed pressure distribution must be such that there are no crossing characteristics in the solution. The same process as above can be used to determine if any crossing occurs.

In order to form the boundary a streamline is traced through this mesh. This can be done by finding the position and flow angle at each intersection point between the boundary and

the characteristic mesh. The boundary is allowed to be found through flow tangency because the nature of the method of characteristics solution satisfies continuity. Thus continuity is satisfied for any stream line in the flow field provided the correct pressure distribution is provided. When the expansion ratio on the boundary is met than continuity has been satisfied for the given contour.

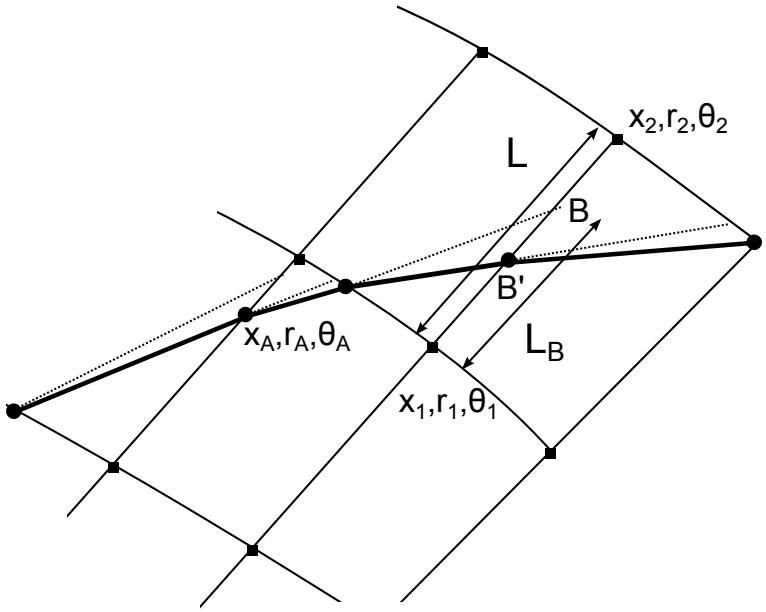

Figure 3.17: Determination of the boundary segments

The point B can be found through

$$x_B = \frac{r_A - r_1 - tan\theta_A x_A + tan(\theta_1 \pm \mu_1)x_1}{tan(\theta_1 \pm \mu) - tan\theta_A} \tag{3.16}$$

$$r_B = r_A + (x_B - x_A)tan\theta_A \tag{3.17}$$

Note that point 1 is always on the inside of the boundary and point 2 is always in the outside of the boundary. This allows the same scheme to be used when the boundary intersects a right running characteristic with only changing the sign of μ in the characteristic

slope term in the above equations. The flow angle at point B is then found by linearly interpolating along the length L between 1 and 2. The flow angle at point B is found through

$$\theta_B = \frac{\theta_2 - \theta_1}{L} L_B + \theta_1 \tag{3.18}$$

To meet flow tangency the segment of the boundary must contain all flow angles between B and A. The boundary must then have a slope that is the average slope of B and A. This changes the slope of line $\bar{BA}$ which is currently $tan\theta_A$. The new location of B is then found.

$$x_{B'} = \frac{r_A - r_1 - \frac{1}{2}(tan\theta_A + tan\theta_B)x_A + tan(\theta_1 \pm \mu_1)x_1}{tan(\theta_1 \pm \mu_1) - \frac{1}{2}(tan\theta_A + tan\theta_B)} \tag{3.19}$$

$$r_{B'} = r_A + (x_{B'} - x_A)\frac{1}{2}(tan\theta_A + tan\theta_{B'}) \tag{3.20}$$

These steps can be repeated until there is no change between point B and B'. The process is then repeated for the next intersection with a characteristic until the boundary is formed at the throat.

3.2 Pressure Distribution Optimization

A viable axis-symmetric method of characteristics solution can be found using an optimizer to find a viable centerline pressure distribution that allows for both the viable solution to the initial MOC mesh and the MOC mesh in the undefined region. The use of Genetic Algorithm/Pattern Search/Particle Swarm Optimization developed by Hartfield, Jenkins and Albarado[28] and the Evolving Swarm Optimizer developed by Jenkins have been used effectively to produce results.

The optimization method of Hartfield, Jenkins and Albarado combines the attributes of particle swarm strategy of Kennedy and Eberhart with the direct search method technique of Hooke and Jeeves[28]. The technique has been proven to be successful in matching solid

rocket motor performances. The method was implemented because of the complexity and interdependence of variables within the design space.

The evolving swarm optimizer of Jenkins is a hybrid particle swarm pattern search optimizer with the addition of the survival of the fittest ideology used in genetic algorithms. There are two fundamental differences between the particle swarm/pattern search optimizers and genetic algorithms. The particle swarm / pattern search optimizer is computationally more efficient with the use of smaller generations. Jenkins recommends 20 - 50 members for a population, whereas binary GA's are often more efficient with large populations of members. When smaller populations are used with a GA the results tend to the same value. The second difference is that the particle swarm pattern search optimizer may take any value for the parameters it is allowed to manipulate. Where a GA can only take discrete values. These values are determined by the a set resolution and the minimum and maximum value limits coded into binary form. Jenkins showed that the %RMS error can be reduced drastically using both a particle swarm / pattern search optimizer and the evolving swarm optimizer. The evolving swarm optimizer has a substantially lower number of calls to the objective function which allow a solution to be found much quicker.

The direct selection method was chosen for finding a viable pressure distribution. Given the chamber conditions, desired exit Mach number, and the number of characteristics that the solution is to be developed over the optimizer selects a normalized pressure for each of the centerline points. The solution is then carried out regardless of its viability as the solution progresses. Once the solution is completed the fitness of the solution is calculated to determine the viability of the pressure distribution.

For both optimizers the same parameters were used to determine a pressure distribution associated with a valid MOC solution. The use of these optimizers is well suited to the direct selection method for determining the pressure distribution. The parameters chosen by the optimizer are the expansion length and the pressure values at each characteristic point that lies on the centerline.

Parameter	Maximum	minimum
Length	1	25
P1	0.1	.99
P2	0.1	.99
P3	0.1	.99
P4	0.1	.99
P5	0.1	.99
P6	0.1	.99
P7	0.1	.99
P8	0.1	.99
P9	0.1	.99
P10	0.1	.99
P11	0.1	.99
P12	0.1	.99
P13	0.1	.99
P14	0.1	.99
P15	0.1	.99
P16	0.1	.99
P17	0.1	.99
P18	0.1	.99

Table 3.1: Pressure distribution optimization parameters for a 20 characteristic solution

The parameters shown above are for a 20 characteristic solution. The first pressure point is always selected as 1 and the last point is always selected as 0. The parameters P1 through P18 are selected at random. Excluding the length selection, the physical meaning to the parameters as they are selected is the percentage of the last parameter selected. this ensures that the pressure distribution selected is always decreasing in pressure. The pressure values are then determined by multiplying the succeeding parameter by the current value. This value is then multiplied by the its succeeding parameter and so on. The result is a percentage of pressure range from the Sauer's solution pressure to the pressure that results in the desired Mach number. With a pressure distribution selected by the optimizer the method can be performed and the solution evaluated. The normalized pressure distribution as selected by the optimizer has the form shown in Fig. 3.18. When these pressure points

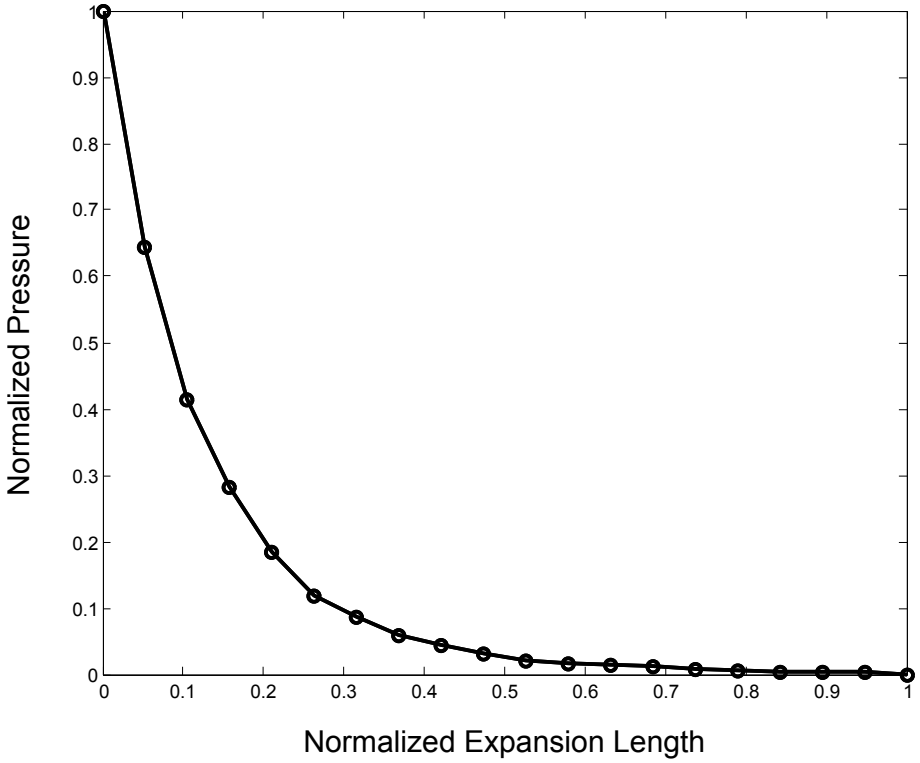

Figure 3.18: Normalized pressure distribution selected from optimizer

are evaluated through

$$p = (p_e - p_s)P_n + p_e \tag{3.21}$$

where p_e is the exit pressure required to achieve the desired exit condition and p_s is the pressure found at the intersection of the Sauer constant Mach line and the centerline. The resulting static pressure distribution along the centerline is shown in Fig. 3.19

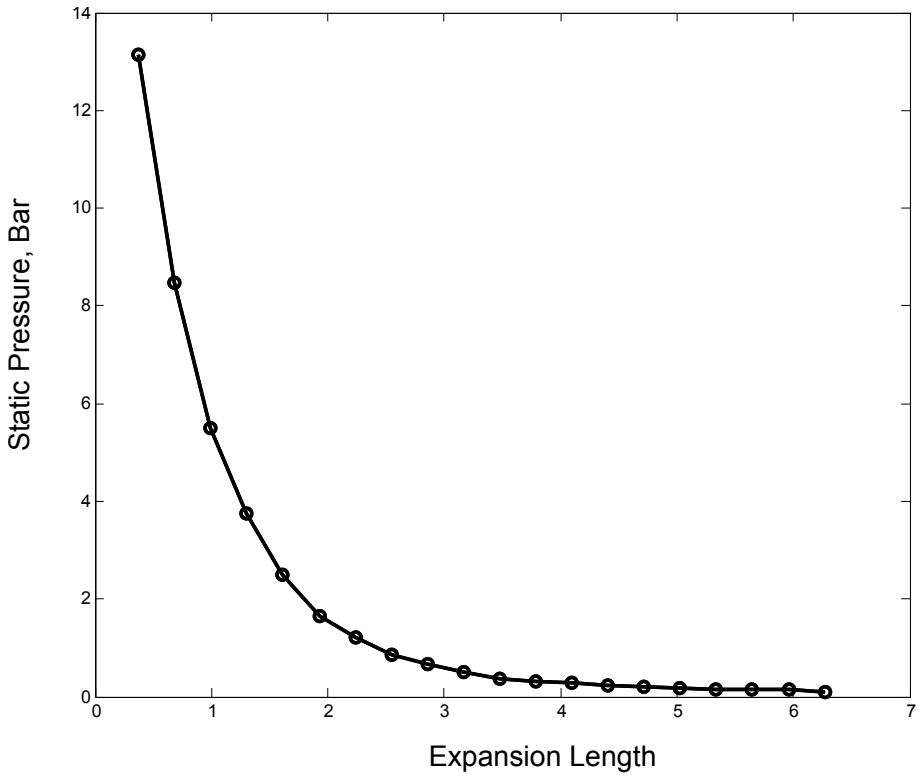

Figure 3.19: Resulting static pressure distribution

3.2.1 Fitness Algorithm

The fitness algorithm analyzes the viability of the pressure distribution through analyzing the solution. For the producing a nozzle contour for a given exit Mach number the fitness algorithm contains two parts. The first algorithm, shown in Fig. 3.20, analyzes the initial MOC solution for viability and the second algorithm, shown in Fig.3.21, analyzes the entire solution given that the initial solution is viable.

In addition to the above evaluation, the addition of solution smoothing terms were added to the fitness evaluation. These functions allowed for better scoring solutions with a more evenly distributed solution mesh and smoother transition along characteristic lines. The resulting solutions are as far away from coalescing solutions as possible. The smoothing fitness for the left running characteristics is

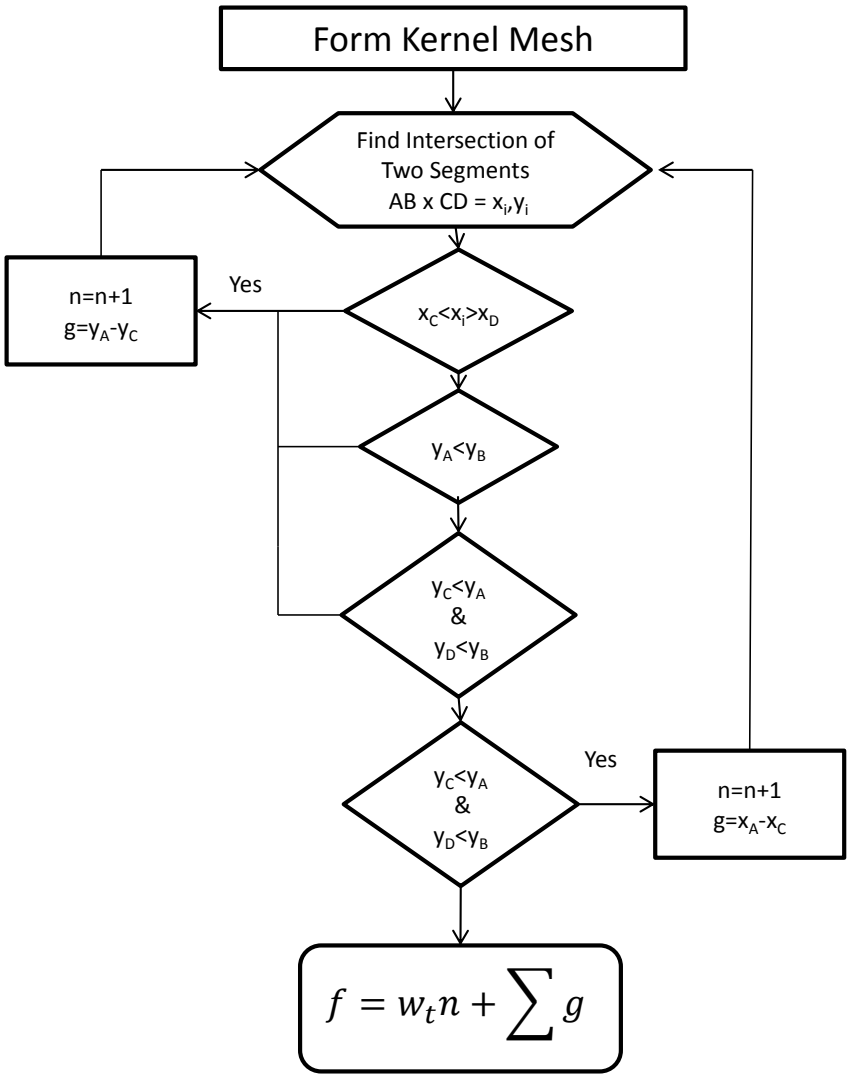

Figure 3.20: Evaluation of fitness through intersection of characteristics

$$d = \sum_{i}^{n_c} \left| x_{i+2} - x_i - 2\frac{x_{i+1} - x_i}{x_{i+2} - x_i} \right| \tag{3.22}$$

The absolute value function, Eq. 3.22, allows for more evenly distributed characteristic to have a lower fitness evaluation, where the x is the x location of the final characteristic point in the kernel. Evaluation of the slope between characteristic points allows for a better transition between points in the solution separating like characteristics further. The smoothing function

that evaluates the characteristic slopes is Eq. 3.23

if $x_C < x_A$ then

$$m_i = |x_C - x_A| \tag{3.23}$$

$$m = \sum m_i \tag{3.24}$$

The smoothing functions are added to the fitness value to allow their influence.

Secondary fitness can only begin if there are no crossing characteristics from the kernel solution. The program also skips the solution of the non-simple region if crossing characteristics have been found; eliminating the processing time required to evaluate the non-simple region.

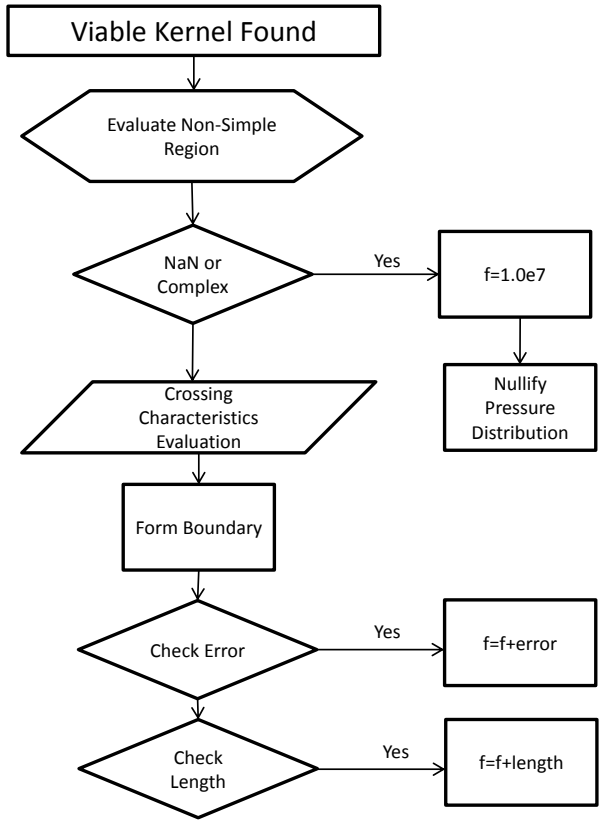

Figure 3.21: Evaluation of fitness for non-simple region and boundary

The fitness factors are weighted so that the optimizer will tend towards the most important factors first. These weights are presented in Table 3.2. The optimizer goals always prefer solutions that have no crossing characteristics as its main objective. It was found that a viable prescribed pressure distribution will allow for a solution that has no crossing characteristics no matter the expansion length. Thus this length is found by meeting requirements by the boundary, and continuity. The expansion length that satisfies these requirements is a unique solution for a selected pressure distribution however the expansion length is not a unique solution for a desired exit Mach number. When nozzle length is of interest the use of the optimizer also allows for the minimization of the expansion length.

The solution must also contain only real numbers. To eliminate in numerical issues that could result in a solution with any variables being read as NaN (not a number) or complex will result in a fitness value that is far greater than the desired result. This situation can occur in the random selection of optimizer parameters.

Parameter	Weight
Crossing in Kernel	3
Crossing in Non-Simple Region	3
Crossing in Boundary Region	1
Area Ratio Error	10
Expansion Length	0.01
Any NaN in solution	1E7
Any Complex in solution	1E7

Table 3.2: Fitness weights

3.3 Uniform Flow Nozzles

The following nozzle contours are nozzles designed for uniform flow at a specified exit Mach number. Table3.3 are the directly chosen expansion lengths and pressure points for the given nozzles. For the following contours the chamber conditions and throat radius for each nozzle was held constant. Figure 3.26 compares the contours.

Normalized Pressures for Viable Solutions				
Mach	2.0	3.0	4.0	5.0
Length	1.1050	2.7463	5.8953	10.9632
P1	1.000	1.000	1.000	1.000
P2	0.9572	0.7943	0.6428	0.4576
P3	0.9034	0.6642	0.4145	0.2187
P4	0.8325	0.5655	0.2809	0.1047
P5	0.6898	0.4610	0.1836	0.0622
P6	0.5668	0.3494	0.1184	0.0372
P7	0.5136	0.2879	0.0856	0.0241
P8	0.4345	0.2273	0.0576	0.0163
P9	0.3774	0.1605	0.0429	0.0106
P10	0.3233	0.1305	0.0311	0.0076
P11	0.2677	0.1028	0.0211	0.0058
P12	0.1940	0.0737	0.0154	0.0039
P13	0.1664	0.0547	0.133	0.0031
P14	0.1350	0.0395	0.0107	0.0022
P15	0.1152	0.0291	0.0069	0.0017
P16	0.0958	0.0262	0.0056	0.0011
P17	0.0832	0.0230	0.039	0.0008
P18	0.0762	0.0201	0.0034	0.0007
P19	0.0561	0.0142	0.0028	0.0006
P20	0.000	0.000	0.000	0.000
*Specific heat ratio, $\gamma = 1.23$ **Pressures Values:$P = (P_e - P_t)P_n + P_e$.				

Table 3.3: Directly prescribed normalized pressure points

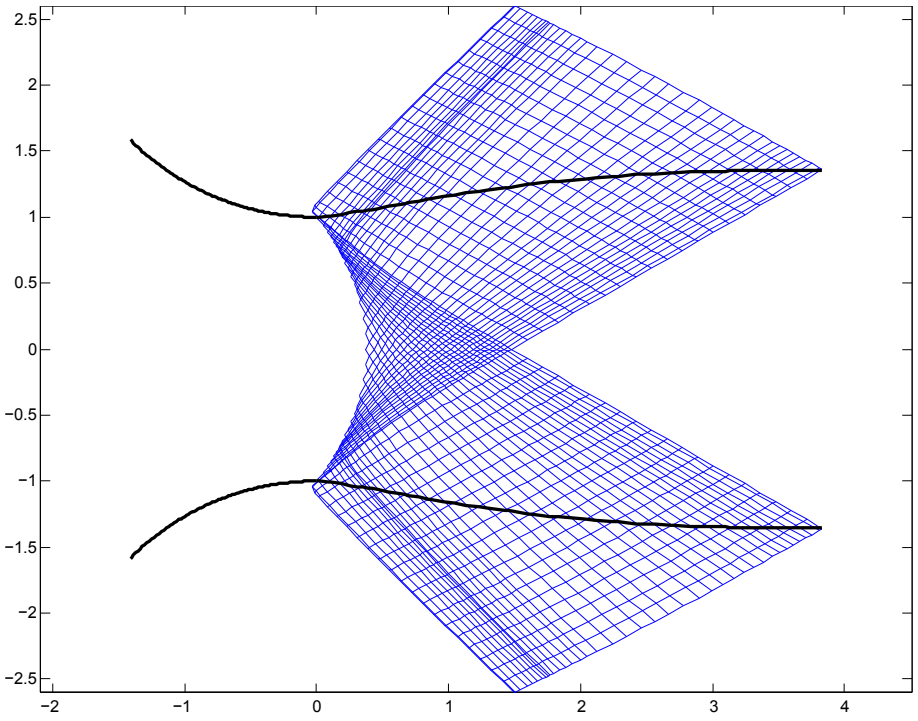

Figure 3.22: Mach 2 Nozzle Contour solved with 20 characteristics, $\gamma = 1.23$

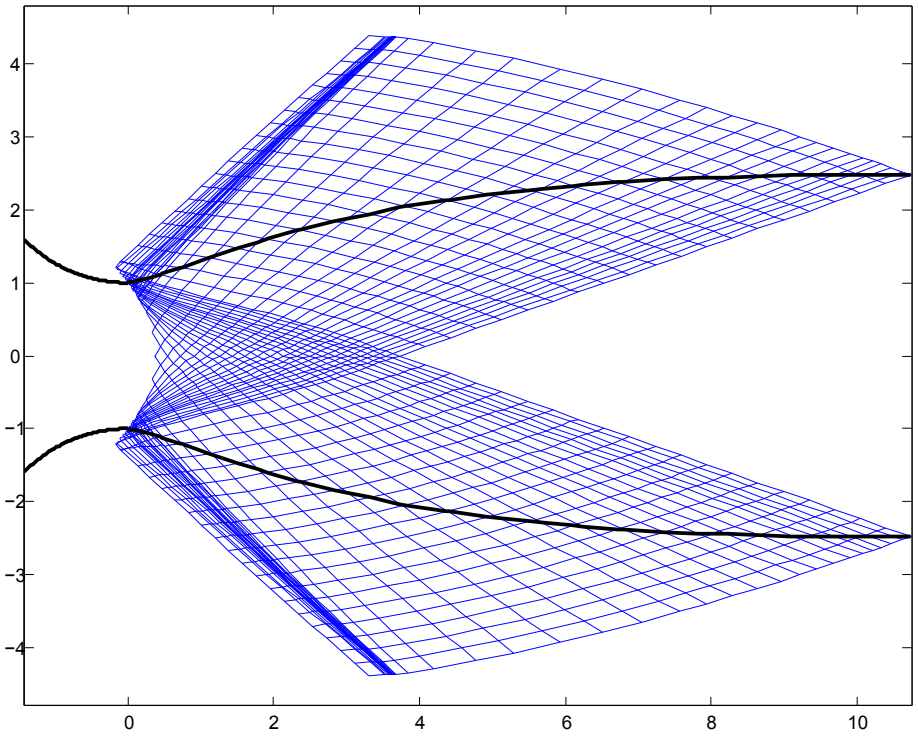

Figure 3.23: Mach 3 Nozzle Contour solved with 20 characteristics, $\gamma = 1.23$

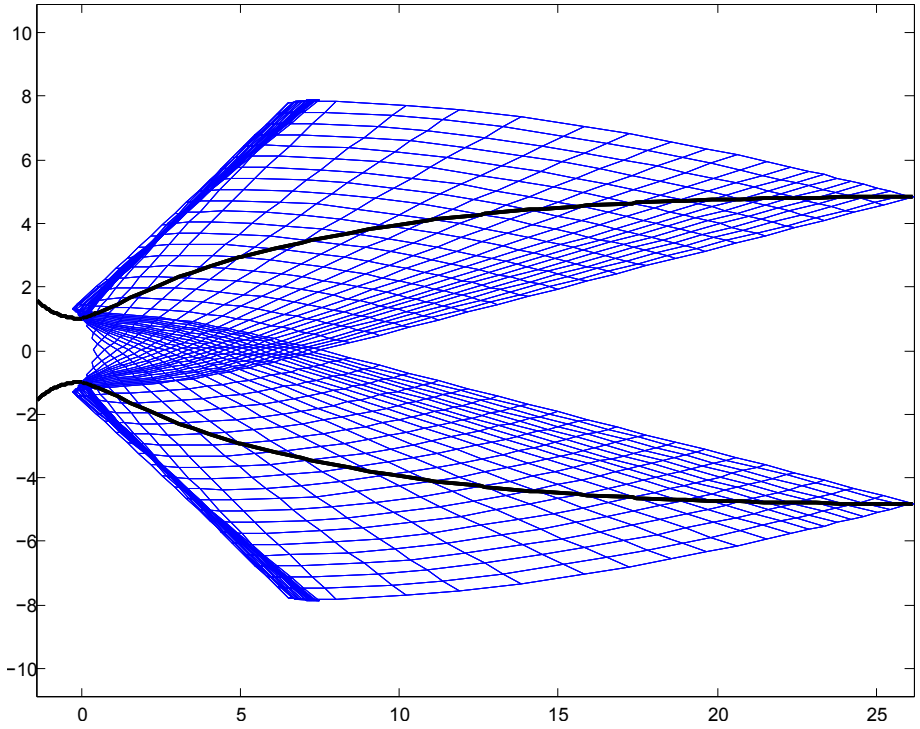

Figure 3.24: Mach 4 Nozzle Contour solved with 20 characteristics, $\gamma = 1.23$

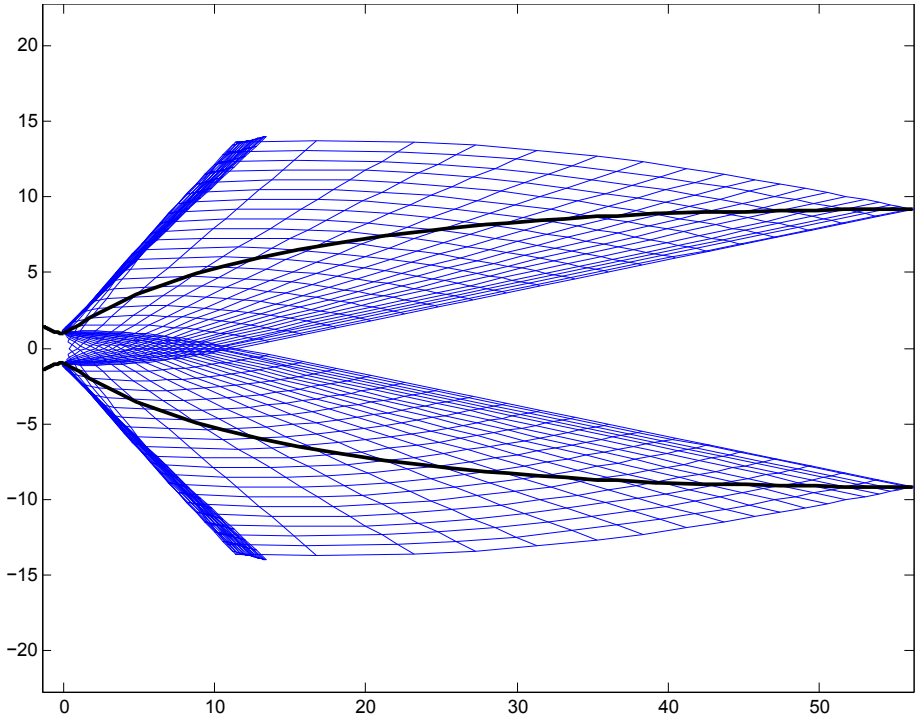

Figure 3.25: Mach 5 Nozzle Contour solved with 20 characteristics, $\gamma = 1.23$

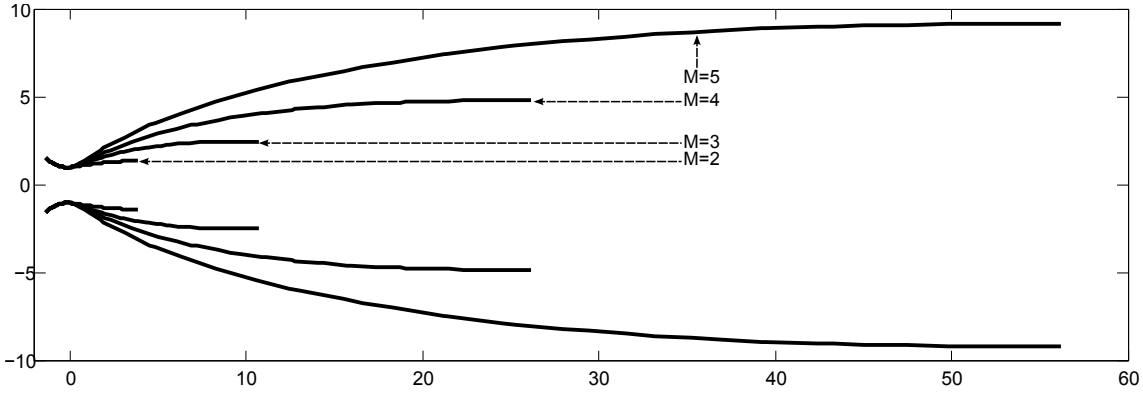

Figure 3.26: Comparison of the above contours

3.4 Nozzle Truncation and Performance Evaluation

Nozzles designed for uniform exit flow can become excessively long. In order to design a nozzle that produces acceptable performance without these lengths a perfect nozzle can be truncated. The exit velocities of a truncated nozzle however will not be uniform or fully axial. The thrust of the truncated nozzle cannot be simply calculated from Eq.(1.3). Instead the mass flow must be integrated along a characteristic to account for the flow being non axial. The integrated mass flow is constant at any cross section of the nozzle, however the mass flow is not uniform across this cross section. Depending on the location of the truncation point the fully axial flow may only occur at the centerline.

The mass flow along a characteristic can be found through integrating the mass flow along a characteristic line.

$$\dot{m} = \int \rho V \left(cos\theta - \frac{sin\theta}{tan(\theta + \mu)} \right) r dr \tag{3.25}$$

Similarly the thrust along a characteristic line can be found through

$$F_t = \int \left(P + \rho V^2 \left(cos\theta - \frac{sin\theta}{tan(\theta + \mu)} \right) \right) 2\pi r dr - \pi r^2 P_a \tag{3.26}$$

The above thrust equation only accounts for the the thrust that is produced by a nozzle truncated where a left running characteristic intersects the nozzle boundary. This does not allow for generic truncation of the nozzle. If the desired truncation length is at a point that does not lie on this intersection the calculated thrust would be not include the portion of the boundary that is between characteristics. A scheme can easily be made to calculate the the thrust associated with the portion of the boundary that does not end at a characteristic intersection.

By definition, the trust is the sum of all pressure forces along the boundary of thrust chamber. Using this the remaining portion of the thrust can be found by integrating the pressure along the remaining boundary.

$$F_t = \int PdA \tag{3.27}$$

In terms of the nozzle radius, and linearly interpolating the pressure along additional boundary section the thrust of the segment becomes

$$F_t = \int_{r_i}^{r_e} 2\pi r(P_i - kr)dr \tag{3.28}$$

where k is the slope of the nozzle segment

This integral can easily be determined numerically and the thrust on this segment of the nozzle can be calculated directly through

$$F = P_i\pi(r_e^2 - r_i^2) - \frac{2\pi k}{3}(r_e^3 - r_i^3) \tag{3.29}$$

The total thrust for the truncated nozzle is found by calculating the characteristic thrust along the first characteristic upstream of the truncation point. The additional thrust from the remaining boundary is then added to this to form the total thrust. With this method the nozzle may be truncated at any distance and the trust can be calculated.

With the thrust calculated the specific impulse can be found in the usual way as presented in Eq. (1.2).

3.4.1 Optimization of Truncated Nozzles

Optimization of a truncated perfect nozzles can be found in multiple ways. One such way would to allow for an external optimization routine to select an exit Mach number for a uniform exit flow nozzle, a optimized pressure distribution would then be found through an internal optimization routine. The external optimization would grade the fitness of the solution by maximizing the thrust, or thrust coefficient of the this contour at a selected truncation point.

This method for optimizing for maximum thrust at a given truncation length would produce the optimum solution, however the approach would have enormous computational expense due to to the shear number of calls to the objective function. The wall clock time to find the solution would also be enormous, because the design space would be very large.

A more intelligent approach to this solution must be made to reduce both computational expense and wall clock time to a solution. This can be done by mapping the thrust coefficient at a given truncation length using pre-specified perfect contours.

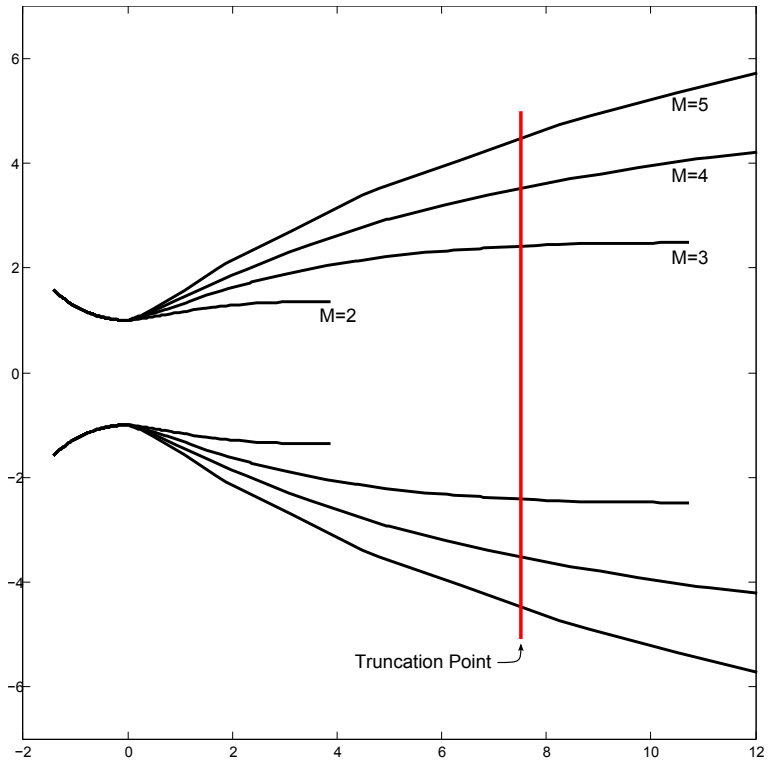

Figure 3.27: Example of contours that can be used for mapping thrust coefficient at a given truncation length

This provides insight to the design space that contains the optimum case for a given length. The exit Mach number for the perfect contour that results in this optimum solution can then be found. Using the process above the MOC solution and contour can then be found.

After the initial process of finding the data to make such performance maps this approach provides a very inexpensive way of finding the optimum solution for a given truncation length.

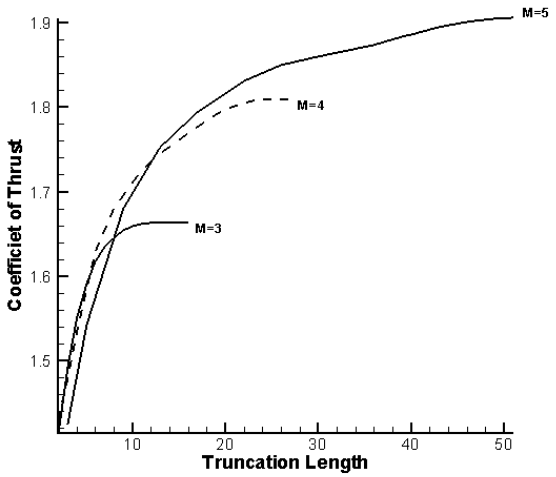

Figure 3.28: Coefficient of thrust versus truncation length for shock free contours

Chapter 4

AXSMOC Nozzle Design with Chemical Kinetics

In order to design a nozzle that takes into consideration the effect of the working fluid being a nonequilibrium chemically reacting mixture the axis-symmetric method of characteristics approach described in Chapter 3 can be coupled with the finite reaction rate analysis of the chemical kinetics. As was explained in Sec 2.4, analysis of finite rate chemistry is not a trivial undertaking; however, the nature of the method of characteristics allows for the MOC solution to be coupled with such an analysis. This chapter will show how the the chemical kinetics can be coupled with the AXSMOC and provides a method for implementing the the coupled approach to existing isentropic solutions. These solutions are chemical kinetics adjusted axis-symmetric method of characteristics solutions.

4.1 Combining Chemical Kinetics with AXSMOC

The axis-symmetric method of characteristics solutions presented thus far have been completed considering isentropic flow. When finding a axis-symmetric method of characteristics solution while considering the working fluid a nonequilibrium chemically reacting gas mixture the computational expense is increased greatly due to the presence of finite rate chemistry.

The governing equations for a steady multidimensional adiabatic, inviscid flow that performs no work and has negligible body forces can be applied with two new considerations.

- The enthalpy of the system is the absolute enthalpy which is comprised of the sensible enthalpy and the energy of formation

- The law of conservation of mass must be applied to each chemical species involved in the nonequilbrium reactions

The governing equations are then

$$\nabla \cdot \left(\rho \vec{V}\right) = 0 \tag{4.1}$$

$$\rho \frac{d\vec{V}}{dt} + \nabla p = 0 \tag{4.2}$$

$$\frac{d}{dt}\left(h + \frac{V^2}{2}\right) = 0 \tag{4.3}$$

$$\nabla \cdot \left(\rho_i \vec{V}\right) = \sigma_i \; i = 1, ..., n \tag{4.4}$$

Where σ is the source function as presented in Eqn. 2.43

$$h = \sum_{i=1}^{n} C_i \left(C_i(h_i + h_i^\circ)\right) \tag{4.5}$$

Noting that i denotes the individual chemical species involved, also note that h_i is the sensible enthalpy and h_i° is the energy of formation of the species.

These governing equations can be arranged to form a set of characteristic equations and compatibility equations.

The relationship $C_i = \rho_i/\rho$ can be substituted into 4.4 to form

$$C_i \nabla \cdot (\rho \vec{V}) + \rho \vec{V} \cdot \nabla C_i \tag{4.6}$$

Substituting4.1 into the above equation will form the continuity equation in terms of global continuity as well as speciese continuity.

$$\rho\vec{V}\cdot\nabla C_i = \sigma_i = \rho\frac{dC_i}{dt} \tag{4.7}$$

This gives way to

$$\rho u C_{i_x} + \rho v C_{i_y} = \sigma_i \tag{4.8}$$

The momentum equation can be rewritten as

$$\rho\vec{V}\cdot\frac{d\vec{V}}{dt} + \vec{V}\cdot\nabla p = 0 \tag{4.9}$$

Rewriting the above momentum equation so that the pressure term is a time derivative yeilds

$$\rho\frac{d}{dt}\frac{V^2}{2} + \frac{dp}{dt} = 0 \tag{4.10}$$

Substituting the energy equation into the form of the momentum equation above forms

$$\rho\frac{dh}{dt} - \frac{dp}{dt} = 0 \tag{4.11}$$

Due to the involvement of change in chemical composition the enthalpy derivative term of the above equation must rewritten to include the species specific enthalpy change per time. With this substitution the above becomes can be rearranged to become

$$\frac{dp}{dt} = \rho\sum_{i=1}^{n}\left(h_i + h_i^\circ\right)\frac{dC_i}{dt} + \rho\sum_{i=1}^{n}C_i\frac{dh_i}{dt} \tag{4.12}$$

Note that the enthalpy of formation is constant for each species resulting in $dh_i^\circ/dt = 0$

The sensible enthalpy h_i is defined as

$$h_i = \int_{T_o}^{T} c_{p_i} dT \tag{4.13}$$

The concentrations derivative can be rewritten in terms of the source function, σ

$$\sigma_i = \rho \frac{dC_i}{dt} \tag{4.14}$$

resulting in the equation

$$\frac{dp}{dt} = \sum_{i=1}^{n} (h_i + h_i^{\circ}) \sigma_i + \rho \sum_{i=1} n C_i c_{p_i} \frac{dT}{dt} \tag{4.15}$$

Substituting the species specific equation of state.

$$p = \rho T \sum_{i=1}^{n} C_i R_i \tag{4.16}$$

Yields

$$\frac{dP}{dt} = \sum_{i=1}^{n} (h_i + h_i^{\circ}) \sigma_i + \rho \sum_{i=1} n C_i c_{pi} \frac{dT}{dt} \tag{4.17}$$

Noting that for a mixture of gases the specific gas constant for the mixture is found through

$$R = \sum_{i=1}^{n} C_i R_i \tag{4.18}$$

The constant pressure specific heat is found through

$$c_p = \sum_{i=1}^{n} C_i c_{pi} \tag{4.19}$$

The resulting specific heat ratio for the mixture is then found in the usual way

$$\gamma = \frac{c_p}{c_p - R} \tag{4.20}$$

The constant pressure specific heat can be rewritten in terms of the specific heat ration and the mixtures specific gas constant as

$$c_p = \frac{\gamma R}{\gamma - 1} \tag{4.21}$$

Using the mixture quantities and the definition of sound speed Eqn. [4.17] can be rewritten as

$$\frac{dp}{dt} - a^2 \frac{d\rho}{dt} = \sum_{i=1}^{n} \left[\gamma RT - (\gamma - 1)(h_i - h_i^\circ)\right] \sigma_i \tag{4.22}$$

For convenience let

$$\psi \equiv \sum_{i=1}^{n} \left[\gamma RT - (\gamma - 1)(h_i - h_i^\circ)\right] \sigma_i \tag{4.23}$$

The governing equations for steady axis-symmetric nonequilibrium chemically reacting gases become

$$\rho u_x + \rho v_r + u\rho_x + v\rho_r + \frac{\rho v}{r} = 0 \tag{4.24}$$

$$\rho u u_x + \rho v u_r + p_x = 0 \tag{4.25}$$

$$\rho u v_x + \rho v v_r + p_r = 0 \tag{4.26}$$

$$u p_x + v p_r - a^2 u \rho_x - a^2 v \rho_r = \psi \tag{4.27}$$

$$\rho u C_{ix} + \rho v C_{ir} = \sigma_i \tag{4.28}$$

With the governing equations containing the source function for finite rate chemical kinetics the characteristic and compatibility equations can be derived. The approach used here for deriving the characteristic and compatibility equations is the approach outlined by Ferri[22] and Zucrow[4].

Multiplying the governing equations above by an unknown factor $\epsilon_{1...4}$ to the global governing equations and summing them yields

$$\begin{aligned}
\epsilon_1(\rho u_x + \rho v_r + u\rho_x + v\rho_r + \frac{\rho v}{r}) + ... \\
\epsilon_2(\rho u u_x + \rho v u_r + p_x) + ... \\
\epsilon_3(\rho u v_x + \rho v v_r + p_r) + ... \\
\epsilon_4(u p_x + v p_r - a^2 u\rho_x - a^2 v\rho_r - \psi) = 0
\end{aligned} \tag{4.29}$$

Factoring the derivative terms of u, v, p, and ρ the above equation can be rewritten in the form

$$\begin{aligned}
(\rho\epsilon_1 + \rho u\epsilon_2)\left[u_x + \frac{\rho v\epsilon_2}{\rho\epsilon_1 + \rho u\epsilon_2}u_r\right] + (\rho u\epsilon_3)\left[v_x + \frac{\rho\epsilon_1 + \rho v\epsilon_3}{\rho u\epsilon_3}v_r\right] \\
+(\epsilon_2 + u\epsilon_4)\left[p_x + \frac{\epsilon_3 + v\epsilon_4}{\epsilon_2 + u\epsilon_4}p_r\right] \\
+(u\epsilon_1 - a^2 u\epsilon_4)\left[\rho_x + \frac{v\epsilon_1 - a^2 v\epsilon_4}{u\epsilon_1 - a^2 u\epsilon_4}\rho_r\right] + \frac{\epsilon_1\rho v}{r} - \epsilon_4\psi = 0
\end{aligned} \tag{4.30}$$

Assuming that u, v, p, and ρ are continuous and that the slope of the characteristic curves is dr/dx then the derivative terms can be written as

$$\frac{du}{dx} = u_x + \frac{dr}{dx}u_r \tag{4.31}$$

$$\frac{du}{dx} = v_x + \frac{dr}{dx}v_r \tag{4.32}$$

$$\frac{du}{dx} = p_x + \frac{dr}{dx}p_r \tag{4.33}$$

$$\frac{du}{dx} = \rho_x + \frac{dr}{dx}\rho_r \tag{4.34}$$

From Eqn. (4.31) the slopes of the characteristic can be rewritten into 4 different and equal expressions

$$\frac{dr}{dx} = \frac{v\epsilon_2}{\epsilon_1 + u\epsilon_2} = \frac{\epsilon_1 + v\epsilon_3}{u\epsilon_3} = \frac{\epsilon_3 + v\epsilon_4}{\epsilon_2 + u\epsilon_4} = \frac{v\epsilon_1 - a^2 v\epsilon_4}{u\epsilon_1 - a^2 u\epsilon_4} \tag{4.35}$$

Yielding the compatibility equation in unknown form

$$\rho(\epsilon_1 + u\epsilon_2)du + \rho u\epsilon_3 dv + (\epsilon_2 + u\epsilon_4)dp + u(\epsilon_1 - a^2\epsilon_4)d\rho + \epsilon_1\frac{\rho v}{r}dx - \epsilon_4\psi dx = 0 \tag{4.36}$$

This compatibility equation is valid along each of the characteristic curves. However the characteristic equation dr/dx has yet to be determined. By the elimination of the unknown parameters in the system of equations in Eqn. (4.35) the characteristic equation can be found. Solving each expression in Eqn. (4.35) for ϵ_1 to ϵ_4 the coefficient matrix for the system can be formed

$$\begin{vmatrix} dr/dx & udr/dx - v & 0 & 0 \\ -1 & 0 & udr/dx - v & 0 \\ 0 & dr/dx & -1 & udr/dx - v \\ udr/dx - v & 0 & 0 & -a^2(udr/dx - v) \end{vmatrix} \tag{4.37}$$

To form a solution to the unknown parameters that is nonzero, the determinant of the above coefficient matrix must be equal zero. This results in

$$(u\frac{dr}{dx} - v)^2 \left[(u\frac{dr}{dx} - v)^2 - a^2 \left(1 + \left(\frac{dr}{dx} \right)^2 \right) \right] = 0 \tag{4.38}$$

Defining $\lambda \equiv dr/dx$ and substituting into the above and letting $S = u\lambda - v$ the above can be rewritten as a fourth-order algebraic equation

$$S^2 \left[S^2 - a^2(1 + \lambda^2) \right] = 0 \tag{4.39}$$

The fourth-order equation can is expressed above as the product of two second order factors. The roots of this fourth-order equation be come the characteristic equation. The first root is repeated and is found to be the differential equation to a streamline.

$$\lambda_{1,2} = \frac{dr}{dx} = v/u \tag{4.40}$$

The other root two roots become the equation of for the Mach lines

$$\lambda_{3,4} = (\frac{dr}{dx})_{\pm} = tan(\theta \pm \mu) \tag{4.41}$$

It is important to note that the characteristic equations are identical for non-equilibrium chemically reacting flow as for isentropic flow. However the compatibility equations are not. Also the species continuity equation Eqn. (4.28) can be placed directly into characteristic form. Allowing the concentrations to be found along a stream line. This is done in the same numerical approach as with a one-dimensional non-equilibrium chemically reacting gas calculation. Rearranging Eqn. (4.28).

$$\rho u(C_{xi} + \frac{v}{u}C_{ri}) = \sigma_i \quad (i = 1...n) \tag{4.42}$$

Rewriting the above equation to the following differential form

$$\frac{dC_i}{dx} = \frac{\sigma_i}{\rho u} \tag{4.43}$$

which can be applied along a stream line.

To form the compatibility equations the unknown parameters must be eliminated from Eqn. (4.36). From the solution to the characteristic equations, the quadratic factor is zero when following Mach lines. Rearranging and substituting this into the system of equations in Eqn. (4.35). Reducing each equation to its simplest form results in

$$\epsilon_2 = -\tan(\theta \pm \mu)\epsilon_3 \tag{4.44}$$

$$\epsilon_1 = (u\tan(\theta \pm \mu) - v)\epsilon_3 \tag{4.45}$$

$$\epsilon_4 = \epsilon_3 \left[\frac{1 + \tan(\theta \pm \mu)^2}{(u\tan(\theta \pm \mu) - v)}\right] \tag{4.46}$$

$$\epsilon_4 = \epsilon_3 \frac{(u\tan(\theta \pm \mu) - v)}{a^2} \tag{4.47}$$

Substituting equations 4.44, 4.45, 4.47 into the unknown compatibility equation 4.36. yields the compatibility equation in velocity component form

$$(\rho v)du - (\rho u)dv + \left[\tan(\theta \pm \mu) - \frac{u(u\ \tan(\theta \pm \mu) - v)}{a^2}\right] dp - (u\ \tan(\theta \pm \mu) - v)\left[\frac{\rho v}{r} - \frac{\psi}{a^2}\right] dx = 0 \tag{4.48}$$

The compatibility equation can be written in the final form as

$$\cot\mu \frac{dV}{V} \mp d\theta - \frac{\sin\mu \sin\theta}{\cos(\theta \pm \mu)} \frac{dx}{r} + \frac{\psi}{\rho V^2 a_f} \frac{dx}{\cos(\theta \pm \mu)} = 0 \tag{4.49}$$

As can be seen from the above equation. The new compatibility equation is the same as the compatibility equation for the axis-symmetric method of characteristics for isentropic flow with the addition of the source term which includes all the changes in chemistry that affect the solution. As shown earlier the characteristic equations remained the same.

Discretizing the compatibility equations yields the finite difference equations including the non-equilibrium chemically reacting term

Solving for v_c through the elimination of θ_C as was done before. The only real change is that $\pounds$ and $\mathfrak{M}$ are adjusted to include the finite rate chemistry term.

Method of Characteristic Equations	
Isentropic Flow	Non-equilibrium Chemically Reacting Flow
Characteristic Equations:	
$dr/dx = \tan(\theta \pm \mu)$	$dr/dx = \tan(\theta \pm \mu)$
Compatibility Equations:	
$\cot\mu \frac{dV}{V} \mp d\theta - \frac{\sin\mu \sin\theta}{cos(\theta \pm \mu)} \frac{dx}{r} = 0$	$\cot\mu \frac{dV}{V} \mp d\theta - \frac{\sin\mu \sin\theta}{\cos(\theta \pm \mu)} \frac{dx}{r} + \frac{\psi}{\rho V^2 a_f} \frac{dx}{\cos(\theta \pm \mu)} = 0$

Table 4.1: Method of Characteristics Equations

$$v_c = \frac{1}{\frac{\cot\mu_A}{v_a} + \frac{\cot\mu_B}{v_B}} \{\cot\mu_A(1 + \pounds(x_c - x_a))(1 + \mathfrak{M}(x_c - x_B)) + \theta_B - \theta_A\} \tag{4.50}$$

where

$$\pounds = \frac{\tan\mu_A \ \sin\mu_A \ \sin\theta_A}{y_A \cos(\theta_A + \mu_A)} - \frac{\psi}{\rho_A v_A^2 \cos(\theta_A + \mu_A)} \tag{4.51}$$

and

$$\mathfrak{M} = \frac{\tan\mu_B \ \sin\mu_B \ \sin\theta_B}{y_B \cos(\theta_B - \mu_B)} - \frac{\psi}{\rho_B v_B^2 \cos(\theta_B - \mu_B)} \tag{4.52}$$

In turn the flow angle of the characteristic may be obtained by solving the compatibility equations for θ_c yeilding:

$$\theta_c = \theta_A + \cot\mu_A \left(\frac{V_c - V_A}{V_A}\right) - \pounds(x_c - x_A)) \tag{4.53}$$

The method may be performed in the same way as with the isentropic flow case however the finite rate analysis must be performed throughout the solution simultaneously to update the chemical species source function as the solution progresses.

To analyze the chemically reacting flow using the intersection of a stream line with the left and the left running characteristic instead of only following the left running and right

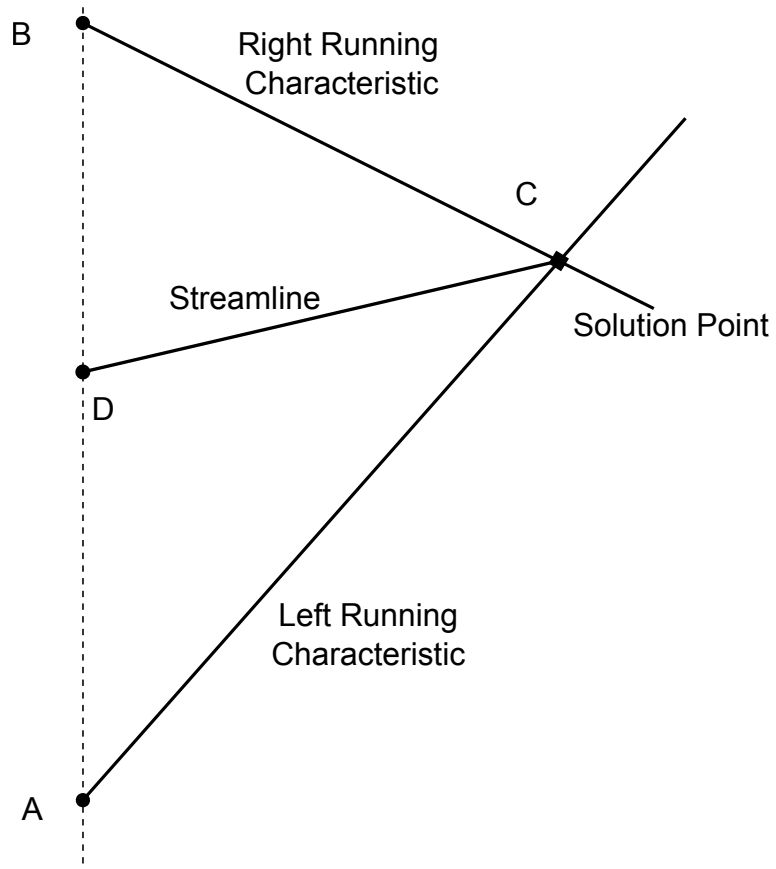

Figure 4.1: Solution can be developed through streamlines[4]

running characteristics through the solution, using the centerline pressure distribution and the Sauer solution constant Mach number line as initial conditions.

The finite difference equations used to analyze the solution with chemistry now add the streamline term for updating the species source function

$$\frac{y_C - y_A}{x_C - x_A} = \tan(\theta_A + \mu_A) \tag{4.54}$$

$$\frac{y_C - y_B}{x_C - x_B} = \tan(\theta_B - \mu_B) \tag{4.55}$$

$$\frac{y_C - y_D}{x_C - x_D} = \frac{\tan(\theta_D + \theta_C)}{2} \tag{4.56}$$

$$\frac{y_D - y_B}{x_D - x_B} = \frac{y_B - y_A}{x_B - x_A} \tag{4.57}$$

The location of point D is found after the location of C, and the properties at D are found through linear interpolation. The location of point D provides the information to calculate a length differential between D and C the finite chemistry scheme is then performed along this differential length allowing for the species source function to be updated at C. Finding the streamline DC is very similar to the method used in determining the boundary. However DC is the streamline that is associated with the intersection of the characteristic lines, the same streamline is not being followed throughout the solution.

For the first iteration for finding the location of point D a prediction of the flow angle by averaging the flow angles of A and B can be made. Point D can be readily found by iteration through

$$x_D = \frac{y_C - y_A - \frac{1}{2}\left(\tan\theta_C + \tan\theta_D\right) x_C + \mathfrak{s} x_D}{\mathfrak{s} - \frac{1}{2}(\tan\theta_C + \tan\theta_D)} \tag{4.58}$$

and

$$r_D = r_C + (x\_x_C)\frac{1}{2}(\tan\theta_C + \tan\theta_D) \tag{4.59}$$

where

$$\mathfrak{s} = \frac{r_A - r_B}{x_A - x_B} \tag{4.60}$$

The flow properties and mass fractions are now linearly interpolated between $\bar{AB}$. The chemical kinetics can now be analyzed along the stream line with the length of $\bar{DC}$ being the differential length of the kinetics problem. Because the line segment represents the stream line $\bar{DC}$ and the flow is supersonic chemical kinetics can be analyzed using the one-dimensional analysis as presented in Section 2.4.

4.2 Nozzle Contour Design Process with Chemistry Included

The approach in design of an axis-symmetric nozzle coupled with finite rate chemistry combines the the three-zone method described with in Chapter 3 with a two-zone down

stream approach to adjust for the chemical kinetics. The addition of the finite rate chemistry allows for the specific heat ratio to be an independent variable instead of a constant.

4.2.1 Nozzle Contour Design Process

The following describes the process for axis-symmetric method of characteristics coupled with finite rate chemistry nozzle design. Providing the chamber conditions, propellant type, mixture ratio, converging curvature, and isentropic exit uniform flow exit Mach number.

1. Select Converging Section Geometry
2. Perform One-Dimensional Finite Rate Analysis
3. Form Isentropic Nozzle Solution
4. Perform MOC Coupled with Chemistry
5. Form Boundary

4.2.2 Converging Section Analysis

The converging section of the nozzle is analyzed with one-dimensional non equilibrium chemically reacting as described in the above section. To initialize the solution the composition of the combustion exhaust gases must be known. To find composition, an equilibrium composition calculation must be performed, using any number of methods to minimize Gibbs free energy[34]. A modified version of the Chemical Equilibrium with Applications (CEA) program developed by Gordon and McBride was used for this calculation[16][17].

The equilibrium calculation can be used to initiate the procedure using the assumption that the gases are reacting at or very near equilibrium in the combustion chamber. This analysis begins directly down stream of the combustion chamber at the start of the nozzle's converging section. To form the required pressure distribution, the converging geometry must be found.

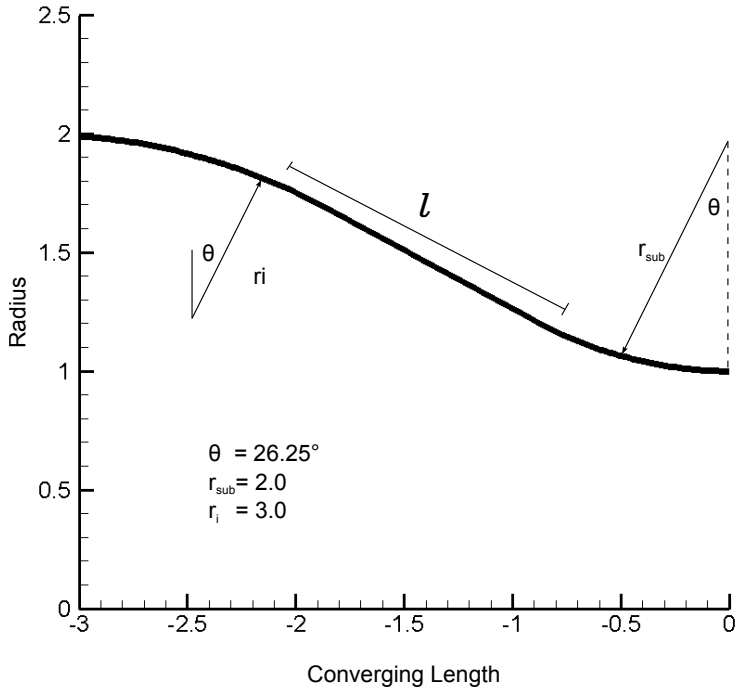

Figure 4.2: Converging section geometry with dimensions normalized by throat radius

The design of the converging section has been simplified for this development. The initial turning radius and the subsonic radius of curvature, along with the turning angles of both curvatures, are held constant for any case. These curvatures were modeled after the converging section of the Pratt and Whitney RL-10 [13] and have also been used in TDK performance calculations[7].

To form the required geometry to produce choked flow at the throat the length l is allowed to change so that the correct expansion ratio is found. The expansion ratio is determined by assuming that the speed of the gases at the beginning of the converging section have a non-zero velocity. For the present development the converging section is assumed to have Mach 0.15 flow at the beginning of the section. This value can be derived from the design of the fuel injection system and combustion chamber design. For this development the expansion ratio for the converging section is only dependent on propellant choice through the specific heat ratio. From the equilibrium calculation the specific heat ratio and assumed Mach number are used in the isentropic relation to determine the initial pressure ratio, and

expansion ratio. Because, the length l is not aligned axially, it is more convenient to evaluate total converging section length.

$$x = -((r_{sub} + r_i)\sin(\theta) + \frac{\sqrt{A_i} - 1 - (r_{sub} + r_i) * (1 - \cos(\theta))}{tan\theta} \tag{4.61}$$

As the required expansion ratio increases the required length l must increase to expand the initial area. This directly results in a change of axial length of the converging section. With the length of the converging section known the area of the converging section and its derivative can be found easily through the following set of equations[7]

When $x < x_1 + r_i + sin(\theta)$

$$A = \sqrt{A_i} - r_i \left(1 - \frac{\sqrt{1 - (x - x_1)^2}}{ri^2}\right)^2 \tag{4.62}$$

$$\frac{dA}{dx} = \frac{-2(x - x_1)}{(r_i^2 - (x - x_1^2)) * *(1/2))}\sqrt{A} \tag{4.63}$$

When $x_+ r_i sin\theta < x \; and \; x < -r_{sub} sin\theta$

$$A = \sqrt{A_i} - r_i\,(1 - \cos\theta) - (x - x_1 - r_i \sin\theta \;\; \tan\theta)^2 \tag{4.64}$$

$$\frac{dA}{dx} = -2\sqrt{A}\tan(\theta) \tag{4.65}$$

When $-r_{sub} sin(\theta)) < x(i) \; and \; x(i) < 0$

$$A = \left(1 + r_{sub}\left(1 - \sqrt{1 - \frac{x^2}{r_{sub}^2}}\right)\right)^2 \tag{4.66}$$

$$\frac{dA}{dx} = \frac{2x}{\sqrt{r_{sub}^2 - x^2}}\sqrt{A} \tag{4.67}$$

As described by Nickerson, et. al.[7][35], the pressure distribution associated with this geometry and chamber conditions can be found. The pressure ratio and its derivative can be determined by using the average equilibrium expansion coefficient and the area of the converging section for every position in x.

The average expansion coefficient can be found through iteration upon the following formula

$$C_e^{n+1} = C_e^n + \frac{\frac{2}{C_e^n+1}^{\frac{C_e^n}{C_e^n-1}} - \frac{P_e^*}{P_c}}{\frac{2}{C_e^n+1}^{\frac{C_e^n}{C_e^n-1}} \frac{1}{C_e^n-1}\left(\frac{1}{C_e^n-1}\ln\left(\frac{2}{C_e^n+1}\right) + \frac{C_e^n}{C_e^n+1}\right)} \tag{4.68}$$

Where P_e^* is the pressure if flow was in chemical equilibrium to the throat. A good starting point for the iteration is 1.2 [7]

With the average expansion coefficient found the pressure ratio at each location of x can now be found. The pressure ratio for the given location is iterated upon through the expression, where P is the ratio P/P_c

$$P_{j+1} = P_j + 2\left\{\frac{C_e-1}{C_e}\left[1-P_j^{\frac{C_e-1}{C_e}}\right]^{-1} P_j^{\frac{-1}{C_e}} - \frac{2}{C_e}P_j^{-1}\right\}^{-1} \cdot\left\{\left[\frac{C_e-1}{2}\frac{\frac{2}{C_e+1}^{\frac{C_e+1}{C_e-1}}}{P_j^{\frac{2}{C_e}}\left[1-P_j^{\frac{C_e-1}{C_e}}\right]}\right]^{-\frac{1}{2}} A - 1\right\} \tag{4.69}$$

The geometry illustrated in Fig. 4.2, was developed for a LOX-Hydrogen engine operating with a chamber pressure of 27.186 Bar. This is similar to that of the RL-10. The pressure distribution prescribed for this engines converging section is depicted in Fig. 4.3.

With the equilibrium condition, geometry, and pressure distribution determined the analysis of the flow including finite rate reactions may take place as described in Sec. 2.4.1. Figure 4.6 shows the general procedure in which the chemistry analysis occurs.

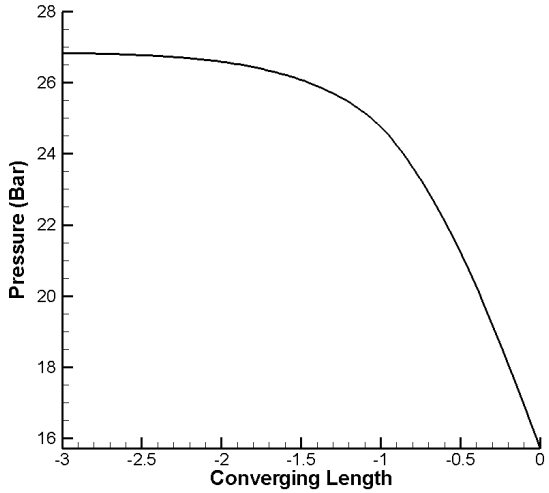

Figure 4.3: Converging section pressure distribution for LOX H_2 with $P_c = 27.186$ Bar

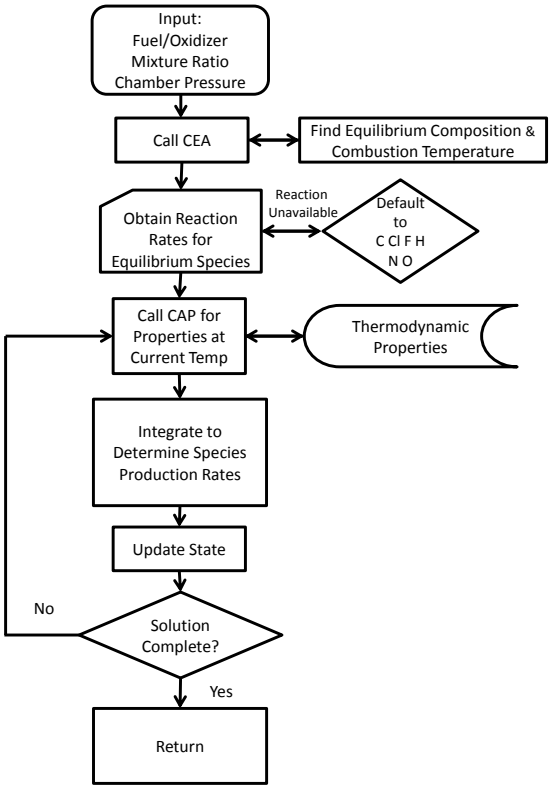

Figure 4.4: Procedure of finite rate chemistry analysis

The finite rate chemistry analysis begins with a library search for the correct set of reactions that can be performed with the species in the equilibrium composition. The reaction rate data available is listed but not limited to that presented in Appendix D. The finite rate chemistry application was developed as a generic tool provided that the correct rate data is provided in the library. If the application cannot find a specific reaction mechanism card it will default to the C, Cl, F, H, N, O reaction card. This card contains the elementary reactions of species that typically could be contained in a liquid propellant. Computationally, a card holding the reaction mechanism with only the available species is preferred.

The propellants in Table 4.2 are some typical liquid propellants that have been used in rockets. Reaction rate data is provided in Appendix D common propellants.

	Propellant Chemistry		
	Elemental Breakdown	Fuel	Oxidizer
1	C , F, H, N	$C_2H_8N_2$	F_2
2	C, F, H, N, O	N_2H_4−$C_2H_8N_2$	OF_2
3*	C, H, O	CH_4, C_3H_8, RP-1	O_2
4	H, O	H_2	O_2
5	F, H,	H_2	F_2
6*	F, H, N	N_2H_4	F_2
7	F, H, N, O	OF_2	N_2H_4
8*	H, N, O	H_2	N_2O_4
*Chemical kinetic rates have been included into the program.			

Table 4.2: Elemental breakdown of propellant fuel oxidizer pairs

Using the appropriate rates for the reaction mechanism the one-dimensional flow analysis of non-equilibrium chemically reacting gases is performed through numerical integration. The scale of the rates of the chemical reactions compared to the scale of the rates of change of the spacial and thermodynamic properties is very large. The extreme scale difference makes the governing equations a system of stiff differential equations. The numerical integration technique used is required to be an implicit scheme so that the scheme remains stable and the solution can be found[7][4][36]. The technique used to numerically integrate the governing equations is fully outlined in the by Nickerson, Coats, Bartz[35].

4.2.3 Isentropic Nozzle Formation

Once the solution has been completed for the converging section, the end result provides the flow properties at the geometric throat. At this point the composition of the fluid and its thermodynamic properties are known. The specific heat ratio for this point will be used for the first estimate of the specific heat ratio for the Sauer solution to the constant Mach number line. The line is formed and one dimensional-flow analysis is performed between the geometric throat and the intersection of the Sauer constant Mach line with the centerline. When the solution converges so that the specific heat ratio is met for the displaced distance from the geometric throat, this composition and thermodynamic properties are assumed to be constant along the constant Mach line.

With the specific heat ratio, location and Mach number known along the Sauer constant Mach line known an axis-symmetric method of characteristics solution can performed for the desired Mach number. If the centerline pressure distribution for this desired Mach number and γ is known the method can be carried out quickly, if not the centerline pressure distribution can be determined and the appropriate solution formed as was done in Chapter 3.

4.2.4 Perform Chemically Coupled MOC

The isentropic nozzle solution will be the basis for the solution coupled with finite rate chemistry. To begin the solution it is necessary to use the the first set of points downstream of the Sauer constant Mach line to begin the solution. The location of these points was determined through the pressure distribution required to achieve correct expansion to the desired Mach number, using these points helps initiate the solution.

The composition and new specific heat ratio is now found at each initiation point through the same means as the would be for an internal point. The solution can now be carried down stream as described is Section4.1, with the exception of finding the points along the centerline. The points on the centerline can be found through symmetry. Here the magnitude of

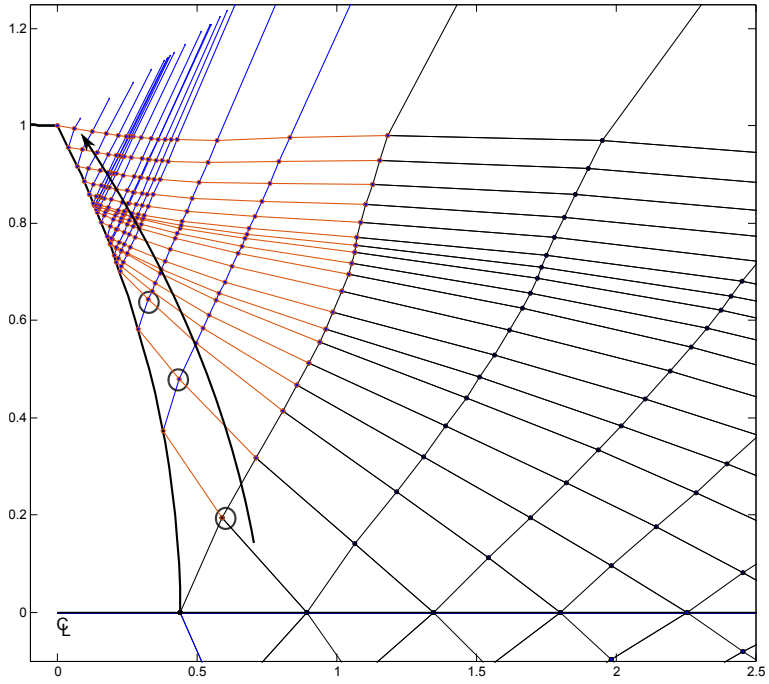

Figure 4.5: Initial Point Selection

the slopes of the left running characteristic of A is the same as the right running characteristic of B, but with opposite signs. This is also true for the flow angles, and the r location of the point. With this exception included the analysis can be completed for the kernel with finite rate chemistry included.

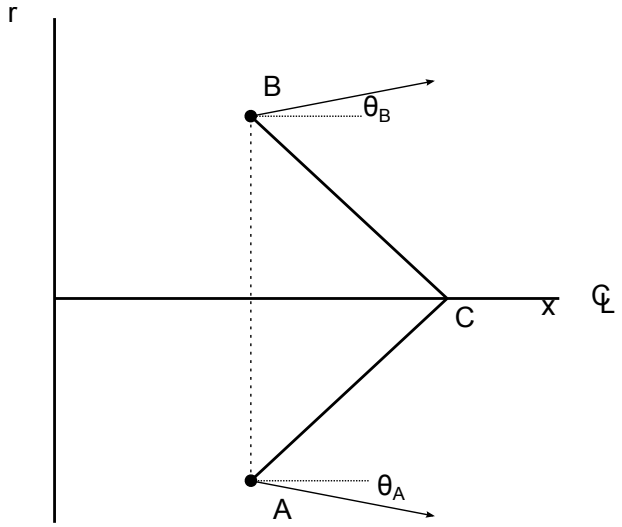

Figure 4.6: Points determined along the centerline through symmetry

Once the the chemically reacting kernel has been found the chemically reacting boundary zone can be found. The process is similar to that of the isentropic case. However, the addition of finite rate complicates the procedure. The difficulty in finding the solution to the boundary region is caused by the need to march down a streamline to update the finite rate chemistry influence. Before the region was simple to find, assuming that the exit flow was uniform and axial, but using those assumptions the solution was marched upstream for the isentropic case. To initiate the chemically reacting MOC scheme an assumption must be made about the position of the next right running characteristic, the flow angle at the first point, and the composition of the working fluid. To initiate the chemically reacting boundary

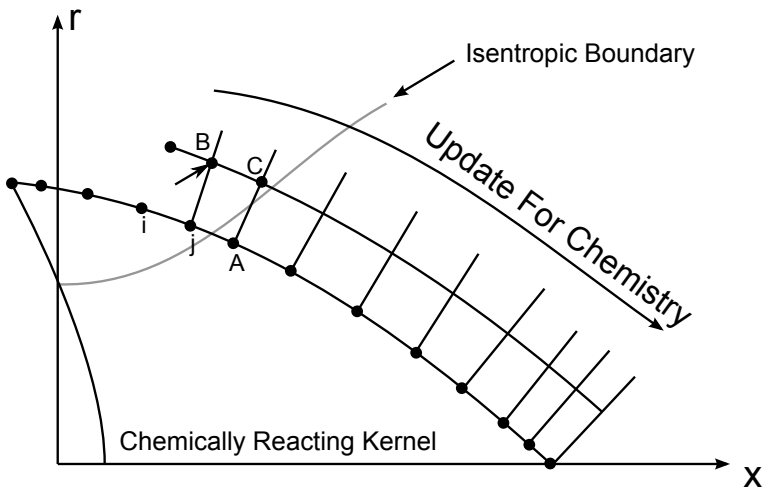

Figure 4.7: Update the boundary region characteristic for chemistry

region, an initial right running characteristic is found using the isentropic boundary region solution. Using a point outside the isentropic boundary an initial estimate of the flow angle is found. The value for ψ is assumed to be the value of ψ for the corresponding left running characteristic at the edge of the kernel. Initializing the right running characteristic in this way allows the method of characteristics with finite rate chemistry to be used. The chemically reacting MOC scheme is used to march downstream updating the location and the chemical source function for each point along the right running characteristic. The next right running characteristic is formed in the same way how ever the initial point should be shifted to the

next left running characteristic, and the assumed values are taken from the previous right running characteristic. The process for forming the right running characteristics for the chemically reacting boundary region is then repeated until ample characteristics have been formed to produce a solution. This solution being overlayed on the isentropic boundary produces a solution mesh as in Fig. 4.8 will show a jump in the non physical boundary mesh. This has no affect on the solution.

The boundary is formed in the same manner as that of the isentropic flow nozzle. The formation of the boundary is described in detail in Section 3.1.9.

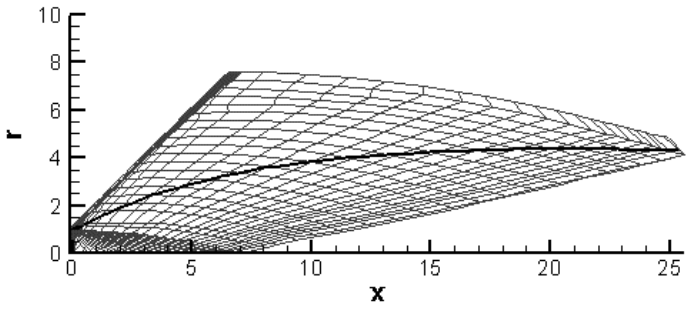

Figure 4.8: Chemically reacting solution mesh for Mach 4 nozzle

4.3 Effects of Finite Rate Chemistry on Nozzle Contour

The addition of finite rate chemistry to the method of characteristics for nozzle design has visible effects on the solution. The effects are more noticeable as the nozzle length increase.

Figure 4.9 shows the difference between the isentropic kernel solution and the kernel solution with the inclusion of finite rate chemistry. Notice that the characteristic lines and points have shifted due to the influence of the chemically reacting system.

The specific heat ratio is no longer constant through out the nozzle. The increase in specific heat ratio tends to be fairly linear along the centerline of the nozzle as depicted in Fig 4.10. For this example, LOX Hydrogen was the propellant choice.

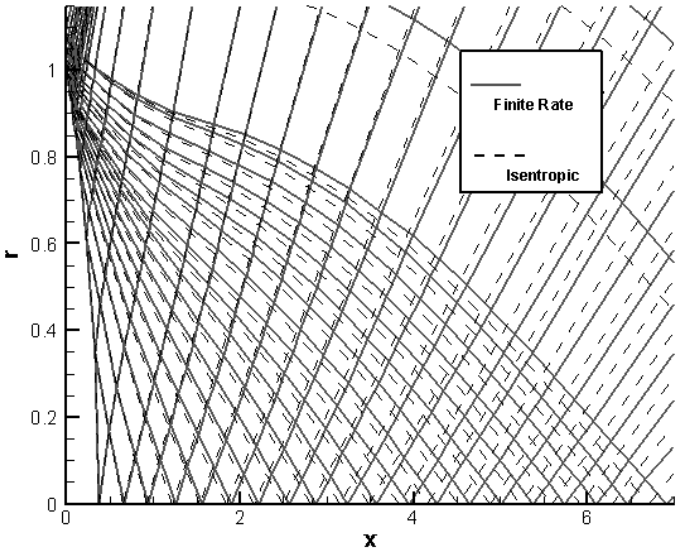

Figure 4.9: Comparison of isentropic kernel to kernel including finite rate chemistry

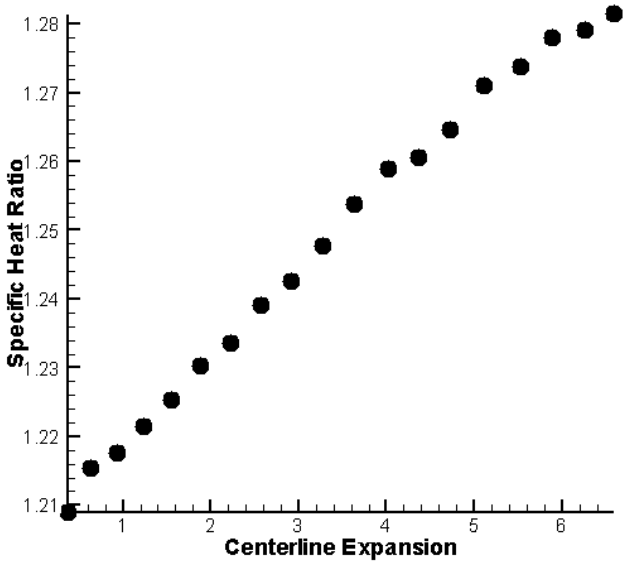

Figure 4.10: Specific heat ratio across expansion length

Referring to Eq 2.1, as γ increases the area ratio to produce a given exit condition decreases. This can be seen in the contour generated including finite rate chemistry. Figure 4.11 shows the effect of finite rate chemistry on the contour of nozzle that was designed for Mach 4 flow at the exit. The turning rate of the contour decreases along the length of the nozzle, as the specific heat ratio increases. This produces a contour that follows the same contour as the isentropic case initially but the exit area is decreased.

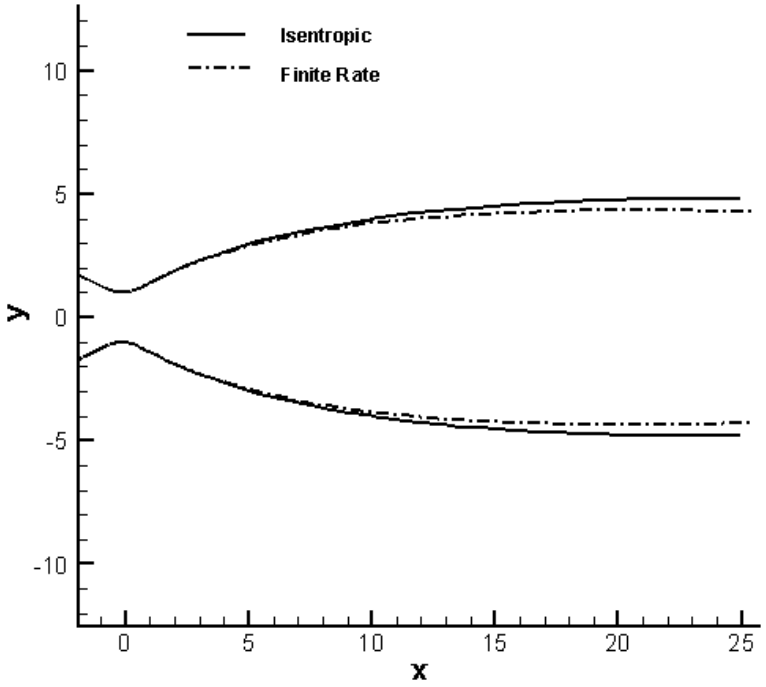

Figure 4.11: Comparison of isentropic Mach 4 nozzle to nozzle including finite rate chemistry

This result shows that the isentropic assumption does not have a drastic effect on the design of truncated nozzles. The contours are only slightly changed from the throat to about 10 time the radius of the throat in length. From this point on the isentropic assumption begins to fail and the inclusion of finite rate chemistry allows for a more accurate contour to produce a shock free nozzle.

Chapter 5

Conclusions and Suggestions for Future Work

A method of designing axis-symmetric nozzles with included finite-rate chemical kinetics has been developed. The method allows for the physical boundary of the nozzle to be determined based on a desired uniform exit Mach number for the isentropic case. The solution is then coupled with and adjusted for finite rate chemistry.

The contours designed in this way can have excessive and undesirable lengths, for use on rocket engines. A method for analysis of truncated nozzle performance was explored. The contour that produces maximum thrust for a given truncation length can be found. A method of simplifying the optimization procedure by reduction of the design space was developed through the use of performance maps. The performance maps can be extended to include a larger number of contours to reduce the design space for the optimum nozzle even further. The truncated nozzle analysis method is not limited to that of isentropic flow nozzles. The process can be extended to contours designed with finite rate chemistry included.

Improvement in contour geometry can be made through the incorporation of boundary layer effects could be added to the methodology developed. This would allow a more accurate physical contour geometry. A simple method for adding a boundary layer to the current development would be to displace the nozzle wall by a distance equal to the estimated boundary layer thickness.

The current development's analysis of the finite rate chemistry in the subsonic portion of the nozzle is limited to a one-dimensional analysis. This could be increased to a higher degree of freedom. In doing so the analysis would consider striated flows. The current development uses a one dimensional analysis becomes the distances traveled by streamlines

in the converging section is approximately equal. With the traversed distance being relatively uniform across the converging section it is a safe assumption that the composition of the product gases are uniform at the sonic line.

Inaccuracies in the finite rate analysis are largely due to provided reaction rate data. The rate data may only be as good as the experimental process to obtain such rates. Techniques for the measurement of reaction rates may become more accurate, and the reaction rate and third-body influence data should be updated accordingly.

The approach to the method of characteristics coupled with finite rate chemistry presented could be extended to analysis of the exhaust plume. This method would allow for the plume composition to be found. This can be useful for missile identification, or optimizing combustion and expansion of the gases to produce desired composition. Such a process would allow reduction of unwanted exhaust chemicals.

The contours designed with the addition of finite rate chemistry provide only a small deviation from the isentropic contour, when the truncation length is kept small. For propulsive nozzles, the truncation length that would typically be selected will be within the range that would see very little differences when designed with or without chemistry. The additional effort may not be worth the slight changes in contour that are formed by the additional analysis. However, if the composition of the exhaust gases needs to be known, as with plume analysis, it is imperative to use the analysis with chemical kinetics included.

Bibliography

[1] Sutton, G. P. and Biblarz, O., *Rocket Propulsion Elements*, John Wiley & Sons, Inc., seventh ed., 2001.

[2] ´Ostlund B. Muhammad-Klingmann, J., "Supersonic Flow Separation with Application to Rocket Engine Nozzles," *Applied Mechanics Reviews, ASME*, Vol. 58, May 2005.

[3] Guentert, E. C. and Neumann, H. E., "Design of Axisymmetric Exhaust Nozzles By Method of Characteristics Incorporating A Variable Isentropic Exponent," NASA TR R-33, 1959.

[4] Zucrow, M. J. and Hoffman, J. D., *Gas Dynamics, Vol II.*, John Wiley and Sons, 1977.

[5] Sauer, R., "General Characteristics of the Flow Through Nozzles at Near Critical Speeds," *National Advisory Committee for Aeronautics*, June 1947.

[6] Dunn, B., "Fuel Table," Tech. rep., 1997 [retrieved 10 March 2012].

[7] Nickerson, G. R., Dang, L. D., and Coats, D. E., "Engineering and Programming Manual : Two-Dimensional Kinetic Reference Computer Program," NASA CR-178628, April 1985.

[8] Anderson, J. D., *Introduction to Flight*, McGraw Hill.

[9] Technologies, G. L., "Brief History of Rockets," `http://www.grc.nasa.gov/WWW/K-12/TRC/Rockets/history_of_rockets.html`, Feb. 2010 [retrieved 24 January 2012].

[10] NASA, "Dr. Robert H. Goddard, American Rocketry Pioneer," `http://www.nasa.gov/centers/goddard/about/history/dr_goddard.html`, June 2009 [retrieved 24 January 2012].

[11] Edwards, T., "Liquid Fuels and Propellants for Aerospace Propulsion: 1903-2003," *Journal of Propulsion and Power*, Vol. 19, No. 6, 2003, pp. 1089–1105.

[12] Huzel, D. K. and Huang, D. H., *Modern Engieering for Design of Liquid-Propellant Rocket Engines*, AIAA.

[13] Pratt and Whitney, "RL10 Rocket Engine A National Historic Mechanical Engineering Landmark," American Society of Mechanical Engineers.

[14] Pratt and Whitney, "Space Shuttle Main Engine," Tech. rep., [retrieved 10 March 2012].

[15] Williams, F. A., *Combustion Theory*, The Benjamin/Cummings Publishing Company, Inc., 1985.

[16] Gordon, S. and McBride, B. J., "Computer Program for Calculation of Complex Chemical Equilibrium Compositions, Rocket Performance, Incident and Reflected Shockes and Chapman-Jouguet Detonations," Nasa sp-273, 1971.

[17] Gordon, S. and McBride, B. J., "Computer Program for Calculation of Complex Chemical Equilibrium Compositions and Applications," NASA RP-1311, 1996.

[18] Anderson, J., *Modern Compressible Flow: with Historical Perspective*, McGraw-Hill.

[19] Rao, G. V. R., "Exhaust Nozzle Contour for Optimum Thrust," *Jet Propulsion*, Vol. 28, No. 6, June 1958, pp. 377–382.

[20] Abbot, M. B., *An Introduction to the Method of Characteristics*, Thames and London.

[21] Hartfield, R. J. and Ahuja, V., "The Closing Boundary Condition for the Axis-Symmetric Method of Characteristics," *Joint Propulsion Conference*, AIAA, San Diego, CA, 2011.

[22] Ferri, A., "The Method of Characteristics," *General Theory of High Speed Aerodynamics*, edited by W. Sears, The Macmillan Co., 1951.

[23] Rao, G., "Contoured Rocket Nozzles," *Proc 9th*, 1958.

[24] Haddad, A. and Mosst, J. B., "Aerodynamic Design for Supersonic Nozzles of Arbitrary Cross Section," Journal of propultion, 1988.

[25] Wang, B. N. and Hoffman, "Calculation of Annular Nozzle Trisonic Flowfields by the Method of Characteristics," Tech. rep.

[26] Allman, J. G. and Hoffman, J. D., "Design of Maximum Thrust Nozzle Contours by Direct Optimization Methods," *AIAA/SAE Joint Propulsion Conference*, Vol. 14, Aug. 1978.

[27] Zucrow, M. J. and Hoffman, J. D., *Gas Dynamics, Vol I.*, John Wiley and Sons, 1976.

[28] Albarado, K. M., Hartfield, R. J., Hurston, B. W., and Jenkins, R. M., "Solid Rocket Motor Performance Matching Using Pattern Search/Particle Swarm Optimization," *Journal of Propulsion and Power*, Vol. 47, 2011.

[29] Quarteroni, A., Sacco, R., and Saleri, F., *Numerical Mathematics*, Springer, 2nd ed., 2007.

[30] Kushida, R., "Revision of CPIA 246, Section 6.2, Reaction Rate Data," Jpl 383cr-76-211, 1976.

[31] Cohen, N. and Westberg, K. R., "Chemical Kinetic Data Sheets for High-Temperature Chemical Reactions," *Journal of Physics*.

[32] Jr., K. W., *Advanced Thermodynamics for Engineers*, McGraw Hill.

[33] Zehe, M. J., Gordon, S., and McBride, B., "CAP: A Computer Code for Generating Tabular Thermodynamic Functions from NASA Lewis Coefficients," NASA/TP- 2001-210959, Oct. 2001.

[34] Anderson, J. D., *Hypersonic and High-Temperature Gas Dynamics*, AIAA, 2006.

[35] Nickerson, G. R., Coats, D. E., and Bartz, J. L., "Two-Dimensional Kinetic Reference Computer Program," NASA CR-152999, Dec. 1973.

[36] Radhakrishnan, K., "Combustion Kinetics and Sensitivity Analysis Computations," *Numerical Approaches to Combustion Modeling*.

Appendices

Appendix A

Sauer's Solution to Transonic Region

Transonic flow occurs in a converging-diverging nozzle near the throat. Unlike in quasi-one-dimensional flow, the sonic line (line where the Mach number of the fluid is unity at all points) is not a vertical line spanning the width of the throat. In fact the sonic line is curved. The region close to this sonic line is the transonic flow zone and contains both subsonic and supersonic portions of the flow. This causes difficulties in the mathematical representation of this region. To describe this zone, the coordinate system used should lie so that the x-axis is the centerline of the nozzle and the origin is placed where the critical velocity first occurs on the axis, see Fig A.1

Considering $\tilde{u}, \tilde{v}$ as the x and r components of the velocity and a^* as the sonic velocity at the throat, the potential equation is written as

$$\frac{\partial U}{\partial x}\left(1 - U^2 - \frac{\gamma-1}{\gamma+1}V^2\right) + \frac{\partial V}{\partial r}\left(1 - \frac{\gamma-1}{\gamma+1}U^2 - V^2\right)$$
$$-\frac{4}{\gamma+1}\frac{\partial U}{\partial r}UV + \sigma\left[1 - \frac{\gamma-1}{\gamma+1}\left(U^2+V^2\right)\right]\frac{V}{r} = 0 \tag{A.1}$$

where

$$U = \frac{\tilde{u}}{a^*}\text{ , and }\ V = \frac{\tilde{v}}{a^*} \tag{A.2}$$

Knowing that the transonic flow is only in the vicinity of the throat define

$$U = 1 + u,\ \text{and}\ V = v \tag{A.3}$$

The quantities of u and v are to be considered small. Substituting Eqn (A.3) into Eqn (A.1) results in the following approximation to be formed. The intermediate steps are found in Sauer[5].

$$(\gamma+1)\,u\frac{\partial u}{\partial x} - \frac{\partial v}{\partial r} - \sigma\frac{v}{r} = 0 \tag{A.4}$$

The following relations must be defined in order to continue. These relations take into account the symmetry around the x-axis

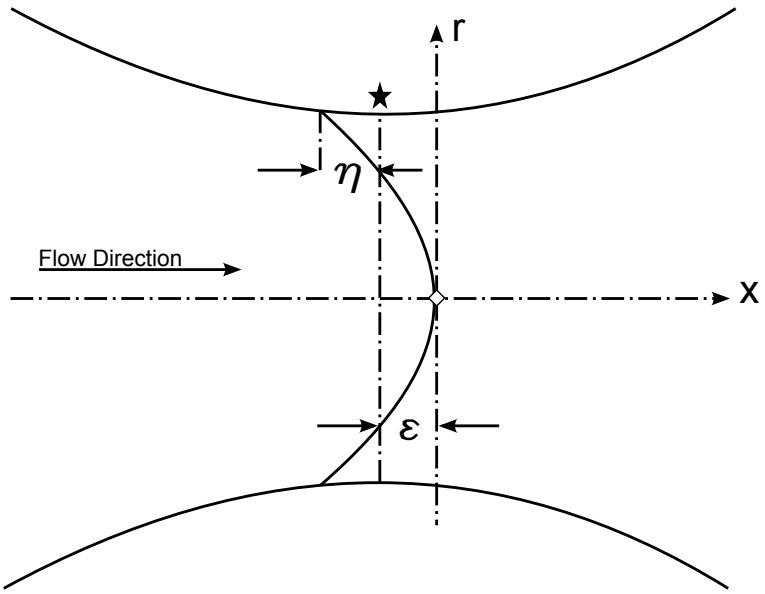

Figure A.1: Transonic Flow Zone[5]

$$\begin{aligned}
\varphi &= f_0(x) + r^2 f_2(x) + r^4 f_4(x) + ... \\
u &= \frac{\partial \varphi}{\partial x} = f_0'(x) + r^2 f_4'(x) ... \\
v &= \frac{\partial \varphi}{\partial r} = 2r f_2(x) + 4r^3 f_4(x) + ...
\end{aligned} \tag{A.5}$$

The primes in the Eq. A.5 represent the first derivatives with respect to x of the appropriate function. From the expressions defined the following can be found through Eqn (A.4).

$$(\gamma+1)(f_0' + r^2 f_2' + ...)(f_0'' + y^2 f_2'' + ...) = 2f_2 + 12r^2 f_4 + ... + 2\sigma(f_2 + 2r^2 f_4 + ...) \tag{A.6}$$

Rearranging Eqn (A.6) in order of powers of r and equating coefficients of the individual powers to zero the following system of equations is obtained.

$$\begin{aligned}
2(1+\sigma) f_2 &= (\gamma+1) f_0' f_0'' \\
2(6+2\sigma^*) f_4 &= (\gamma+1)(f_0' f_2'' + f_0'' f_2')
\end{aligned} \tag{A.7}$$

The function

$$f_0' = u_o(x)$$

characterizes the velocity distribution along the nozzle axis. This flow velocity distribution can be set given

$$f_0' = u_o(x) = \alpha x \tag{A.8}$$

Given $u_o(y)$ and understanding that the nozzle wall can be assumed to be a curve that is revolved about the x-axis. This provides that the flow is completely established in the nozzle. With this being said Eqn (A.8) can be substituted into the system of equations in Eqn (A.7) and solved for the functions f_2 and f_4 yielding the following equations

$$f_2 = \frac{\gamma+1}{4}\alpha^2 x \tag{A.9}$$

$$f_4 = \frac{(\gamma+1)^2}{64}\alpha^3 \tag{A.10}$$

Because the nozzles being considered are three dimensional $\sigma = 1$, substituting Eqn (A.9) and (A.10) into Eqn (A.5) results in

$$u = \alpha x + \frac{\gamma+1}{4}\alpha^2 r^2 + ... \tag{A.11}$$

$$v = \frac{\gamma+1}{2}\alpha^2 xr + \frac{(\gamma+1)^2}{16}\alpha^3 r^3 + ... \tag{A.12}$$

where higher order terms have been neglected. This result are the components of the velocity as a function of x and r in the nozzle. From (A.11) and (A.12) the sonic line can be obtained when the following requirement is met

$$(1+u)^2 + v^2 = 1 \tag{A.13}$$

When this condition met the following curve can be projected through the transonic region

$$x_K = -\frac{\gamma+1}{4}\alpha r_k^2 \tag{A.14}$$

This curve crosses through the axis of symmetry normally at the point $x = 0, y = 0$. At this location its curvature is

$$\frac{1}{\rho_K} = \frac{\gamma+1}{2}\alpha \tag{A.15}$$

Considering where the flow is tangent to the boundary, the flow here is thus parallel to the axis of the nozzle. At this point $v = 0$, this being so allows for the location of the minimum area point to be found through

$$\epsilon = x_s = -\frac{\gamma+1}{8}\alpha y_s^2 \tag{A.16}$$

From the location of the minimum area point and the curve of the sonic line the distance behind the minimum area point where the flow becomes sonic can be defined through

$$\eta = -(x_k - x_s) = \frac{1}{8}(\gamma+1)\alpha y_s^2 = \epsilon \tag{A.17}$$

With the minimum area point and the sonic point at the wall of the nozzle known the radius of curvature of the throat can be found. Following the assumption that the curvature follows a circular arc the radius of curvature can be found to be

$$\rho_s = \frac{2}{(\gamma+1)\alpha^2 y_s} \tag{A.18}$$

The preceding equations have been presented as if the velocity components of the flow field are known and the radius of curvature needs to be found. Typically the opposite occurs. In use of Sauer's solution in developing an automated nozzle design program neither is known and no assumptions could be made about the flow field beyond reasonable doubt. This being said a radius of curvature of the subsonic portion of the throat is allowable, especially with the use of an optimizer. Thus the flow field was determined by an assumed radius of curvature. Solving a few of the equations so that one of the dependent variables is the radius of curvature is completed below.

$$\alpha = sqrt\frac{2}{(\gamma+1)\rho_s y_s} \tag{A.19}$$

$$\eta = \epsilon = \frac{y_s}{8}\sqrt{2(\gamma+1)\frac{y_s}{\rho_s}} \tag{A.20}$$

The use of (A.11) and (A.12) along with the solution to (A.19) the Mach number within the transonic region can be found.

Appendix B

Chemical Equilibrium with Applications

The development of a computer program for the calculation of complex chemical equilibrium began in the 1940's through the NASA Lewis Research Center[16]. Sanford Gordon and Bonnie McBride developed a series of software applications that allow for such calculation as well as application of chemical equilibrium flow such as rocket performance calculations. The software is readily available at `www.grc.nasa.gov/WWW/CEAWeb/`. The fortran source code can be found and modified as needed to fit the application at hand.

The approach used by Gordon and MacBride was a free-energy minimization technique, formed in a generic sense as to beable to calculate the equilibrium compositions of any specified mixture of propellants.

Appendix C

Thermodynamic Properties Database

As with applications such as CEA, the development at hand required the availability of thermodynamic data of all species involved in the calculation performed. NASA Glen Research Center maintains a database of over 2000 species[33]. The database has been compiled into the Coefficients and Properties (CAP) program.

The database uses a 9-constant empirical representation of the thermodynamic data of each species. The thermodynamic coefficients are generated by a least-squares fit to measured thermodynamic functions of condensed and gas phase species[33]. The database is contiually updated to reflect new species, improved measurements for current species, and newer physical constants.

The properties available in the database include

- C_p° Molar Constant Pressure Specific Heat
- $G^\circ(T)$ Molar Gibbs energy at temperature T
- $H^\circ(T)$ Molar Enthalpy
- K Equilibrium Constant
- M Molecular Weight
- $S^\circ(T)$ Entropy at temperture T

The program also has the ability of changing the reference state. As well as compare some of the above properties to the properties at the reference state.

For the development in hand the CAP program was used internally. The reference state used was $298.15K$. The source code can easily be found through `www.grc.nasa.gov/WWW/CEAWeb/`. This is the same thermodynamic database used in the version of CEA employed in the current development.

Appendix D

Reaction Mechanisms

The following tables provide the forward reaction rate coefficients and mechanisms that can be used in this development.

	O-H Reactions				
	Elementary Reaction	3rd Body	A	N	B
1	$2H + M \rightleftharpoons H_2 + M$	M1	6.4E17	1.0	0.0
2	$H + OH + M \rightleftharpoons H_2O + M$	M2	8.4E21	2.0	0.0
3	$O + H + M \rightleftharpoons OH + M$	M3	1.9E13	0.0	-1.79
4	$O + O + M \rightleftharpoons O_2$	M4	3.62E18	1.0	0.0
5	$O_2 + H \rightleftharpoons O + OH$	0	2.2E14	0.0	16.8
6	$H_2 + O \rightleftharpoons H + OH$	0	1.8E10	-1.0	8.9
7	$H_2 + OH \rightleftharpoons H_2O + H$	0	2.2E13	0.0	5.15
8	$OH + OH \rightleftharpoons H_2O + O$	0	6.3E12	0.0	1.09
* Forward Rate: $K = AT^{-N}EXP(-1000B/R_uT)$					

Table D.1: Simple reaction mechanism for Hydrogen/Oxygen combustion[7]

Third-Body Ratios of H,O system				
Species	M1	M2	M3	M4
H	25.0	12.5	12.5	12.5
H_2	4.0	5.0	5.0	5.0
H_2O	10.0	17.0	5.0	5.0
O	25.0	12.5	12.5	12.5
OH	25.0	12.5	12.5	12.5
O_2	1.5	6.0	5.0.0	11.0

Table D.2: Third-body efficiency ratios for Hydrogen/Oxygen

	Carbon-Hydrogen-Oxygen Nitrogen Reactions				
	Elementary Reaction	3rd Body	A	N	B
1	$2H + M \rightleftharpoons H_2 + M$	M1	6.4E17	1.0	0.0
2	$H + OH + M \rightleftharpoons H_2O + M$	M2	8.4E21	2.0	0.0
3	$O + H + M \rightleftharpoons OH + M$	M3	1.9E13	0.0	-1.79
4	$O + O + M \rightleftharpoons O_2$	M4	3.62E18	1.0	0.0
5	$N + O + M \rightleftharpoons NO + M$	M5	6.4E16	0.5	0.0
6	$N + N \rightleftharpoons N_2 + M$	M6	3.0E14	0.0	-0.99
7	$CO + O + M \rightleftharpoons CO_2 + M$	M7	1.0E14	0.0	0.0
8	$O_2 + H \rightleftharpoons O + OH$	0	2.2E14	0.0	16.8
9	$H_2 + O \rightleftharpoons H + OH$	0	1.8E10	-1.0	8.9
10	$H_2 + OH \rightleftharpoons H_2O + H$	0	2.2E13	0.0	5.15
11	$OH + OH \rightleftharpoons H_2O + O$	0	6.3E12	0.0	1.09
12	$CO + OH \rightleftharpoons CO_2 + H$	0	1.5E7	-1.3	-0.765
13	$N_2 + O \rightleftharpoons NO + N$	0	7.6E13	0.0	75.5
14	$O_2 + N \rightleftharpoons NO + N$	0	6.4E9	-1.0	6.25
15	$CO + O \rightleftharpoons CO_2$	0	2.5E6	0.0	3.18
16	$CO_2 + O \rightleftharpoons CO + O_2$	0	1.7E13	0.0	52.7
* Forward Rate: $K = AT^{-N}EXP(-1000B/R_uT)$					

Table D.3: Simple reaction mechanism for CHON combustion[7]

	Third-Body Effeciency of CHON						
Species	M1	M2	M3	M4	M5	M6	M7
Ar	1.0	1.0	1.0	1.0	0.8	1.0	1.0
CO	1.5	3.0	4.0	4.0	1.0	1.0	1.0
CO_2	6.4	4.0	5.0	8.0	3.0	2.0	5.0
H	25.0	12.5	12.5	12.5	10.0	10.0	1.0
H_2	4.0	5.0	5.0	5.0	2.0	2.0	1.0
H_2O	10.0	17.0	5.0	5.0	7.0	3.0	1.0
N	1.0	1.0	1.0	10.0	10.0	10.0	1.0
NO	1.5	3.0	4.0	4.0	1.0	1.0	1.0
N_2	1.5	3.0	4.0	4.0	1.0	1.0	2.0
O	25.0	12.5	12.5	12.5	10.0	10.0	1.0
OH	25.0	12.5	12.5	12.5	10.0	10.0	1.0
O_2	1.5	6.0	5.0.0	11.0	1.0	1.0	25.0
*Argon only present in combustion with air							

Table D.4: Third-body efficiency ratios for CHON[7]

	C,Cl,F,H,N,O Reactions				
	Elementary Reaction	3rd Body	A	N	B
1	$2H + M \rightleftharpoons H_2 + M$	M1	6.4E17	1.0	0.0
2	$H + OH + M \rightleftharpoons H_2O + M$	M2	8.4E21	2.0	0.0
3	$O + H + M \rightleftharpoons OH + M$	M3	1.9E13	0.0	-1.79
4	$O + O + M \rightleftharpoons O_2$	M4	3.62E18	1.0	0.0
5	$N + O + M \rightleftharpoons NO + M$	M5	6.4E16	0.5	0.0
6	$N + N \rightleftharpoons N_2 + M$	M6	3.0E14	0.0	-0.99
7	$CO + O + M \rightleftharpoons CO_2 + M$	M7	1.0E14	0.0	0.0
8	$F + F + M \rightleftharpoons F_2 + M$	M8	3.25E8	-1.0	-6.38
9	$H + F + M \rightleftharpoons HF + M$	M9	7.5E12	0.0	-35.13
10	$CL + CL + M \rightleftharpoons CL_2 + M$	M10	2.23E14	0.0	-1.81
11	$H + CL + M \rightleftharpoons HCL + M$	M11	2.6E13	0.0	-19.9
12	$CL + F + M \rightleftharpoons CLF + M$	M12	3.0E16	0.5	0.0
13	$O_2 + H \rightleftharpoons O + OH$	0	2.2E14	0.0	16.8
14	$H_2 + O \rightleftharpoons H + OH$	0	1.8E10	-1.0	8.9
15	$H_2 + OH \rightleftharpoons H_2O + H$	0	2.2E13	0.0	5.15
16	$OH + OH \rightleftharpoons H_2O + O$	0	6.3E12	0.0	1.09
17	$CO + OH \rightleftharpoons CO_2 + H$	0	1.5E7	-1.3	-0.765
18	$N_2 + O \rightleftharpoons NO + N$	0	7.6E13	0.0	75.5
19	$O_2 + N \rightleftharpoons NO + N$	0	6.4E9	-1.0	6.25
20	$CO + O \rightleftharpoons CO_2$	0	2.5E6	0.0	3.18
21	$CO_2 + O \rightleftharpoons CO + O_2$	0	1.7E13	0.0	52.7
22	$F + H2 \rightleftharpoons HF + F$	0	9.2E13	0.0	1.08
23	$H + F_2 \rightleftharpoons HF + F$	0	8.8E13	0.0	2.40
24	$Cl_2 + H \rightleftharpoons HCl + Cl$	0	8.6E13	0.0	1.2
25	$Cl + H_2 \rightleftharpoons HCl + H$	0	1.45E13	0.0	4.4
26	$HCl + F \rightleftharpoons HF + Cl$	0	1.9E12	-0.68	0.6
27	$Cl_2 + F \rightleftharpoons Cl + ClF$	0	6.2E12	-0.68	0.5
28	$Cl + F_2 \rightleftharpoons F + ClF$	0	7.6E12	-0.68	0.3
29	$ClF + H \rightleftharpoons HF + Cl$	0	1.8E12	-0.58	3.2
30	$ClF + F \rightleftharpoons HCl + F$	0	5.6E12	-0.68	1.9
31	$ClF + H_2 \rightleftharpoons HCl + HF$	0	1.8e10	-0.5	46.34
32	$F_2 + HCl \rightleftharpoons HF + ClF$	0	1.8E10	-0.5	39.43
33	$ClF + HCl \rightleftharpoons HF + Cl_2$	0	1.8E10	-0.5	46.03
34	$F_2 + Cl_2 \rightleftharpoons ClF + ClF$	0	1.8E10	-0.5	26.76
35	$OH + F \rightleftharpoons HF + OH$	0	2.9E12	-0.68	0.2
36	$H_2O + F \rightleftharpoons HF + OH$	0	1.4E10	-0.68	.6
37	$Cl + OH \rightleftharpoons HCl + O$	0	5.9E10	-0.5	39.43
38	$HCL + OH \rightleftharpoons H_2O + Cl$	0	2.25E12	0.0	1.02

Table D.5: Reaction mechanism for C,Cl,F,H,N,O system combustion[7]

	Third-Body Effeciency of C,Cl,F,H,N,O											
Species	M1	M2	M3	M4	M5	M6	M7	M8	M9	M10	M11	M12
Ar	1.0	1.0	1.0	1.0	0.8	1.0	1.0	0.0	0.0	0.0	1.0	1.0
CO	1.5	3.0	4.0	4.0	1.0	1.0	1.0	0.0	0.0	0.0	1.0	1.0
CO_2	6.4	4.0	5.0	8.0	3.0	2.0	5.0	0.0	0.0	0.0	1.0	1.0
H	25.0	12.5	12.5	12.5	10.0	10.0	1.0	1.0	20.0	0.0	1.0	1.0
H_2	4.0	5.0	5.0	5.0	2.0	2.0	1.0	1.0	8.0	0.0	1.0	1.0
H_2O	10.0	17.0	5.0	5.0	7.0	3.0	1.0	0.0	0.0	0.0	1.0	1.0
N	1.0	1.0	1.0	10.0	10.0	10.0	1.0	1.0	1.0	0.0	1.0	1.0
NO	1.5	3.0	4.0	4.0	1.0	1.0	1.0	0.0	0.0	0.0	1.0	1.0
N_2	1.5	3.0	4.0	4.0	1.0	1.0	2.0	1.0	0.0	0.0	1.0	1.0
O	25.0	12.5	12.5	12.5	10.0	10.0	1.0	0.0	0.0	0.0	1.0	1.0
OH	25.0	12.5	12.5	12.5	10.0	10.0	1.0	0.0	0.0	0.0	1.0	1.0
O_2	1.5	6.0	5.0.0	11.0	1.0	1.0	25.0	0.0	0.0	0.0	1.0	1.0
HF	2.0	0.0	0.0	0.0	0.0	0.0	0.0	1.0	1.0	0.0	1.0	1.0
F	4.0	0.0	0.0	0.0	0.0	0.0	0.0	2.4	4.0	0.0	1.0	1.0
HCl	0.0	0.0	0.0	0.0	0.0	0.0	0.0	1.0	0.0	1.0	1.0	1.0
Cl_2	0.0	0.0	0.0	0.0	0.0	0.0	0.0	0.0	0.0	5.0	1.0	1.0
CL	0.0	0.0	0.0	0.0	0.0	0.0	0.0	0.0	0.0	1.0	1.0	1.0
*Argon only present in combustion with air												

Table D.6: Third-body efficiency ratios for C,Cl,F,H,N,O system[7]

Appendix E

One-dimensional Finite Rate Chemistry Data

The following plots are mole fractions of the chemical species in one-dimensional finite rate chemistry analysis of the converging sections for LOX-Hydrogen and LOX-RP1 propellant mixtures.

E.1 LOX-Hydrogen

Analysis was made with LOX-Hydrogen propellant. Chamber pressure was set to 27.186 Bar and the mixture ratio was 6.0.

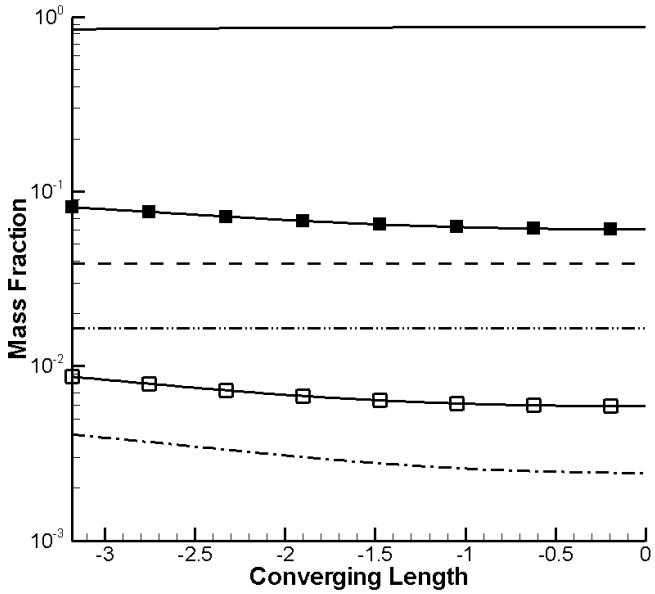

Figure E.1: Mass fraction of LOX Hydrogen system in converging section

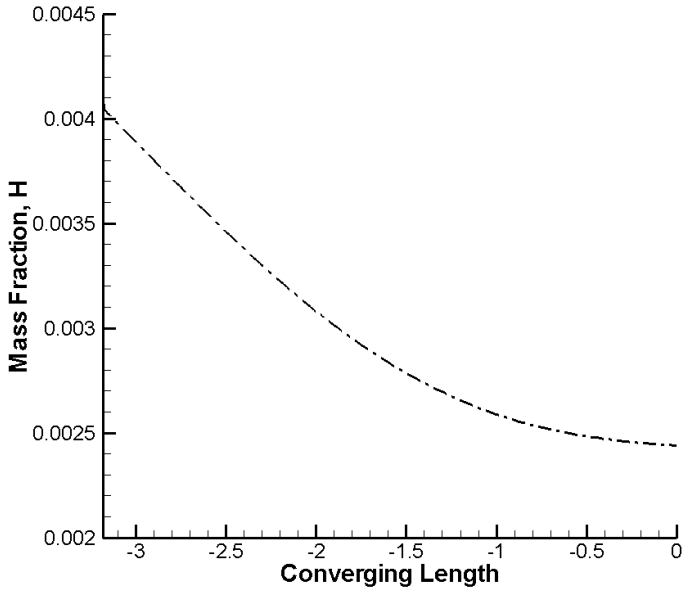

Figure E.2: Mass fraction of H in converging section

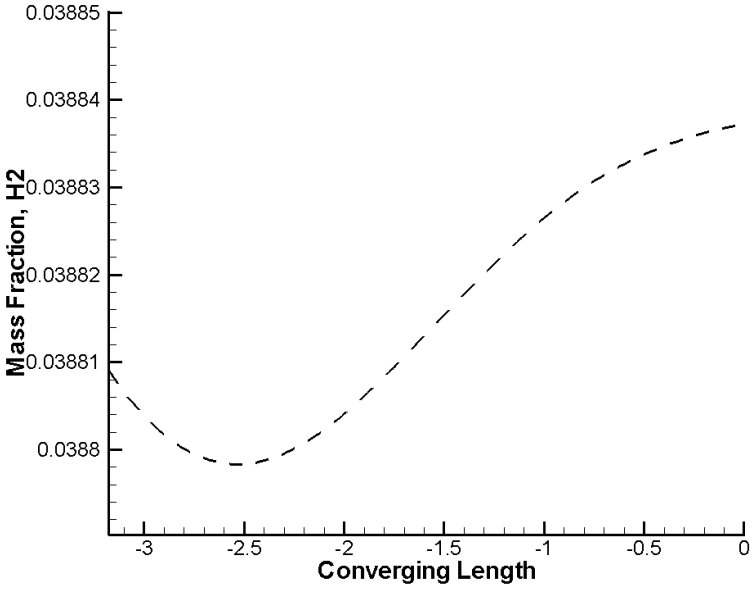

Figure E.3: Mass fraction of H_2 in converging section

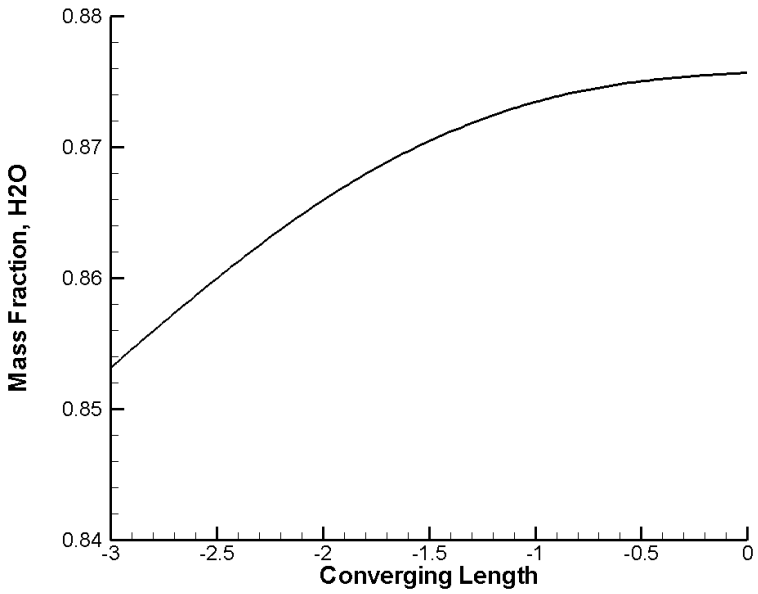

Figure E.4: Mass fraction of H_2O in converging section

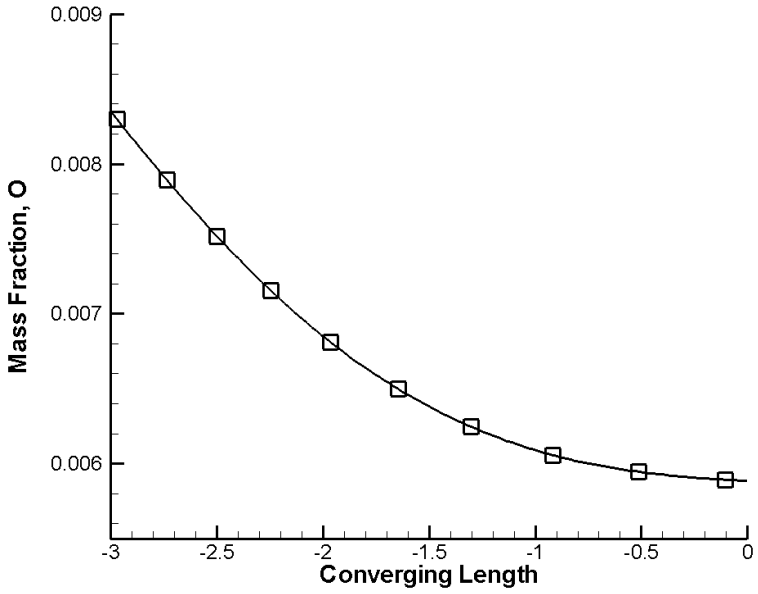

Figure E.5: Mole fraction of O in converging section

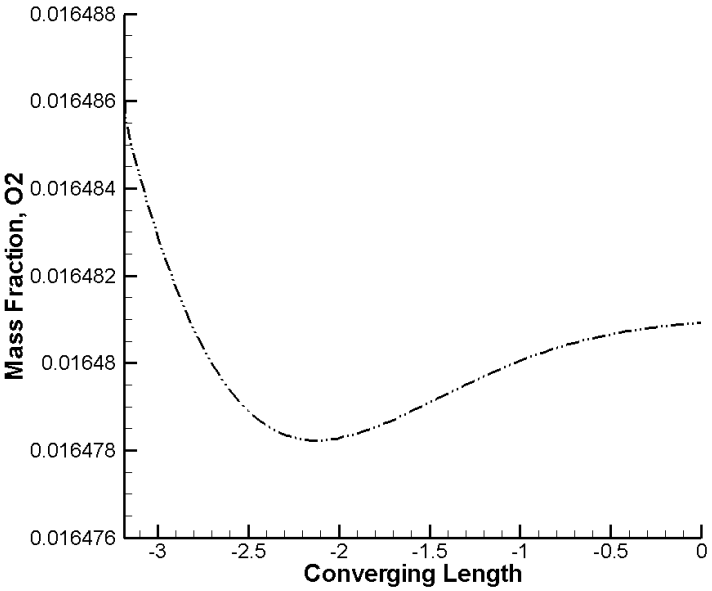

Figure E.6: Mole fraction of O_2 in converging section

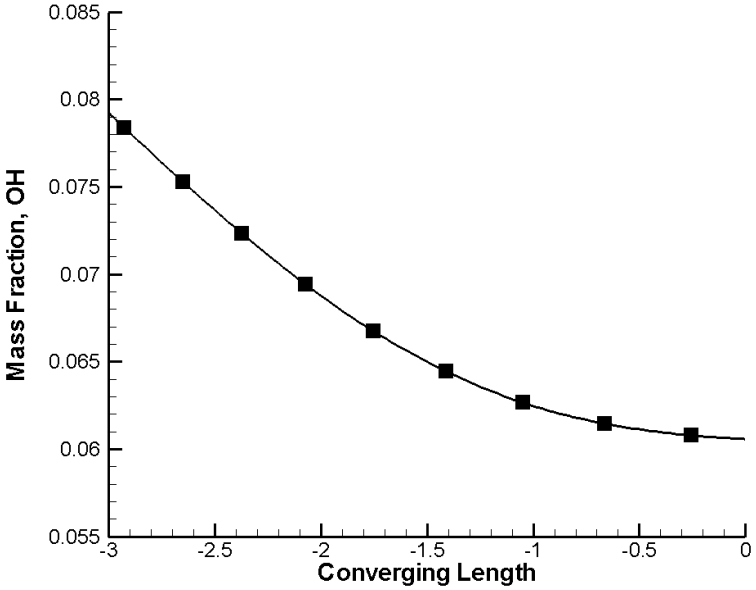

Figure E.7: Mole fraction of OH